Alma Mater Studiorum - Università di Bologna

DOTTORATO DI RICERCA

Scienze Ambientali: tutela e gestione delle risorse naturali

Ciclo XXI

Settore/i scientifico disciplinari di afferenza: GEO/12 Oceanografia e Fisica dell'atmosfera

TITOLO TESI

Modelling coupled physical-biogeochemical processes in ice-covered oceans

Presentata da: Letizia Tedesco

Coordinatore Dottorato
Prof. Elena Fabbri

Tutor
Prof. Nadia Pinardi

Supervisore
Dr. Marcello Vichi

Co–supervisori
Dr. Jari Haapala
Dr. Tapani Stipa

Esame finale anno 2009

University of Bologna
PhD course in Environmental Sciences

A dissertation submitted for the Degree of Doctor of Philosophy and Doctor Europaeus

MODELLING COUPLED PHYSICAL-BIOGEOCHEMICAL PROCESSES IN ICE-COVERED OCEANS

Letizia TEDESCO

June 2009

Prof. Marco ACULEO (committee)

Prof. Terenzio BERNARDI (committee)

Prof. Antonio PUSCEDDU (committee)

Prof. David N. THOMAS (external committee)

Dr. Mats A. GRANSKOG (referee)

Prof. Harri KUOSA (referee)

Prof. Nadia PINARDI (tutor)

Dr. Marcello VICHI (supervisor)

Dr. Jari HAAPALA (co-supervisor)

Dr. Tapani STIPA (co-supervisor)

To Miikka,
my lighthouse in the storm.

Abstract

The last decades have seen a large effort of the scientific community to study and understand the physics of sea ice. We currently have a wide - even though still not exhaustive - knowledge of the sea ice dynamics and thermodynamics and of their temporal and spatial variability. Sea ice biogeochemistry is instead largely unknown. Sea ice algae production may account for up to 25% of overall primary production in ice-covered waters of the Southern Ocean. However, the influence of physical factors, such as the location of ice formation, the role of snow cover and light availability on sea ice primary production is poorly understood. There are only sparse localized observations and little knowledge of the functioning of sea ice biogeochemistry at larger scales. Modelling becomes then an auxiliary tool to help qualifying and quantifying the role of sea ice biogeochemistry in the ocean dynamics. In this thesis, a novel approach is used for the modelling and coupling of sea ice biogeochemistry - and in particular its primary production - to sea ice physics. Previous attempts were based on the coupling of rather complex sea ice physical models to empirical or relatively simple biological or biogeochemical models. The focus is moved here to a more biologically-oriented point of view. A simple, however comprehensive, physical model of the sea ice thermodynamics (ESIM) was developed and coupled to a novel sea ice implementation (BFM-SI) of the Biogeochemical Flux Model (BFM). The BFM is a comprehensive model, largely used and validated in the open ocean environment and in regional seas. The physical model has been developed having in mind the biogeochemical properties of sea ice and the physical inputs required to model sea ice biogeochemistry. The central concept of the coupling is the modelling of the Biologically-Active-Layer (BAL), which is the time-varying fraction of sea ice that is continuously connected to the ocean via brines pockets and channels and it acts as rich habitat for many microorganisms. The physical model provides the key physical properties of the BAL (e.g., brines volume, temperature and salinity), and the BFM-SI simulates the physiological and ecological response of the biological community to the physical enviroment. The new biogeochemical model is also coupled to the pelagic BFM through the exchange of organic and inorganic matter at the boundaries between the two systems . This is done by computing the entrapment of matter and gases when sea ice grows and release to the ocean when sea ice melts to ensure mass conservation. The model was tested in different ice-covered regions of the world ocean to test the generality of the parameterizations. The focus was particularly on the regions of landfast ice, where primary production is generally large. The implementation of the BFM in sea ice and the coupling structure in General Circulation Models will add a new component to the latters (and in general to Earth System Models), which will be able to provide adequate estimate of the role and importance of sea ice biogeochemistry in the global carbon cycle.

Abstract

Nelle ultime decadi la comunità scientifica ha impiegato molte risorse nello studio e nella comprensione della fisica del ghiaccio marino. Abbiamo attualmente un'ampia conoscienza, sebbene non ancora esaustiva, della dinamica e termodinamica dei ghiacci marini e della loro variabilità spaziale e temporale. La biogeochimica dei ghiacci è invece ancora in gran parte sconosciuta. La produzione delle alghe del ghiaccio raggiunge il 25% della produzione totale in alcune aree dell'Oceano Meridionale. Nonostante ciò, l'influenza dei fattori fisici, quali ad esempio la disponibilità di luce sulla produzione primaria sono ancora scarsamente conosciuti. Sono disponibili solo poche osservazioni localizzate in zone limitate e la funzione della biogeochimica dei ghiacci a scale più larghe è ancora poco compresa. L'utilizzo di modelli matematici diventa quindi un importante strumento ausiliario nella comprensione del ruolo qualitativo e quantitativo che la biogeochimica dei ghiacci svolge rispetto alla dinamica degli oceani. In questa tesi è stato utilizzato un approccio innovativo per modellizzare e accoppiare la biogeochimica, e in particolare la produzione primaria, alla fisica dei ghiacci. I tentativi precedenti si erano basati sull'accoppiamento di modelli fisici piuttosto complessi con modelli empirici o biogeochimici relativamente semplici. Il centro dell'attenzione è stato qui spostato verso uno di tipo maggiormente biologico. Un modello fisico relativamente semplice ma completo, della termodinamica dei ghiacci marini (ESIM) è stato sviluppato e accoppiato a una nuova implementazione nel ghiaccio (BFM-SI) del Biogeochemical Flux Model (BFM). Il BFM è un modello completo, largamente utilizzato e validato in ambiente oceanico aperto e in mari regionali. Il modello fisico è stato sviluppato avendo in mente le caratteristiche biogeochimiche del ghiaccio e gli input fisici richiesti per modellizzarne la biogeochimica. Il concetto principale per l'accoppiamento è quello di strato di ghiaccio biologicamente-attivo (Biologically-Active-Layer), ovvero quello frazione di ghiaccio il cui spessore varia nel tempo e all'interno del quale il liquido interstiziale (brines) è connesso fisicamente con l'oceano sottostante e dove è possibile la vita per numerosi microorganismi. Il modello fisico passa le informazioni-chiave del BAL (e.g, la temperatura, salinità e volume delle brines) e il BFM-SI simula la risposta fisiologica ed ecologica della comunità biologica all'ambiente fisico. BFM-SI è inoltre accoppiato al BFM pelagico attraverso lo scambio di sostanza organica e inorganica fra i due sistemi, considerando il passaggio di gas e particolato durante l'accrescimento e lo scioglimento del ghiaccio, conservando quindi la massa totale di scambio fra i due sistemi. Il modello è stato testato in differenti regioni per verificare la generalità delle parametrizzazioni. In particolare, l'attenzione è stata posta sulle regioni di landfast ice dove la produzione primaria è generalmente abbondante. L'implementazione di BFM-SI e la sua struttura di accoppiamento con Modelli di Circolazione Generale aggiungerà una nuova componente a questi ultimi (e in generale ai Modelli di Sistema Terra), che saranno in grado di poter stimare adeguatamente il ruolo e l'importanza della biogeochimica del ghiaccio nel ciclo globale del carbonio.

Contents

Overview

The topic of this thesis deals with the unique nature of sea ice and the unique biological and physical interactions occurring within the system itself and with the atmosphere and the ocean.

Chemically, sea ice is less dense than seawater and this allows sea ice to float and act as a buffer for the exchange of heat, moisture and momentum between the ocean and the atmosphere. Despite the fact of being rather thin if compared to the ocean or to the thickness of the polar ice caps, sea ice is a strong insulating medium from a physical point of view. Biologically, sea ice is a surprising habitat for many microorganisms, which actively grow and create complex ecosystems, closely related to their polar oceanic counterpart. Climatically, sea ice is a very sensitive indicator of global climate change. Because sea ice is very thin and, at the same time, is very vulnerable to small perturbations within the ocean and/or the atmosphere, any modification in its thickness and extent due to warming is strongly amplified than in non-ice-covered oceans. Finally, sea ice covers about 7% of our planet and its formation and movements are important information required for navigation purposes.

The main properties of sea ice, together with the role it plays and the description of some regional differences are reviewed in the Introduction (Chapter 1).

Chapter 2 summarizes the state-of-the-art of the modelling of sea ice thermodynamics and introduces and describes a new physical model (ESIM1), developed having in mind the biogeochemical and ecosystem properties that characterize it. The model is applied in several stations of the Baltic Sea, which was used as a central test-case for the large availability of observations to be compared with model simulations. The calibration and sensitivity of the model to some physical parameters and to the addition of new physical processes are also discussed together with the assessment of the robustness of the model to large scale atmospheric forcing.

Chapter 3 introduces the importance of considering the salt evolution in sea ice for more general sea ice models applications. First, an introduction on the previous studies on the salinity dependence of some sea ice physical parameters and a review on the most significant desalination processes are given. Then, an improvement of ESIM1 (ESIM2) is presented. ESIM2 embeds some thermodynamic improvements with respect to ESIM1, and a new halodynamic component is added in order to allow its application in non-brackish waters. Model results are compared with observations in the Gulf of Finland (Baltic Sea) and Kobbefjord (Western Greenland). Some of the outcomes of ESIM1 results are here generalized and a sensitivity analysis to desalination processes is applied.

Chapter 4 presents the new implementation of the Biogeochemical Flux Model in a sea ice system (BFM-SI) and the novel concept of the Biologically-Active-Layer (BAL), which is the main link for coupling the physics of sea ice of ESIM2 and the ecosystem properties of BFM-SI, and it also allows a direct coupling between the pelagic biogeochemistry and the sea ice biogeochemistry. After describing the sea ice habitat and the previous attempts of modelling sea ice biogeochemistry, the already-developed and comprehensive pelagic Biogeochemical Flux Model is shortly presented. Hence, the new BFM-SI is described, with special emphasis on some important biological process, such as primary production and chlorophyll synthesis. New physiological and ecological parameters are assigned to the sea ice community and a simplified version of the pelagic BFM in ice-covered oceans is described.

In Chapter 5, some numerical simulations of the biogeochemistry of ice-covered oceans are shown and analyzed. The BAL environmental variables are discussed together with the sensitivity of the model to those parameters which depend on environmental conditions. The main biological controlling factors, such as nutrient availability and grazing pressure, are also described. The new biogeochemical model allows process-studies of important ecological functions: for instance, on the composition of the sea ice and pelagic communities, on the importance of light availability, on different strategies of photoadaptation and photoacclimatation and on the fate of the sea ice biomass.

Finally, the main results and conclusions of this thesis are reported together with an outlook at the potentialities of this work for large-scale studies and applications (Chapter 6) .

Chapter 1

Introduction

All men by nature desire to know.

(Aristotle)

1.1 The growth and decay of sea ice[1]

Sea ice differs from lake ice for the fact that it embeds not only a solid fraction, but also a liquid fraction. The solid fraction of sea ice is made of pure solid ice, while the liquid fraction is made of very salty water. This liquid fraction is entrapped in the so-called brine pockets and channels. Lake ice grows differently, with the interface between liquid and solid being planar rather than lamellar as in the case with sea ice. Hence, almost all of the impurities, such as ions dissolved in lake water are expelled from the ice cover. In sea ice, instead, brine is trapped between the lamallae at the bottom of the ice, allowing for a retention of up to 40% of the ions in sea ice (Eicken, 2003). These peculiar features brought to the definition of sea ice as a mushy layer, an active porous medium made of a two phases (solid and liquid) and two components (water and salt), together with a minor fraction consisting of gas and particulate inclusions (Feltham et al., 2006). The amount of brines in sea ice depends on the ice temperature, salinity and age. While microorganisms cannot survive in the pure solid ice matrix, a plentiful biological community is able to grow in the brine pockets and channels (Fig. 1.1), which are closely connected to the oceanic ecosystem (Gosselin et al., 1997).

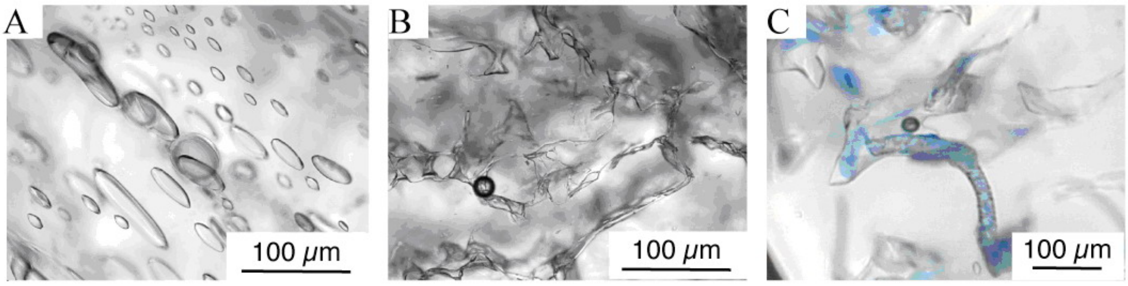

Figure 1.1: Microscopic photographs depicting brine pores of laboratory-grown, organic-free sea ice (A), ice grown in the presence of algal-derived organic materials that sculpt the brine pores (B), and the naturally sculpted habitat of sea ice off the coast of Alaska with organic material stained blue and an algal filament extending from one of the pores near the bottom of the ice (C) (From C. Krembs and J. Deming).

---

[1] Strictly speaking, sea ice should be spelled without hyphenation ("sea ice") when it is a noun and hyphenated ("sea-ice") when it is an adjective. The purpose of hyphenation is to remove ambiguity when sea ice is not thought as a single entity. However, sea ice is often an adjective. In order to simplify the reading, in this thesis "sea ice" always refer to a compound noun. If ambiguity may raise, "sea-ice" is used.

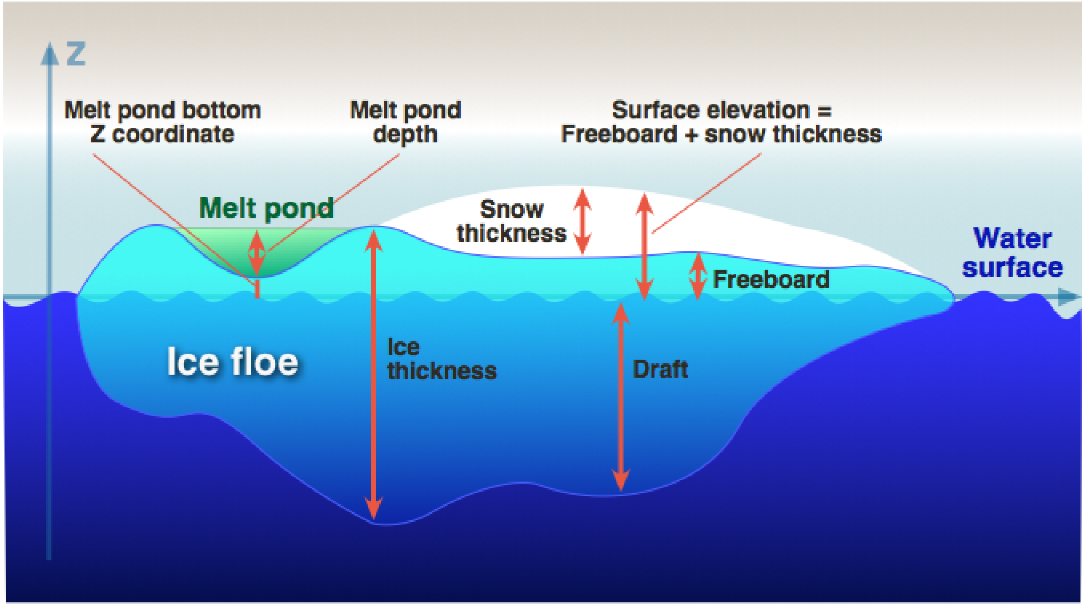

Figure 1.2: Some typical ice floe parameters (From A. Grobe and H. Grobe).

When seawater reaches its freezing temperature, which is dependent on its salinity[2], sea ice starts growing as single ice crystals of few millimeters with the shape of needles, spicules and platelets. When thermohaline mixing and wind stress are reduced, ice crystals consolidate in a slush layer of frazil ice. Once layer upon layer are added at the bottom of the ice sheet, sea ice grows vertically as congelation ice. Some typical ice floe parameters are shown in Fig. 1.2. The seasonal cycle of sea ice is not always preceded by frazil ice formation. In the Arctic ocean, surrounded by lands and with perennial ice cover, 60% to 80% of the ice cover is composed of congelation ice, while frazil ice plays an important role only in marginal seas, leads or other openings in the pack (Eicken, 2003). In the Antarctic, the formation of frazil ice is, instead, enhanced by turbulent conditions, such as higher wind speed, ocean swell penetrating from higher latitudes and large numbers of opening in the pack, resulting in 60-80% of ice thickness constituting of frazil ice in some regions (Eicken, 2003).

Sea ice growth rate is fast when sea ice is very thin and free of snow. Once it becomes thicker and a snow layer covers it, the growth rate lowers. In both cases, the growth

---

[2] In this thesis, salinity refers to Practical Salinity SP, unitless, for the variables that are measured at sea, since it is a usual oceanographic practice, while refers to absolute salinity SA, in g/kg, for model prognostic variables, as suggested by McDougall et al. (2009). Even though SI unit of absolute salinity is kg/kg, absolute salinity in g/Kg is used here since it takes numerical values close to those of Practical Salinity. One of the advantage to adopt absolute salinity in preference to Practical Salinity is its generality with respect to the the range to which SP was limited, that is $2 < SP < 42$, while sea ice bulk sanity and brine salinity may often be well below and above those thresholds.

rate is approximately linear, depending mainly on the local temperature gradient, which is stronger in snow for its higher thermal conductivity. Hence, the colder the air, the thicker the ice due to greater temperature gradients. Once the oceanic heat flux into the ice-water interface exceeds the conductive heat flux out of the interface, ice starts melting at the bottom. The thermodynamic growth of sea ice will be described more in details in Chapter 2.

It is important to point out here that the melting process is usually faster - sometimes all seasonal ice melts away in few days - than the growing process, which is typically lasting several weeks. These rapid changes affect many physical and biological process, such as the salt entrapment and release and, consequently, also nutrients content.

One of the most evident feature of sea ice is the physical barrier that it creates between the ocean and the atmosphere. However, sea ice does not prevent the atmosphere to be physically, chemically and biologically connected to the ocean, but simply it reduces the response to changes at the interface. Basically, it acts as a filter for the exchange of momentum, heat and gases between the two mediums. The influence of sea ice on the ocean is manifold, covering a wide range of processes and spatial and temporal scales. In both hemispheres, shelf waters initiate the formation of sea ice. In the Arctic, surface waters are strongly diluted by large river run off. In the Southern Ocean, brines rejection, that is the rejection of salt from forming sea ice, causes deep convection. The deep and bottom waters produced by the polar oceans are an important part of the global thermohaline circulation. Sea ice and its snow cover also prevent the ocean from heating the lower atmosphere. The high surface albedo and the reduced short-wave radiation in the darker season also support a cooler atmosphere, only mitigated by clouds cover.

Sea ice conditions are also very much driven by atmospheric and ocean dynamics. Under the action of winds and currents, sea ice is drifting and transporting latent heat and freshwater far away from its place of origin. During a divergent situation of the drift, an open water is generated (Fig 1.3, right) and in the convergent situation, pack ice is compressing and forming thick ridged ice (Fig 1.3, left). As a results of the thermodynamical and dynamical processes, pack ice is a mixture of the different ice types and thicknesses which can be described by the probability density function of the sea ice thickness distribution (Thorndike et al., 1975). Hence, the ultimate variable to assess is the ice volume, which is the mathematical product of the ice thickness and areal ice coverage. While ice coverage estimates are well-supported by satellite monitoring, ice thickness remains largely unknown.

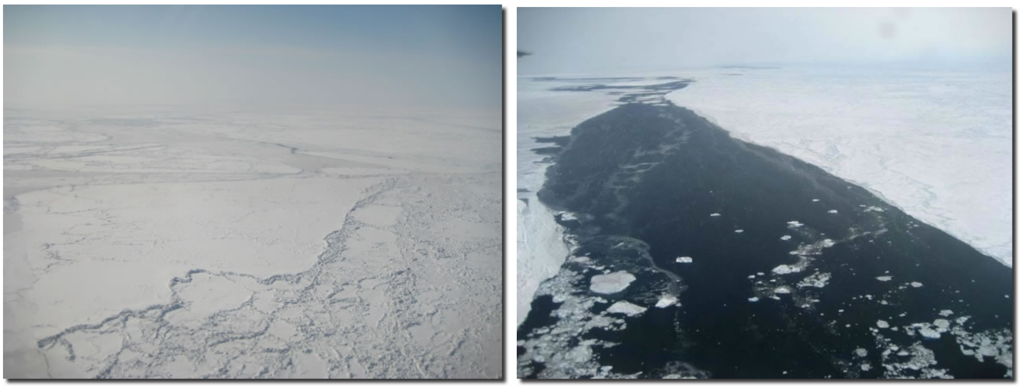

Figure 1.3: Ice dynamics: Arctic pressure ridges (left) and leads (right) (Helicopter photos from National Oceanic and Atmospheric Administration of USA, NOAA).

Considering both its thermodynamics, which is basically a vertical process, and its dynamics, which is basically a horizontal process, sea ice is a very complex 3-dimensional medium. Its small scale structure properties can effectively modify many large scale process in the world's climate system, as it will described more in detail in Sect. 1.5.

1.2 Spatial and temporal variation of sea ice

Sea ice covers annually up to more than 5% of the oceans of the northern hemisphere and about up to 8% of the oceans of the southern hemisphere. It globally attains up to 70% of the ice-covered areas on Earth, even if it accounts for only 1% of the total ice volume (Maykut, 1985). This is due to the fact that sea ice is rather thin if compared to the very thick continental ice caps which cover Antarctica and Greenland. However, the thinner the ice is, the more sensitive is its response to climate fluctuations.

In the northern hemisphere, winter sea ice is found as far south as the coast of Labrador, Cook Inlet in Alaska, in the Sea of Okhotsk, in the Bohai Sea and in the Baltic Sea (Fig. 1.4). Boreal summer coverage is confined mainly to the central Arctic Ocean, the Greenland Sea and Canada's Arctic archipelago. Sea ice reaches its maximum extent of about 15.5 x 10^6 km^2 in March and its minimum extent of about 4.2 x 10^6 km^2 in September (Fig. 1.5) (Comiso et al., 2008; Maslanik et al., 2008).

In the southern hemisphere, sea ice cover surrounds the Antarctic continent with the highest latitude being 80°N. During winter it is expanding as a continuous ring around the continent and spreads largely in the Atlantic, Pacific and Indian Ocean, reaching its maximum of about 19 x 10^6 km^2 in September (Fig. 1.5). Antarctic sea ice reaches its

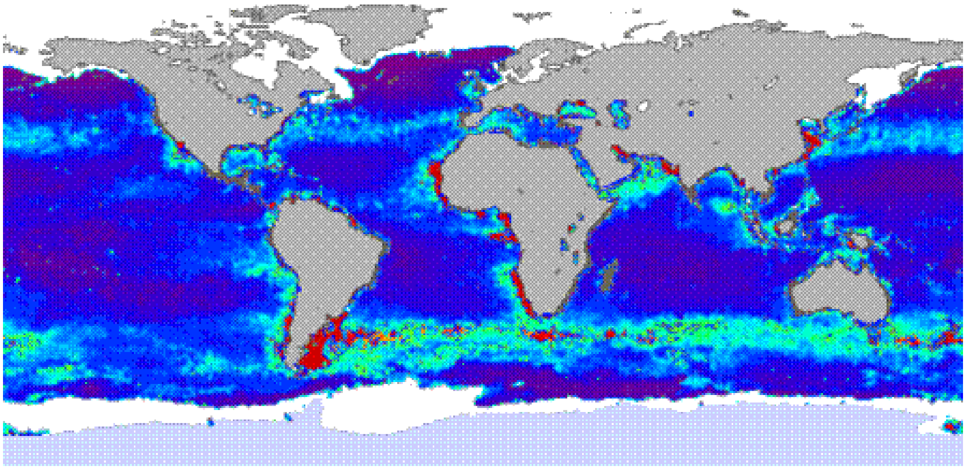

Figure 1.4: Sea ice cover in the boreal winter season (Satellite image from SeaWifs, http://www.oceancolor.nasa.gov).

minimum of about 3.8 x 10^6 km^2 in February, when its cover is fragmented and limited to the Weddell Sea, Bellinghausen Sea, Amundsen Sea and only partly in the Ross Sea and in the Indian Ocean (Fig. 1.5) (Comiso, 2003).

Due to geographical constrains, the perennial ice regions are thus much more extended in the northern hemisphere, while the seasonal sea ice is more extended in the southern hemisphere. In the northern hemisphere the growth and decay periods last approximately the same length, while the southern hemisphere is characterized by a longer growth period, approximately 7 months, and consequently, a shorter decay period, typically 5 months. This fact is again due to different environmental and geographical conditions. The Antarctic sea ice is directly affected by intrusion of warm waters from lower latitudes and large ocean waves directly breaks sea ice up. On the other hand, the lands surrounding the Arctic cool faster than the ocean and can partly accelerate the ice growth rate.

Because of important positive feedbacks, such as the ice and snow albedo feedbacks - which will be discussed more in details in Sect. 1.5 - global climate change are expected to be amplified in the polar regions (Räisänen, 2002; Holland and Bitz, 2003). Sea ice extent has been measured since 1979 from passive microwave instruments on board of NOAA (National Oceanic and Atmospheric Administration of USA) satellites. A linear

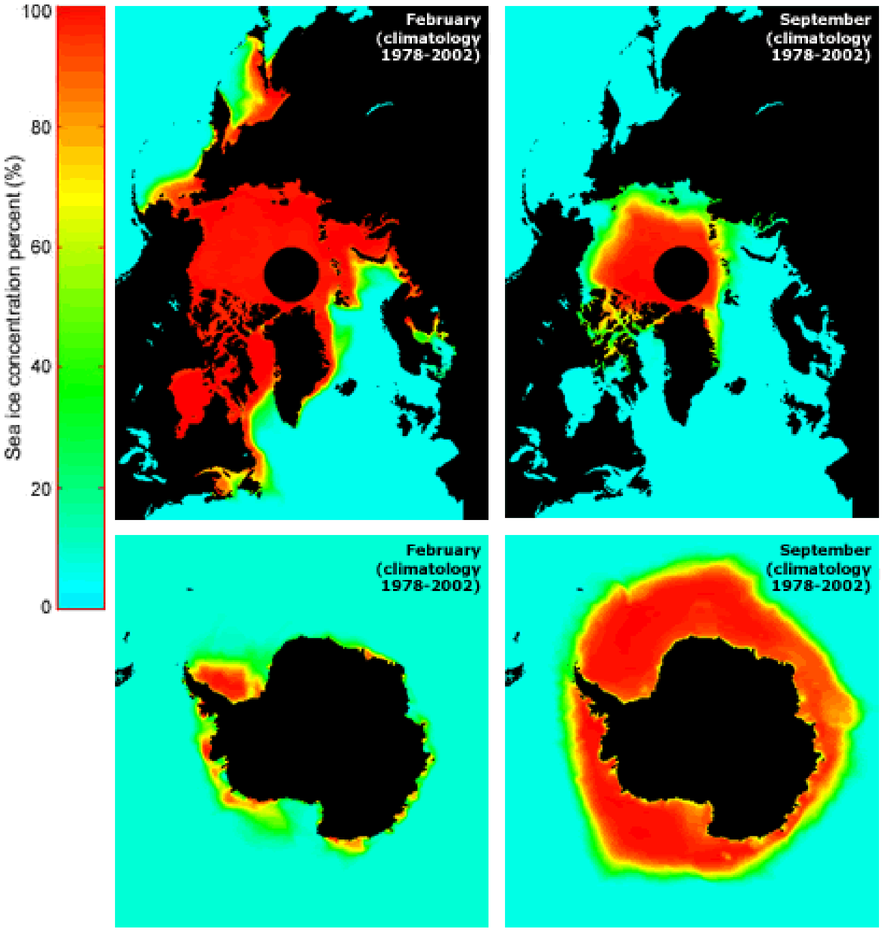

Figure 1.5: Average (1978–2002) sea ice extent in February (left) and September (right) in the northern (above) and southern (below) hemispheres based on monthly climatology (From National Snow and Ice Data Center, NSIDC).

regression analysis for mean sea ice extent in both hemisphere for March and September during 1979–2008 is shown in Fig. 1.6 and Fig.1.7.

The trend is negative in the northern hemisphere for both periods, more consistently for the minimum sea ice extent. While temperatures in the northern hemisphere have risen at a rate of approximately 0.37°C per decade over the same period (source: NOAA), for March sea ice extent has decreased at a rate of 2.8% per decade, while at a rate of 11.1% per decade in September. If the timeseries would have be limited to the period 1979–2000, the trend would be less negative: -0.8% per decade in winter and -4.1% per decade in summer. This is a remarkable point to consider when making considerations on a general trend, which is characterized by the addition or subtraction of very different values at the beginning or at the end of the studied time series. A more detailed analysis (Comiso, 2003, not shown here) reports that regionally, the negative trend is basically controlled by peripheral seas; however, the most rapid decline is happening for the perennial Arctic

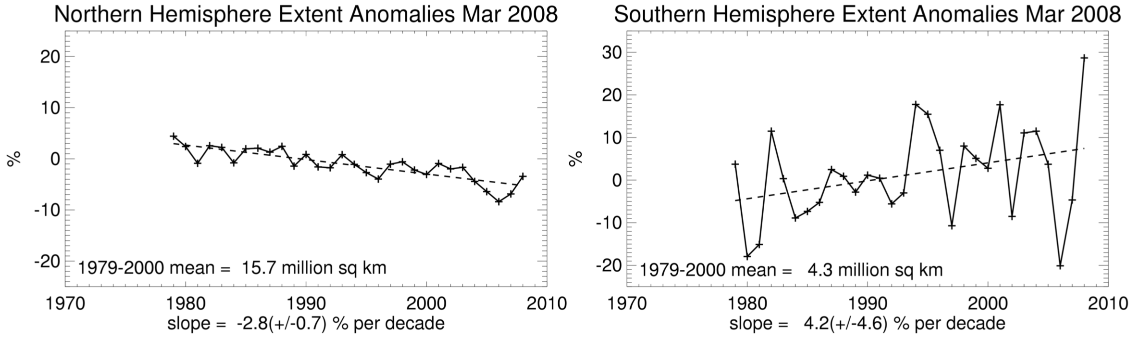

Figure 1.6: March's northern (left) and southern (right) hemispheres sea ice extent in 1979–2008. The anomalies are computed with respect to the 1979–2000 mean (From NSIDC).

sea ice, which consists mainly of multi-year ice cover that basically controls the thickness distribution and limits the retreat during summer.

In the southern hemisphere, there are no such significant variations. However, a general positive trend is found, especially for the austral winter (Fig. 1.6). In fact, sea ice extent for March has increased at a rate of 4.2% per decade. Besides, the March 2008 sea ice extent was much above the 1979–2000 mean and it was the largest sea ice extent in March (28.6% above the 1979–2000 mean) over the 30-year historical period, surpassing the previous record set in 1994 by 10.9%. Sea ice minimum, instead, has slowly increased at a rate of 0.6% per decade. There are several fluctuations from year to year, which can partly be explained by the Antarctic Circumpolar Current waters that propagate clockwise around the continent (Comiso, 2003). Regionally, a strong positive trend (7% per decade) is detected in the Ross Sea, while a strong negative trend (-8.1% per decade) is

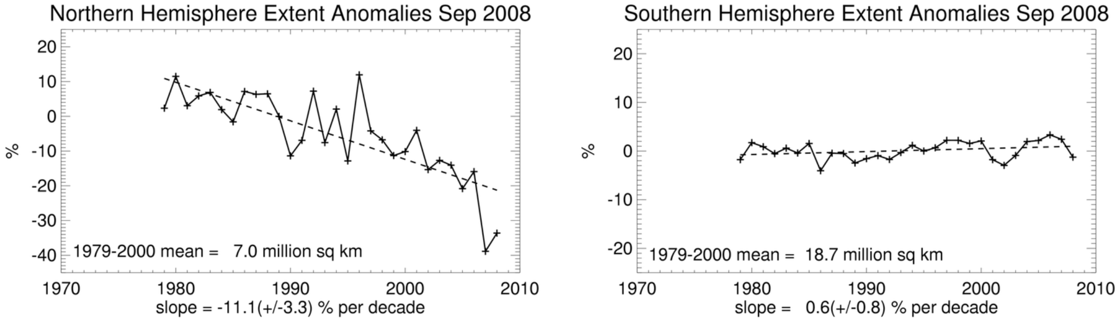

Figure 1.7: September's northern (left) and southern(right) hemispheres sea ice extent in 1979–2008.The anomalies are computed with respect to the 1979–2000 mean (From NSIDC).

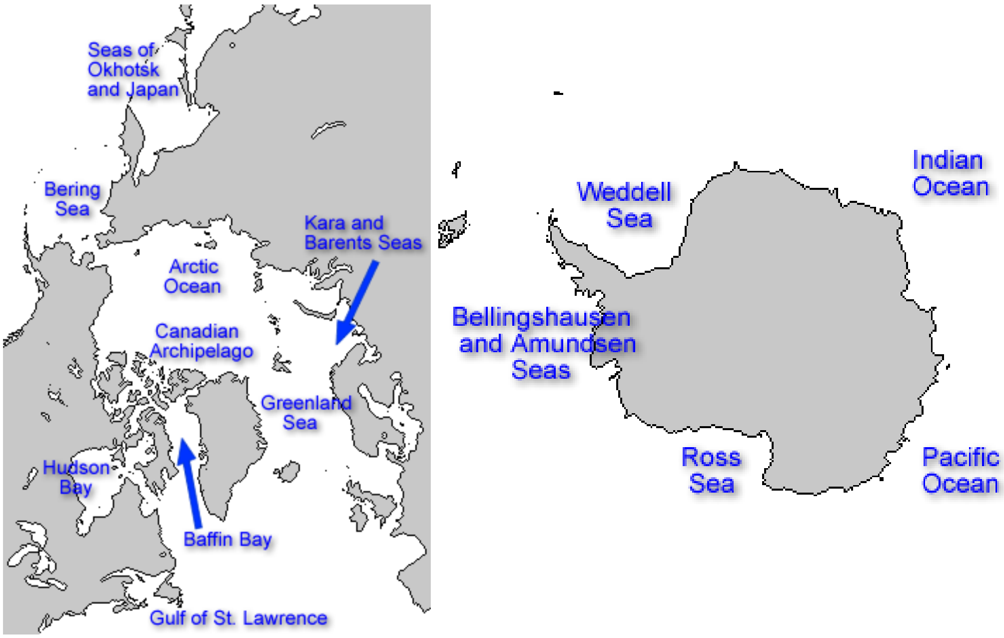

Figure 1.8: Map of the Northern and Southern hemispheres (From NSIDC).

instead found in the Bellinghausen/Amundsen Seas. Since those sectors are adjacent to each other, the opposite trend can also be explained by advection of ice (Comiso, 2003). Other sectors, such as the Weddell Sea, Indian Ocean and Western pacific Ocean do no show any significant trend. Generally, Antarctic onset of sea ice is currently occurring earlier and breaking up slightly later (Comiso, 2003).

1.3 Arctic versus Antarctic sea ice

The most evident difference between the Arctic and the Antarctic is physiographic. The Arctic is a closed basin surrounded by land with only one deep passage through which the water can be exchanged with the rest of the other oceans, while the Antarctic Ocean is circumpolar and connected to the Indian, Pacific and Atlantic oceans (Fig. 1.8). This fact affects the dynamics and thermodynamics of sea ice and brings to a different seasonal cycle: Antarctic annual sea ice has a much higher amplitude and variability than the Arctic (Dieckmann and Hellmer, 2003).

Dynamically, the extent of the Arctic sea ice, being limited by the surrounding lands, results in sea ice having a much longer residence time, ranging between 5 and 7 years, being mostly multi-year ice with an average thickness of about 3 m, and receiving a smaller precipitation input. Typical winds are convergent, that is ice movements are mostly opposite to the natural southwards ice growth, bringing ice floes to crash and form ridges, increasing ice thickness and enhancing multi-year ice formation. The Antarctic sea ice, being surrounded by oceans, has instead a potentially infinite extension northwards, typically from 75°S to 55°S. It is characterized by mostly first-year ice with an average thickness of 0.5 m (Wadhams, 2000), has a shorter residence time - usually 1–2 years - and receives a larger amount of precipitation. Typical winds are divergent, leading to the generation of open water and enhancing more sea ice growth (Kottmeier et al., 1992).

Thermodynamically, sea ice growth and melting depend on the conductive heat fluxes at the boundaries and within sea ice. The most notable difference between the two polar regions consists in different oceanic heat fluxes. The average heat flux in the Arctic is estimated to be about 2 W m^{-2} (Wadhams, 2000), whereas the average annual flux in the Southern Ocean may be up to 30 W m^{-2} (Lytle et al., 2000). Arctic sea ice is subjected to considerable terrestrial input due to river run-off. The large amount of riverine input lowers sea ice and seawater salinities and stabilizes the water column underneath sea ice, limiting the oceanic heat flux. The terrestrial input to Antarctic sea ice is, instead, considered insignificant, thus resulting in a well-mixed water column and larger amount of heat received by sea ice at the bottom of the ice floes.

Another important difference between the two polar regions lies in the fact that the large eolian, riverine and terrestrial inputs received by Arctic sea ice result in considerable pollution (Leventer, 2003; Thomas and Papadimitriou, 2003), while Antarctic sea ice can still be considered pristine.

Sea ice algal biomass accumulation is extremely variable, depending upon location, environmental conditions as well as biological factors. Several studies based on *in situ* measurements (see Arrigo, 2003, for a review) suggest that Antarctic sea ice support higher algal biomass (mean 133 mg chl-*a* m^{-2}) than Arctic ice (spring-summer mean of 87.5 mg chl-a^{-2}). The highest algal biomass ever reported is 300 mg chl-*a* m^{-2} in the congelation ice of Resolute Passage during springtime for Arctic sea ice (Welch and Bergmann, 1989) and more than 1000 mg chl-*a* m^{-2} in two different studies on platelet ice of McMurdo Sound (Arrigo et al., 1993; Bunt and Lee, 1970). However, it should be noted that the higher level of accumulation in the Antarctic is due entirely to the contribution of additional biomass by platelet ice; removing it from the above analysis reduce the mean accumulated algal biomass to 88.1 mg chl-*a* m^{-2}, which is within 1 % of the estimate of the Arctic (Arrigo, 2003). In Antarctica, algal colonization in sea ice is vertically more extensive than in the Arctic (Ackley and Sullivan, 1994). Ice algae are common at the snow-ice interface, within the congelation ice (typically, the lower 20 cm) and in the platelet layer. In Arctic first-year ice, 95% of the biomass is typically found in the bottom

2 cm of the ice (Perovich, 1993), consisting of the so called skeletal layer. More than 100 species of diatoms have been found in sea ice, the most important being *Fragilariopsis curta* and *Fragilariopsis cylindrus*, which are bipolar (Dieckmann and Hellmer, 2003).

Sea ice algae are also an important energy and nutritional source for invertebrates such as juvenile krill, especially in the Antarctic (Arrigo and Thomas, 2004). In the Arctic, instead, krill species occur but do not reach the biomass reported in Antarctic waters and the most dominant crustaceans are amphipods, which are on the other hand not frequently found in Antarctic sea ice (Dieckmann and Hellmer, 2003).

The most important fish species in the Arctic is the arctic cod (*Boreogadus saida*), while in Antarctica is the broadhead fish (*Pagothenia borchgrevinki*). They occupy similar niches, often living among ice-crystals, and have developed almost the same antifreeze proteins in response to similar environmental conditions (Dieckmann and Hellmer, 2003).

1.4 Baltic sea ice

The Baltic Sea will be largely used in this thesis as a test-bed for comparing model simulations with observations. The Baltic Sea is a semi-enclosed basin surrounded by several countries , sea ice covers annually about 40 % of it and ice seasons have been studied for a long time for navigation purposes (see Vihma and Haapala, 2009, for a review on Baltic sea ice). Consequently, there is a large availability of information on coastal sea ice and snow thicknesses, which are important requirements for model validations. Moreover, Granskog et al. (2006a) suggested that the low-salinity Baltic Sea, and the processes associate with it could potentially be used as a model for Arctic sea ice (or region of the Arctic such as the White Sea) in a climate change induced warming, especially where high river discharge reduces coastal salinities to a significant degree.

There are many differences and similarities between the Baltic Sea and other polar seas and oceans (e.g. Leppäranta and Myrberg, 2009). The Baltic Sea has a mean depth of about 55 m and features brackish waters (salinity < 24); it receives heavy discharge river inputs and only intermittent inflow of saline water from the Danish Strait (Stigebrandt, 2001). The mean surface salinity varies from 9 to less than 1, while sea ice bulk salinity is generally less than 2. The variation in salinity both in seawater and in sea ice are thus rather insignificant and brine volume is proportionally reduced, despite the quite high temperatures. Hence, many physical parameters, which are typically dependent on salinity, may be considered constant in the Baltic sea ice, following the assumption of

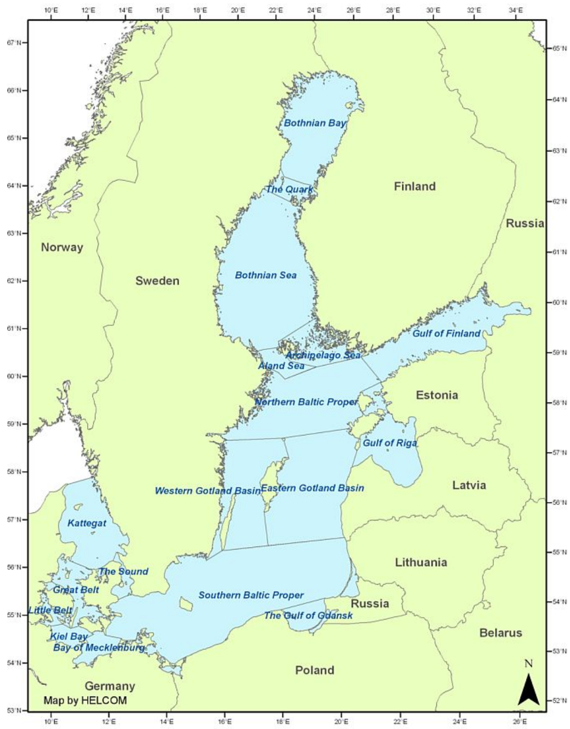

Figure 1.9: Map of the sub-basins of the Baltic Sea (Font: HELCOM).

constant salinity. According to the law of fives (Golden et al., 1998), at a temperature of -5 °C and salinity of 5 sea ice has a brine volume of 5%, which is the threshold for brines to be interconnected. Obviously, the law of fives does not hold true in the Baltic Sea, which very seldom reaches bulk salinity greater than 5. Leppäranta and Manninen (1983) studied the brine content of sea ice with particular attention to low bulk salinities and according to them, sea ice with a bulk salinity of 1 needs a temperature as high as -1°C for Baltic sea ice to become permeable.

Ice formation begins in October at the earliest in the northern Bothnian Bay. First, ice starts forming along the coast and ice edges move outward progressively. Land-fast sea ice usually extends until the water depth is between 5 and 15 m, while further offshore sea ice is highly dynamic (Leppäranta, 1981). Sea ice starts melting in the southern regions and by early June it completely disappears. A Baltic ice season typically lasts from 20–30 days in the Baltic proper to more than 6 months in the northern Bay of Bothnia (Granskog et al., 2006a). In a warming scenario, if winter air temperature would increase of about 4° C, while Omstedt and Hansson (2006) reported that Baltic Sea may become completely ice-free , other studies, based on more advanced models, do predict large changes in the ice conditions, but not totally ice free conditions (Haapala et al., 2001; BAAC, 2008).

Baltic sea ice is typically divided in two layers: a granular upper layer made of frazil ice, snow ice and superimposed ice and a lower layer made of columnar ice (Granskog et al., 2003b). In the Gulf of Finland, Granskog et al. (2004) found that snow contributed up to 35 % of the sea ice mass, while superimposed ice up to 22 %. Besides, Baltic Sea ice is relatively thin and even small snow loads may cause flooding, supporting snow ice formation. In fact, the Baltic Sea ice is usually characterized by rather complex melt-freeze cycles and a high proportion of meteoric ice resulting from the formation of snow ice and superimposed ice (e.g., Granskog et al., 2004), which leads to the necessity of considering snow metamorphism to assess the total ice/snow mass balance.

Even though brine volumes in the Baltic Sea are rather small compared to those found in polar sea ice, high-diversity of sea ice associated microbes also occur in its interior habitats (e.g., Meiners et al., 2002). Pennate diatoms are, in terms of biomass, the dominant algae in several sub-basins (e.g., Ikävalko, 1998). Other important algal groups are small autotrophic flagellates and dinoflagellates (e.g., Ikävalko, 1998). The main heterotrophic organisms are flagellates and ciliates of various sizes and heterotrophic bacteria (Kaartokallio, 2004). Ciliates, in particular, have a important role, being either grazers, mixotrophs and autotrophs. Under-ice blooms have been studied limited to the Gulf of Finland, where the dominant group was found to be dinoflagellates (Larsen et al., 1995). Since the small brine volume excludes larger grazers, it is obvious that the main group of grazers reported in Baltic sea ice is made of small rotifers and copepods, whose importance increases during the late and post algal bloom (e.g., Kaartokallio, 2004). Typical values for chl-a range between 0.2 and 5.5 mg m^{-2} (e.g., Granskog et al., 2003a; Kuosa and Kaartokallio, 2006). Even though small brine volumes simplifies the ecosystem lowering the diversity of ecological relationships (Granskog et al., 2006a), quantification of sea ice food webs are still limited (Lizotte, 2003). Trophic shortcuts such as herbivory by ciliates and flagellates, ciliates bacterivory and direct utilization of Dissolved Organic Matter (DOM) by flagellates are typical. Of these, only direct utilization of DOM and ciliate grazing are suggested to be functional in the Baltic Sea ice (e.g., Kaartokallio, 2004). Contrary to other polar seas (Thomas and Papadimitriou, 2003), concentrations of Dissolved Organic Carbon (DOC) in Baltic sea ice are generally lower than in underlying waters, due to the high concentrations of terrestrial-derived DOC (Hägstrom et al., 2001). Based on observations by Kaartokallio et al. (2006), ice bacteria may be dependent on autochtonous DOM produced in sea ice. The main source of nutrients in sea ice is the initial entrapment when ice forms and later movements along with brines porosity, as it will be further discussed (Sect. 4.8 and Sect. 5.3.1). Recycling of nutrients from allochtonous and autochtonous biomass in the ice through decomposition and nutrient regeneration by ice heterotrophs is also an important source (Cota et al., 1991). Sea ice seems to be sequentially light- and nutrient-limited along with the winter progression, being phosphorous probably the most important limiting nutrient for algal growth (e.g., Kuosa and Kaartokallio, 2006). An important source of nutrients in the Baltic comes from snow deposition, which accounts for 5% of the total annual flux of nitrogen and phosphorous and up to 40 % of cadmium and lead (Granskog and Kaartokallio, 2004). Atmospheric nutrients are incorporated in the ice sheet via snow ice and superimposed ice formation and later trough melting become a major source for surface waters of the Baltic Sea (Granskog and Kaartokallio, 2004).

1.5 Sea ice in the climate system

Though sea ice is only a very thin layer between the ocean and the atmosphere, it plays an important role in the Earth's climate system. The high albedo and its positive feedback, the strong insulating effect, the physical barrier that it creates between the atmosphere and the ocean and its impact on the large-scale thermohaline structure of water masses make sea ice an active component of the climate system. It is thus likely that sea ice acts as a very sensitive indicator of global climate change (Eicken, 2003) and has become one of the most components in the study of the past, present and future climate.

One of the most pressing issues is whether the observed changes in sea ice cover, especially in the Arctic, are part of some natural cycle or represent a climatic regime shift in which the feedbacks associated with the presence of sea ice play an important role. There are still fundamental problems in the study of sea ice at a larger scale. Ice thickness remains often a largely unknown parameter, supported only by sparse observations. New remote sensing technology, which is able to monitor sea ice cover, can nowadays support validation of sea ice dynamical models. Even though plastic rheology of sea ice captures all the main features of the ice dynamics (Hibler, 1979) and it has been successfully used in numerical investigations of climate, only few global climate models use the same approach and many AOGCM's use simplified sea ice dynamics models.

Finally, the retreat of an ice edge is the result of an equilibrium between ice drift, air temperature and ocean heat flux, the latter being a function of the velocity and heat contents of ocean currents, whose origin is usually in non-polar regions. Thus, the retreat of an ice edge is not necessarily the consequence of a decrease in ice volume, but it may be linked to the complexities of interactions among atmosphere, ice and oceans.

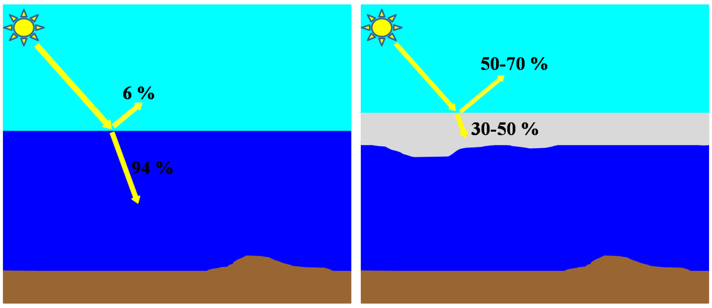

Figure 1.10: General scheme of seawater and sea ice typical albedo values.

1.5.1 The albedo feedback

Sea ice albedo is up to 11.7-folds higher than seawater albedo (Fig. 1.10). A perturbation in the surface energy balance resulting in a decrease in ice extent due to warming may propagate and amplify since the reduction in ice extent increases the amount of solar energy absorbed by the system: this is the so-called “ice-albedo feedback” (Curry et al., 1995).

A global warming scenario, which may prelude a reduction in sea ice cover and thickness, has thus positive albedo feedbacks in ice-covered regions. Once more open water, previously ice-covered, is exposed to sunlight, the ocean gets warmer, and ocean albedo is very small (0.06, Perovich, 1996) comparing to sea ice and snow albedos. Consequently, the ocean increases its heat content and its potential to laterally melt an ice edge (Fig. 1.11). In a similar way, a thinner sea ice cover brings to a higher fractions of short-wave radiation penetrating sea ice and reaching the underneath seawater, thus increasing its heat content. This last process is not directly related to albedo but, more in general, to the amount of short-wave radiation reaching the surface.

1.5.2 The influence on water mass

During ice growth, the salt that is dissolved in seawater cannot be incorporated into the forming ice crystals and is expelled into the liquid solution between the crystals. The more crystals forms, the more brine salinity increases. At the same time, some of the saline liquid is not trapped in brines, but is released to the underneath water, increasing the salinity. The initial distribution of salt between the ice and the water depends on an effective segregation coefficient (Weeks and Ackley, 1986), which is proportional to the ice growth rate, and it will be mathematically described in Sect. 3.2. The slower the growth, the more liquid fraction is trapped between ice crystals, and less saline water is

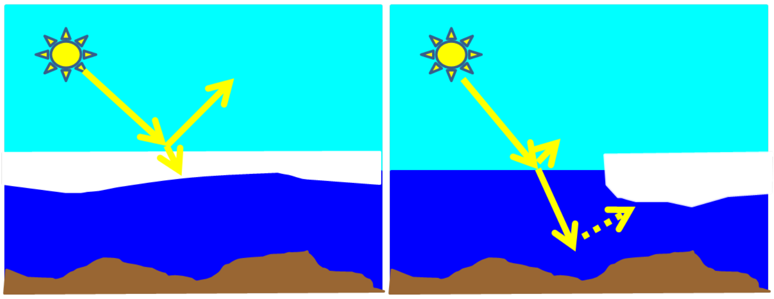

Figure 1.11: Ice-albedo feedback mechanism in a scenario of sea ice retreating.

released to the ocean. In the more salty waters of the Southern Ocean, when seawater salinity exceeds 34.46, these waters have the potential to initiate deep and bottom water formation during mixing with open ocean components (Gill, 1973). The deep and bottom waters produced by the polar oceans have not only local effects in modifying the ocean properties and water mass structure, but are also connected to the rest of the world's oceans, forming and affecting part of the global thermohaline circulation.

In the Arctic, surface waters are strongly diluted by large river run off, buffering most of the salt input during autumn. During the spring, instead, snow and sea ice melt, producing zero- or low-salinity melt water both at the surface and at the bottom of the ice. The obvious consequence is the formation of a well-stratified layer, which plays an important role from physical and biological points of view. Convection is thus restricted to the upper 50-100 m and deeper layers are renewed only by advection of water masses of Atlantic origin entering trough the Fram Strait and across the Barents Sea. The stabilization of the water column also favors the algal bloom event until nutrients are exhausted, thus becoming a limiting factor for phytoplankton growth.

1.5.3 The role of snow

Snow has a key-role in the heat budget of ice-covered oceans. Comparing to bare sea ice, snow albedos are consistently higher (up to 0.87, Perovich, 1996), thus enhancing the amount of short-wave radiation reflected back to the atmosphere (Fig. 1.12). Snow is also characterized by a higher extinction coefficient (up to 27 m^{-1}), affecting the amount of short-wave radiation that penetrates to the bottom sea ice and the underlying water. Finally, snow thermal conductivity is also much lower (0.056 for new fresh snow) than sea ice and its insulating properties can impede ice growth by reducing the conductive heat flux.

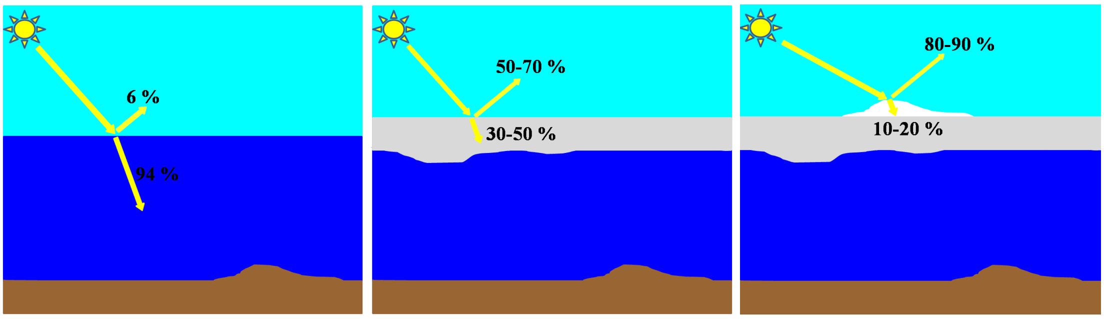

Figure 1.12: Comparison among seawater (left), sea ice (center) and snow (right) typical albedo values.

Snow may also transform, changing its properties, to snow ice and superimposed ice (see Sect. 2.2 for a mathematical description). When heavy snow loads depress the ice surface below the sea surface (such as the ones typical of the northern Baltic Sea and of large areas of the Southern Ocean) seawater and brine may percolate vertically and laterally through the ice cover. As the flooded snow refreezes, a new layer made of snow mixed to seawater forms. Hence, the conductive heat flux increases, allowing more ice to grow. Numerous studies in the Southern Ocean have established that snow ice accounts for up to 50% of the total ice thickness, with the actual meteoric fraction - that is the total contribution of precipitation - generally less than 20%.

When snow starts melting, it may eventually re-freeze in contact with a cold ice layer and starts forming superimposed ice. This physical processes is relevant in the Baltic Sea, which is characterized by complex melt-freeze cycles (e.g. Granskog et al., 2003b) and in the lowest Arctic (e.g. Svalbard area, Nicolaus et al., 2003). Snow ice usually plays a more important role than superimposed ice in the total ice mass balance. However, in a climate change scenario of thinning of the ice and increasing of precipitation (e.g. Alexander et al., 2004), snow ice and superimposed ice may both become even more common and important. Besides, from an ecological point of view, snow ice and superimposed ice may create suitable habitats for sea ice algae, bringing nutrients - by flooding events and melt-refreeze cycles - where the light is more available, and allowing the formation of surface and infiltration communities. Although snow cover has the negative effect of reducing the amount of light available for algal growth, it is also responsible for providing nutrients to the surface community, which are very productive in Antarctic sea ice (Legendre et al., 1992).

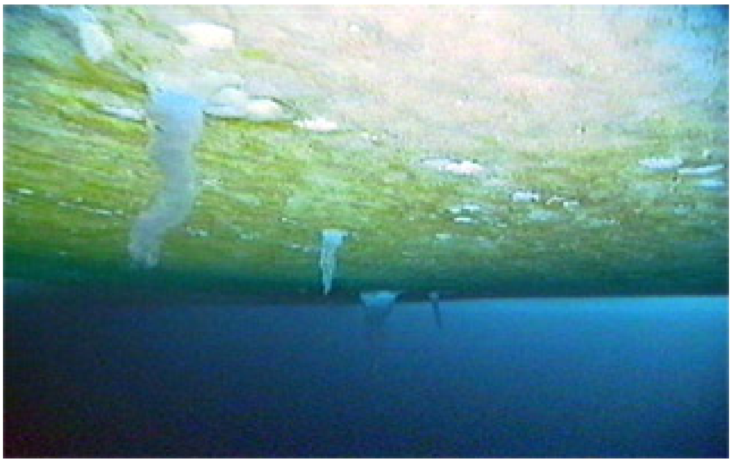

Figure 1.13: Ice algae communities living on the under-surface of sea ice (Photo from D. Allen).

1.5.4 The role of sea ice in the carbon cycle

Sea ice is a rich habitat for microbial community. The most abundant species found are unicellular microalgae, mostly diatoms. When sea ice forms, many organisms are passively or actively entrapped in the salty brines. Their rate of survival in the new habitat depends on their adaptation and/or acclimation to the new environmental conditions (low temperature, high salinity and low light intensities) and on the external supply of nutrients and gases from seawater. Some organisms may die in isolated brines, some may survive or encyst, some may find a favorable habitat and actively grow. Primary producers, such as some diatoms and small flagellates, are very adapted to the sea ice environment and may be limited only by the lack of a sufficient amount of light to allow photosynthesis. The grazing pressure is in fact very low, depending on the size of the predators which are able to penetrate the larger brines. Besides, sea ice is a stable environment where the vertical sinking is prevented and many organism have developed several strategies to anchor to the ice matrix (Thomas and Papadimitriou, 2003). Once the snow cover has melted, light is usually not a limiting factor anymore and an algae bloom usually occurs in and underneath sea ice (Lavoie et al., 2005). Concentrations up to 1000 mg $m^{-3}$of diatom chlorophyll have been found in Antarctic sea ice (Thomas and Dieckmann, 2002).

The sea ice biogeochemical cycle is strongly related to its oceanic counterpart. This is of extreme biological importance at the end of the ice season, when sea ice starts melting and a sea ice algae bloom occurs. The fate of this biomass depends on the rate of melting and on the vertical stability of the water column. If the stratification is high and the rate of

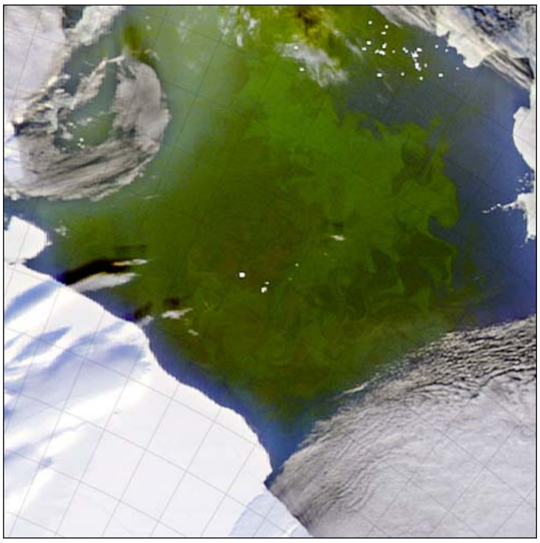

Figure 1.14: Typical Ross Sea phytoplankton bloom in February (Satellite image from NASA Earth Observatory).

melting is low, sea ice algae may stay long time in the upper part of the water column and may seed a pelagic phytoplankton bloom. Polar blooms represent a relevant fraction of the carbon production in some regions of the world, such as the Ross Sea (see Fig. 1.14) and the Weddell Sea in Antarctica, and the Barents Sea in the Arctic (see Fig. 1.15). If the rate of melting is high and the stratification is low, the sea ice biomass may rapidly sink to the bottom of the ocean and likely become a sink for the atmospheric CO_2. In both cases, the size and weight of the organisms affect the sinking velocity, together with the grazing rate by zooplankton.

Most Arctic and Antarctic marine species depend upon the presence of sea ice (Ainley et al., 2003). The polar marine food chain begins with ice algae that cling within and to the underside of the dark ice pack all winter and creates a dense mat within and under the ice with the end of the long darkness in spring. Once sea ice has almost completely melted away, a phytoplankton bloom develops in the water beneath the ice, spreading for dozen of kilometers, surrounding the ice edge. This highly productive ice-edge ecosystem is home to numerous crustaceans and other invertebrates. These in turn are eaten by fish species. Organic material released from the ice algae mat and the phytoplankton bloom enriches the sea floor, also supporting a benthic (sea bottom) community of shellfish and other invertebrates. Unique among the world's ecosystems, the ice-edge zone moves thousands

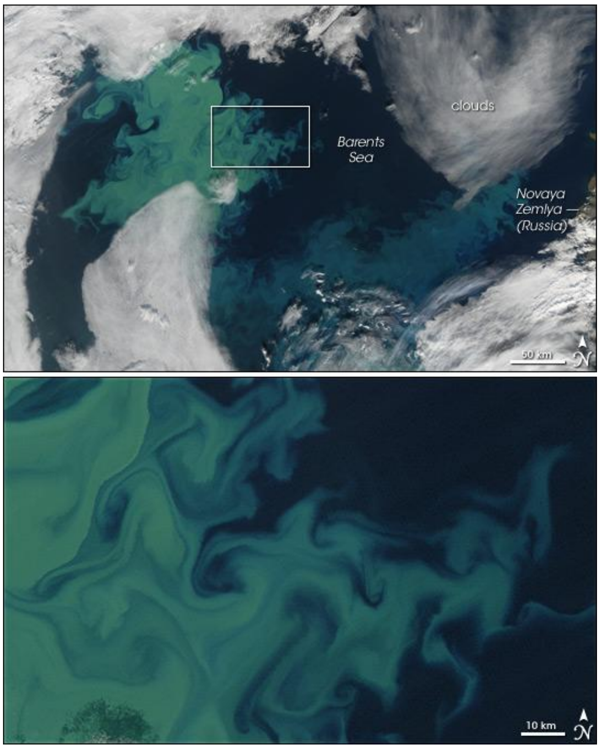

Figure 1.15: Phytoplankton bloom in the Barents Sea during August 2006 (Satellite image from NASA Earth Observatory).

of kilometers each year, north in spring and south in fall in the northern hemisphere and viceversa in the southern hemisphere. Walrus, penguins, numerous species of seals and cetaceans follow the ice-edge, taking advantage of the ready access to food, mating and raising pups. Seals are also in turn preyed on by polar bears in the Arctic.

In a global warming scenario, the almost complete elimination of multi-year ice in the Arctic Ocean and the thinning or disappearing of seasonal sea ice in both hemispheres are likely to be immensely disruptive to all the ice-dependent microorganisms, which will lack a permanent habitat. And consequently, all the polar food chains may be disrupted.

1.6 Summary

In this first chapter, the main properties of sea ice have been reviewed.

From the smallest scale, sea ice is a complex medium made of two phases (liquid and solid) and two components (water and salt). Its particular nature allows sea ice to be lighter than seawater and to float over the oceans, becoming a physical semi-permeable barrier between the ocean and the atmosphere. Its influence on the ocean results in relevant modifications of the salinity of the water masses both in the Arctic and in the Antarctic. Sea ice prevent the ocean heat to reach the atmosphere, which is thus cooler and thinner in polar regions than in warmer latitudes. This fact brings to a small requirement of energy input per degree for the temperature to increase.

Its thermal properties largely differ from those of seawater, turning sea ice in a strong insulating medium. Sea ice grows vertically as a result of the thermodynamic equilibrium between the ocean and the atmosphere and it moves laterally under the influence of solar heating, ocean currents, wind stress and tidal forcing. Sea ice total volume is the key information that scientists need for studies of past, present and future climate; this however is a difficult state variable to monitor and model at large scales.

Sea ice is also a rich habitat for many microorganisms. Its productivity is closely related to that of polar waters. Many species, from small to top predators are ice-dependent for their life, as a habitat, source of food or place for mating.

Despite the numerous efforts, the increasing available information and the attempts of modelling, sea ice still remains a largely unexplored realm for many aspects. This is mostly due to its inaccessibility, complexity and heterogeneity. Many small scale properties, such as its microstructure, have large scale effects, and the link between the two scales is still difficult to achieve. Sea ice research is costly and remote-sensing information are limited to its cover. Hence, sea ice thickness is still largely unknown at large scale. Longer time-series are necessary, particularly during the colder season. More modelling attempts and validations are required to improve our knowledge on ice thickness variability. Sea ice is even more unknown from a biological point of view. Interdisciplinary research which may link physical and biological process in sea ice is still scarce. Yet, and even more, sea ice remains a fascinating subject of the scientific research, and any attempt to further improve our knowledge is important both at local and global scales.

Chapter 2

Modelling sea ice physics: thermodynamics

Where the midnight sun blows
hundred thousand lakes glow
in the land of ice and snow.

(Stratovarious)

2.1 Sea ice thermodynamics

The evolution of the pack ice is driven by heat, radiation and momentum exchanges between the ocean and the atmosphere, which can be decomposed in thermodynamic (thermal growth/decay) and dynamic processes (drift, lead openings, ridging). In the coastal fast-ice regions, sea ice evolution is determined fully by thermodynamic processes. These regions are indeed spatially limited, but are key to the functioning of high latitude ecosystems. Landfast ice accumulates, in fact, more algal biomass than pack ice in both Arctic and Antarctic regions (Arrigo, 2003).

Sea ice growth rate is determined by the magnitude of the conductive heat flux, which is dependent on the surface temperature. In order to determine the surface temperature, it is necessary to compute the surface energy balance. The total surface fluxes include shortwave (F_{sw}) and long-wave radiation (F_{lw}), sensible (F_{se}) and latent (F_{la}) heat, which are dependent directly or indirectly on the surface temperature. Hence, a proper treatment of the sea ice growth requires some numerical techniques.

However, the first attempt to study sea ice thermodynamics was an analytical model, which was developed by Stefan (1891). Through some simplifications, he developed the so-called degree-day model, which may actually give fairly accurate predictions of ice growth. Assuming a linear temperature profile, the growth rate is given by:

$$\frac{dH}{dt} = \frac{k_i}{H\rho_i L_f}\left(T_0 - T_f\right) \tag{2.1}$$

where H is the ice thickness, k_i is the ice thermal conductivity, ρ_i is the ice density, L_f is the latent heat of fusion, T_0 and T_f are the surface and freezing temperatures, respectively. In order to simplify his model, Stefan (1891) ignored the short-wave radiation, since its contribution during winter is negligible. And in order to avoid a rigorous mathematical treatment, he assumed that the ice temperature was equal to the air temperature, given that air and surface temperatures are closely coupled. Thus, substituting in Eq. 2.1 T_0 with the air temperature T_a and integrating over time, he obtained:

$$\frac{1}{2}H^2 = \frac{k_i}{\rho_i L_f}\int_0^{t_e}\left(T_f - T_a\right)dt \tag{2.2}$$

where the last term integrated over time in the right side is referred to as the number of freezing days.

Later, Untersteiner (1964) and Maykut and Untersteiner (1971) moved to rather complex numerical modelling, which included the effects of snow cover, ice salinity, and internal heating due to penetration of solar radiation. The incoming radiative and turbulent fluxes, oceanic heat flux, ice salinity, snow accumulation, and surface albedo were specified as functions of time. Starting from an arbitrary initial condition of the Arctic, the model was integrated numerically until annual equilibrium patterns of temperature and thickness were achieved.

Semtner (1976) simplified their model for numerical investigations of climate. In the Semtner 3-layer model, the ice conductivity and heat capacity are assumed to be constant. The upward long-wave is calculated using the Stefan–Boltzmann relation, and the upward shortwave by applying a surface albedo. He also parametrized the ice brine content dynamic. A certain fraction of the solar radiation impinging upon the ice is stored in a brine pocket variable that releases energy to the upper half of the ice under cooling conditions, maintaining its temperature at the freezing until the brine energy is exhausted. In spite of its simplicity, the ice model accurately reproduced the results of Maykut and Untersteiner for a wide variety of environmental conditions. The Semtner-like model has fewer computational requirements than one layer of ocean in polar regions, and it can be further simplified to a 0-layer model as it will show later on.

Leppäranta (1983) introduced also snow compaction and snow ice formation, since these processes are of great importance in subarctic regions. In fact, if snow falls on ice, the air temperature is no more a reasonable estimator of the ice temperature and the Stefan analytical model does not hold anymore . In addition, if the snow input is large enough some of it will be transformed into snow ice.

Saloranta (2000) studied the effect of the flooding and snow ice formation for the mass balance of the Baltic Sea with a Maykut-Untersteiner type model. He also estimated the sea ice sensitivity to changes in winter precipitation. Increased precipitation led to an increase only in snow ice thickness with little change in total ice thickness, while a reduction in precipitation of more than - 50% caused a significant increase in total ice thickness. The difference in modeled total ice thickness for the case of artificially neglecting snow ice physics was about 25%, which indicates the importance of including snow ice physics in a sea ice model dealing with a seasonal sea ice zone.

Later Cheng et al. (2006) modeled the superimposed ice formation during melting periods. They used a high-resolution one-dimensional thermodynamic snow/ice model to simulate this process in the Gulf of Bothnia (Baltic Sea), where during 4 weeks in the early melt season of 2004, 90% of the snow layer was transformed into superimposed ice, while the rest sublimated.

During the last decades other variations of such numerical models have been developed, with different complexity aiming at different applications from the smallest to the largest temporal and spatial scales. However, not much effort has been done to analyze the properties of sea ice thermodynamic models from a biogeochemical perspective.

2.2 Enhanced Sea Ice Model version1 (ESIM1)[1]

ESIM1 (Enhanced Sea Ice Model 1) is the first attempt to model the sea ice physical environment from a more biologically-oriented point of view - that is, having in mind that its development is finalized at the coupling with biological processes. At the same time, it is a very comprehensive Semtner-like model – in terms of number of physical processes that have been included. Its simplicity keeps the computational requirements very low and allow the coupling with other models of higher complexity.

The Baltic Sea was chosen as a test-bed for model simulations. The results have been compared with observations at four different stations of the Baltic Sea. The sensitivity of the model to some of the physical parameters, such as the albedo and the oceanic heat flux is further discussed together with the new addition of relevant physical processes. Finally, the robustness to changes in the physical forcing are assessed.

2.2.1 Description of ESIM1

Following the Semtner 0-layer model (Semtner, 1976, hereafter referred to as S0), the sea ice system consists of one layer of ice and one layer of snow on top. The model is constructed in such a way that, depending on the required complexity, more layers of sea ice can be added. Differently from S0, the prognostic variables of ESIM1 includes two layers of snow (two density classes), three layers of ice (superimposed ice, snow ice and sea ice), temperature at the surface and in each layer. Sea ice stays isosaline with S=5‰. The numerical step is 1.5 hours. A schematic drawing of the model is presented in Fig. 2.1.

Table 2.1 presents the values of the model parameters. In all the following equations the subscript *s* indicates snow, *i* ice, *sn* snow ice, *ss* superimposed ice, *si* sea ice and *w* seawater, while the subscript *mi* refers to meteoric ice, that is snow ice and superimposed ice together.

In S0, a 1-dimensional heat conduction equation governs the vertical heat fluxes, defined positive downwards, at the boundaries and among different layers:

$$\rho_s c_s \frac{\partial T_s}{\partial t} = \frac{\partial}{\partial z} k_s \frac{\partial T_s}{\partial z} \tag{2.3}$$

where ρ is the density, c is the heat capacity, T is the temperature, which is a function of time t and the vertical coordinate z, and k is the thermal conductivity.

---

[1] Parts of this section are published in Tedesco et al. (2009a)

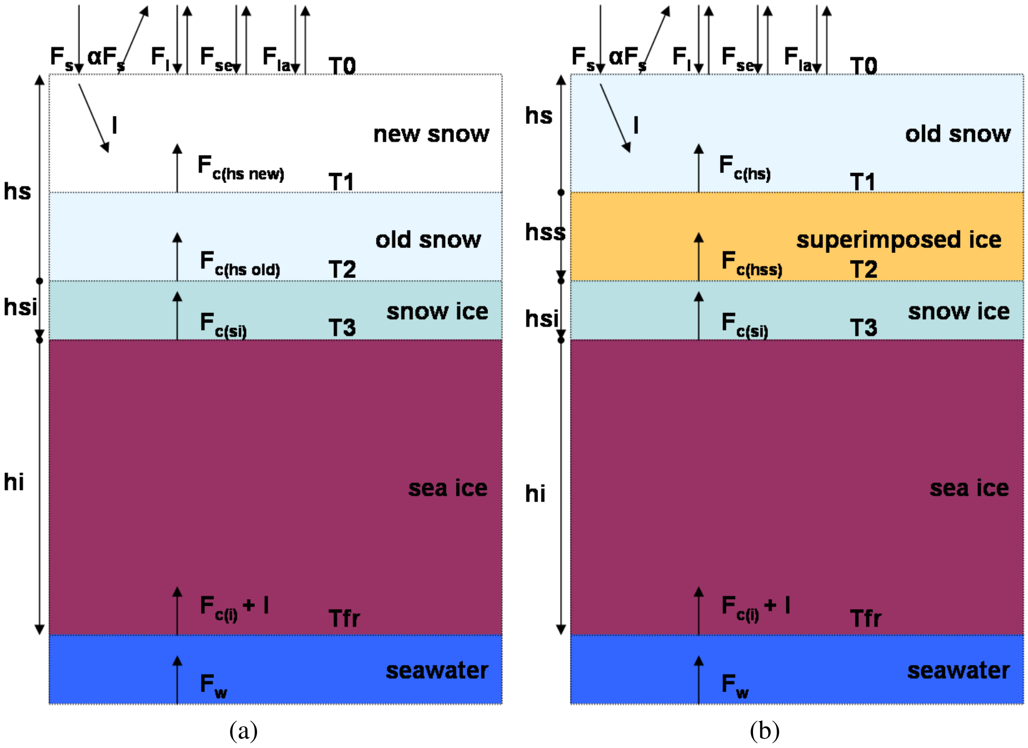

(a) (b)

Figure 2.1: General structure of the ESIM1 (heat fluxes, temperatures, snow and ice layers) during growth (left) and melting (right) periods.

Unlike S0, when sea ice is the only layer of the ice sheet, the sea ice temperature equation also embeds the presence of the penetrating solar radiation which depends on the albedo α and on the extinction coefficient κ:

$$\rho_i c_i \frac{\partial T_i}{\partial t} = \frac{\partial}{\partial z} k_i \frac{\partial T_i}{\partial z} + (1-\alpha_i) F_{sw} e^{-\kappa_i z} \tag{2.4}$$

where F_{sw} is the incoming solar radiation.

The different layers are supposed to be in thermal equilibrium and the temperatures at the interfaces are derived from the continuity of the heat fluxes (Fig. 2.1):

$$\frac{\partial}{\partial z} k_i \frac{\partial T_i}{\partial z} = \frac{\partial}{\partial z} k_s \frac{\partial T_s}{\partial z}. \tag{2.5}$$

The surface temperature is obtained by linearly approximating the surface fluxes, expanding in a Taylor series and iterating according to the Newton-Raphson method for 20 times with a convergence criterion of 0.01 K:

$$T_0^{n+1} = T_0^n - \frac{F(T_0^n)}{F'(T_0^n)} \tag{2.6}$$

Surface, snow, snow ice, superimposed ice and sea ice temperatures are computed

Table 2.1: ESIM1 parameters.

Symbol	Description	Value	Unit	Reference
ρ	Density of air	1.225	kg m^{-3}	
ρ_s	Density of snow	200	kg m^{-3}	
$(\rho_s)_y$	Density of new snow	400	kg m^{-3}	
ρ_{sn}	Density of snow ice	880	kg m^{-3}	
ρ_{ss}	Density of superimposed ice	850	kg m^{-3}	
ρ_{si}	Density of sea ice	900	kg m^{-3}	
ρ_w	Density of seawater	1026	kg m^{-3}	
$(k_s)_y$	Thermal conductivity of new snow	0.056	W m^{-1} K^{-1}	
k_s	Thermal conductivity of snow	0.180	W m^{-1} K^{-1}	
k_{sn}	Thermal conductivity of snow ice	0.950	W m^{-1}K^{-1}	
k_{ss}	Thermal conductivity of superimposed ice	0.9	W m^{-1} K^{-1}	
k_{si}	Thermal conductivity of sea ice	2.0	W m^{-1} K^{-1}	Maykut and Untersteiner, 1971
κ_{si}	Extinction coefficient of sea ice	1.5 – 17.1	m^{-1}	
c_{si}	Heat capacity of sea ice	2093	J kg^{-1} K^{-1}	
c_{sn}	Heat capacity of snow ice	2093	J kg^{-1} K^{-1}	
c_{ss}	Heat capacity of superimposed ice	2093	J kg^{-1} K^{-1}	
c_s	Heat capacity of snow	2093	J kg^{-1} K^{-1}	
c_a	Specific heat of air	1004	J kg^{-1} K^{-1}	
c_w	Specific heat of seawater	4186	J kg^{-1} K^{-1}	
α_s	Surface albedo of snow	0.75	—	Flato and Brown, 1996
$\alpha_{sn,ss}$	Surface albedo of snow/superimposed ice	0.56 – 0.7	—	Perovich, 1996
α_{si}	Surface albedo of sea ice	$(f\,of\,h_{i,}h_s)$	—	Flato and Brown, 1996
α_w	Surface albedo of seawater	0.06	—	Perovich, 1996

implicitly by solving a tridiagonal matrix of the heat conduction equation in each layer.

The snow compaction, snow ice and superimposed ice formation are fast processes and their thicknesses are assumed to reach an instantaneous equilibrium. The model is structured in such a way that, when snow compaction, snow ice and superimposed ice formation are initiated, the snow and ice fractions are transformed instantaneously at the next time step, thus changing their properties, namely density, thermal conductivity, heat capacity and albedo, Table 2.1.

Snow accumulates on top of the surface layer whenever the air temperature is below the freezing point of snow (273.15 K) and an ice layer is already present. If young fallen snow $(h_s)_y$ accumulates on an already present snow layer, snow compaction initiates by specifying the following instantaneous equilibrium:

$$h_s = (h_s)_y \frac{(\rho_s)_y}{\rho_s} \tag{2.7}$$

The total surface fluxes include shortwave (F_{sw}) and long-wave radiation (F_{lw}), sensible (F_{se}) and latent (F_{la}) heat (Fig. 2.1). At the surface, snow, snow ice, superimposed ice and sea ice melt whenever the surface temperature is at the melting point and the rate of melting is determined by the net heat flux balance between the surface fluxes and the conductive fluxes.

$$-k_{i,s}\left.\frac{\partial T_{i,s}}{\partial z}\right|_{z=0} + (1-\alpha_{i,s})F_{sw} - (1-\alpha_i)F_{sw}\,e^{-\kappa_i z} + F_{lw} + F_{se} + F_{la} = -\rho_{i,s}(L_f)_{i,s}\frac{dh_{i,s}}{dt} \tag{2.8}$$

As in S0, if the surface heat fluxes exceed the conductive fluxes, the imbalance in the surface energy budget contributes to increase the conductive flux of the surface layer and the surface energy balance changes accordingly:

$$-k_{i,s}\left.\frac{\partial T_{i,s}}{\partial z}\right|_{z=0} + (1-\alpha_{i,s})F_{sw} - (1-\alpha_i)F_{sw}e^{-\kappa_i z} + F_{lw} + F_{se} + F_{la} = 0 \tag{2.9}$$

The temperature at the bottom of the ice sheet is set constant at the freezing point of seawater at the given salinity (272.88 K). The oceanic heat flux at the ice-water interface is represented by constant values depending on the model location (ranging between 0 and 9 W m^{-2}). At the bottom, ice growth or melting is regulated by the net heat flux balance between the oceanic and conductive fluxes:

$$-\rho_i(L_f)_i\frac{dh_i}{dt} = -k_i\left.\frac{\partial T_i}{\partial z}\right|_{z=-H} + F_w \tag{2.10}$$

As originally proposed in Fichefet and Maqueda (1999), if the ice draft exceeds the ice thickness, i.e.

$$\frac{h_s\rho_s - h_{sn}(\rho_w - \rho)}{(\rho_w - \rho_{si})} > h_{si} \tag{2.11}$$

then snow ice formation is initiated. Snow density and compaction are changed accordingly and a new isostatic equilibrium is prescribed. No addition of seawater mass is currently assumed. Snow is compressed to an amount of new snow ice equal to the initial depression below the water line, as originally in Schmidt et al. (2004):

$$h_{sn} = \frac{h_s\rho_s + h_{si}(\rho_{si} - \rho_w) + h_{mi}(\rho_{mi} - \rho_w)}{\rho_w - \rho_{mi} + \beta\rho_s} \tag{2.12}$$

$$h_s = (h_s)_y - \beta(h_{sn} + \frac{(\rho_s)_y(h_s)_y}{\rho_w + \beta\rho_s - \rho_{mi}}) \tag{2.13}$$

where β is an empirical coefficient of conversion between snow ice and sea ice, after Leppäranta (1983). Snow ice melts according to the same energy balance previously described for snow and sea ice.

If melted snow re-freezes in contact with an ice layer, superimposed ice formation begins by transforming a fraction of snow, depending on snow properties, in superimposed ice (Cheng et al., 2006):

$$h_{ss} = \phi (h_s)_{melt} \frac{\rho_s}{\rho_{ss}} \tag{2.14}$$

where ϕ is the fraction of refreezing snow.

In order to properly simulate the onset and melting of sea ice, ESIM1 is coupled to a simple ocean mixed-layer with a depth of 10 m. During ice-free periods, the slab ocean computes an heat budget equation and resolves the mixed-layer temperature of this isothermal layer as:

$$\frac{\partial T_w}{\partial t} = \frac{F_{tot}}{\rho_w c_w h_w} \tag{2.15}$$

where h_w stands for the depth of the layer, T_w for its temperature and F_{tot} for the net heat flux at the surface.

2.2.2 Test-case: the Baltic Sea

The Baltic Sea is characterized by rather complex melt-freeze cycles and more snow ice formation than any other sea (Sect. 1.4). Because weather conditions in the Baltic are very variable, short periods when surface air temperature exceeds freezing point lead to the melting of the snow and ice, commonly even in the mid-winter. This leads to the importance of including the superimposed ice and snow ice layers to compute the total ice/snow mass balance (Saloranta, 2000; Cheng et al., 2006). The ocean is usually stratified and the oceanic heat flux remains small. The flux can thus be assumed constant allowing to use only one sea ice layer.

Model results, in terms of seasonal evolutions of snow, snow ice, superimposed ice and sea ice thickness and inter-annual variability of the thermal growth of sea ice, were assessed by comparison with regular sea ice observations. The model was implemented in the Baltic Sea at four different stations (Fig. 2.2): Ajos (65° 39.8’ N, 24° 31.4’ E), Kummelgrund (62° 09.3’ N, 21° 09.5’ E), Jussarö (59° 53.4’ N, 23° 31.1’ E) and Kotka (60° 27.3’ N, 26° 57.2’ E). Ajos is the northernmost station and it is characterized by the most severe winters, more ice formation, snow accumulation, snow ice formation and faster melting with minor superimposed ice growth. Jussarö is the southernmost station and it

Figure 2.2: Location of the stations (Ajos, Kummelgrund, Jussarö and Kotka) for comparing ESIM1 with observations.

is characterized by less severe winter, less sea ice growth and snow precipitation, though consistent superimposed ice grows during the melting period. Kummelgrund is latitudinally located between Ajos and Jussarö and has intermediate characteristics between the two. Kotka is the easternmost station and shows similar characteristics to Jussarö, but since it is located north of Jussarö the area is affected by higher sea ice growth rate.

2.2.3 Experiment design

The meteorological data were taken from ECMWF ERA-15 6h Reanalysis data at 2.5 degrees resolution (Gibson et al., 1997) considering air temperature at 2 m height, total cloud cover, wind speed at 10 m height, large scale precipitation and convective precipitation. Due to biases in the ERA-15 database, NCEP 6h Reanalysis (Kalnay et al., 1994) were used for irradiance and specific humidity at the surface and at 2 m height. The weekly observations of snow, snow ice, superimposed ice and sea ice thicknesses were provided by the Ice Service at the Finnish Institute of Marine Research. The chosen simulation period was 1979–1993.

Assuming the normality in the distribution of the residuals of ice thickness, the best fit for every station was chosen with respect to the following criteria:

i. Mean

ii. Variance

iii. Linear correlation

iv. Centered-root-mean-square-error

v. Kurtosis index

vi. Skewness index

Model sensitivity analysis was performed by using an index S, which considers both the variation of the input parameter and the consequent changes of the output variables (Saltelli, 2005), i. e.

$$S = \frac{\frac{O^{+}-O^{-}}{\sigma_O}}{\frac{I^{+}-I^{-}}{\bar{I}}} \tag{2.16}$$

where I represents the chosen parameter (for instance, albedo) and

$$I^{+} = (1+\gamma)\bar{I} \tag{2.17}$$

$$I^{-} = (1-\gamma)\bar{I} \tag{2.18}$$

where γ is 0.1. O^{+} and O^{-} are the outputs of the studied model variable (total ice thickness) corresponding to I^{+} and I^{-}, respectively, while σ_O is the standard deviation of total ice thickness for the control simulation. When the S index is close to 0, the relative changes in the model output (with respect to the observed standard deviation) are smaller than changes in the value of the parameter. If, on the other hand, S value is closer to 1, changes in the model output are larger than variations in the parameter, and the model sensitivity exceeds natural variability. .

The sensitivity of the model to the new physical processes, such as the inclusion of meteoric ice dynamics, is also analyzed and graphically represented. Finally, the dependence on the NCEP and ERA-15 Reanalysis data resolution, by perturbing of 10% their value at every time step, is tested. The statistical results are graphically shown in a Taylor diagram.

2.2.4 ESIM1 results and comparison

Fig. 2.3 presents the simulation results of the thicknesses plotted against observations at every station. The two types of snow are grouped together (hs) and plotted in the positive ordinate. Snow ice and superimposed ice are also grouped together as an intermediate layer (hmi) and plotted in the negative ordinate. The total ice thickness (hi tot) is shown in the negative ordinate as the sum between the intermediate layer and the sea ice thickness. These results were obtained by calibrating the following model parameters (see following section on model calibration and sensitivity):

i. Albedo

ii. Oceanic heat flux

The model seems to reproduce well the dominant physical features: timing of growth and melting and thickness of the ice layers are in general good agreement with observations at all stations, except few cases – for example in Ajos, Jussarö and Kotka during the ice season 1985–1986. On the contrary, the model generally underestimated the maximum thickness of the snow layer, especially in Ajos station – for example during the ice seasons 1980–1981 and 1987–1988. This is probably due to the fact that snow compaction is initiated when new precipitation falls on old snow. However, since the total weight of snow on ice is conserved, the mismatch between simulations and observations do not affect the total ice thickness.

In Fig. 2.4 observations of the ice thickness are plotted on the x-axis against the model control run in the y-axis. The red line is the perfect fit with observations, while the dashed blue and green lines represent the 5% and 95% confidence intervals of every distributions of residuals (difference between observed ice thickness and modeled ice thickness), which are assumed to be normal.

The statistical analysis (Table 2.2) of the residuals reveals low variance values, ranging between 0.93 cm to 1.89 cm. The linear correlation coefficient is also high, from 0.7375 in Kotka to 0.9012 in Kummelgrund. The root mean square errors also stays low, between 9.65 and 11.14 cm. The kurtosis index is, instead, always greater than 3, showing that all of the distributions are more outlier-prone than a normal distribution is. Also the Skewness index reveals that 3 out of 4 of the residuals distributions spread out more to the left, while only the Ajos residuals distribution spreads out slightly to the right.

Fig. 2.4 shows that most of the mismatches between observations and model runs are generally larger at the beginning and/or at the end of the ice season. The largest discrepancy is in Kummelgrund, where, despite the fact that the oceanic heat flux is set to $0\,W\,m^{-2}$(Table 2.2), the mean residual value is -3.93 cm, indicating a general underestimation of the modeled total ice thickness.

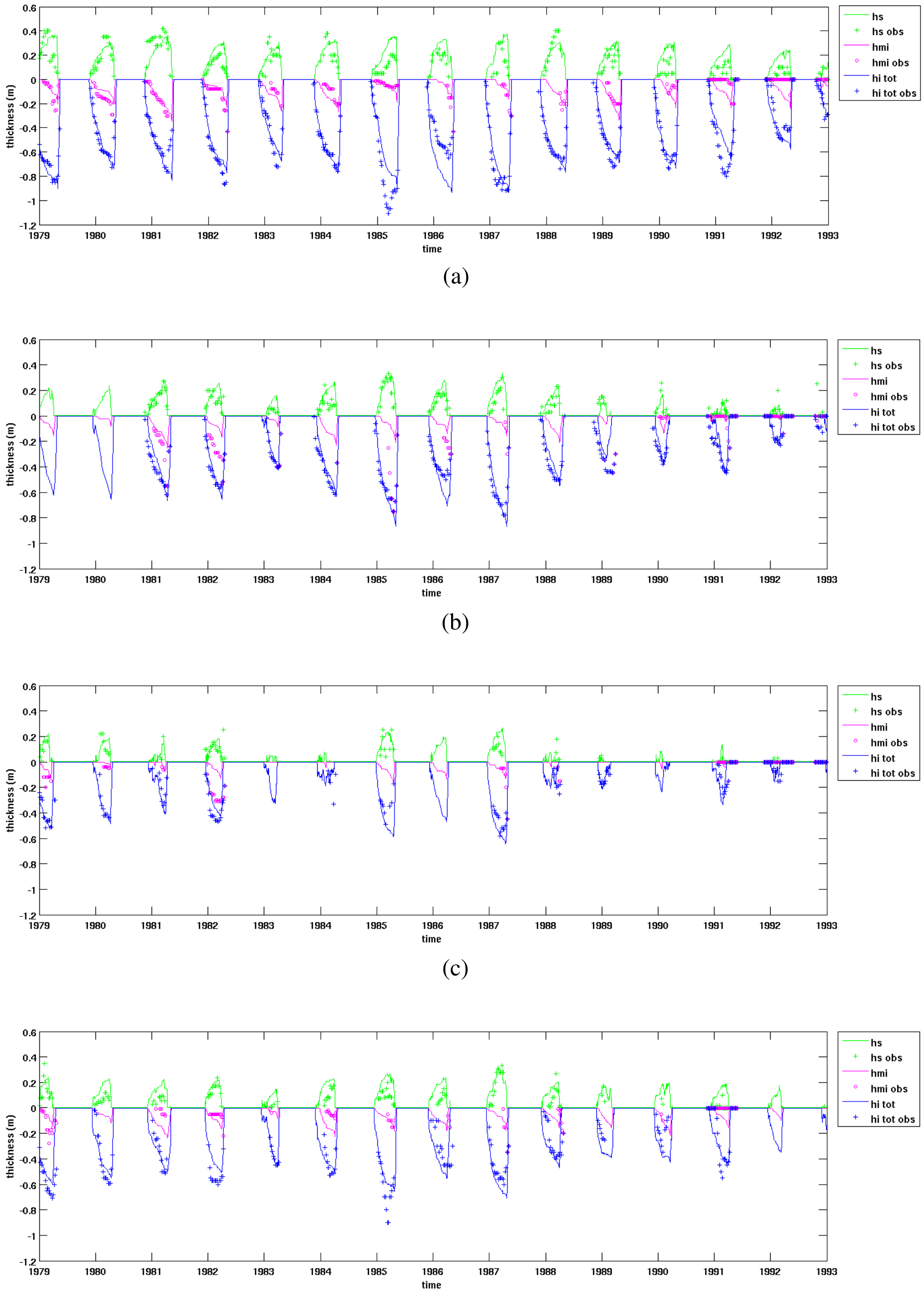

(a)

(b)

(c)

(d)

Figure 2.3: Observations and model simulations in 1979–1993. From above, Ajos, Kummelgrund, Jussarö and Kotka stations (hs: snow; hmi: snow ice + superimposed ice; hi tot: total ice thickness).

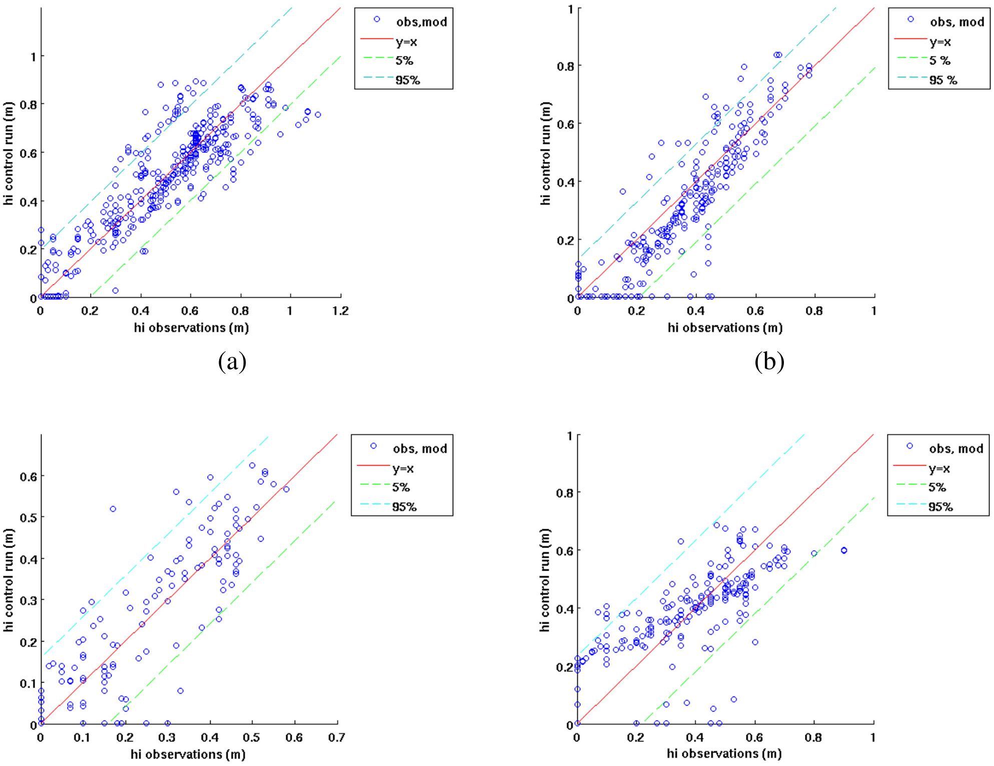

(a) (b)

(c) (d)

Figure 2.4: Observations of ice thickness plotted against control simulations at Ajos, Kummelgrund, Jussarö and Kotka (from above, clockwise).

2.2.5 ESIM1 calibration and sensitivity

In model developments, the choice of the tuning parameters to adjust the model results is usually guided by considering their uncertainties and sensitivities, choosing justifiable values, minimizing the number of parameters, whose values must be changed once at a time. The model has been initially calibrated by testing several albedo parametrizations and oceanic heat fluxes and analyzed the model sensitivity to their values.

Sea ice is known to be very sensitive to albedo (e.g. Shine and Pederson-Heller, 1985), which is the ratio of the reflected and absorbed radiation. The higher is the albedo, the smaller is the absorbed heat and the larger is the reflected radiation. Surface albedo depends on the surface type (snow or ice, see Fig. 2.5), on the surface temperature and on the age of the surface layer. In order to calibrate the model, the discrete parametrization of albedo developed by Perovich (1996, hereafter referred to as PE96) for the Central Arctic and the continue algorithms developed by Flato and Brown (1996, hereafter referred to as FB96) for the Arctic land-fast sea ice and by Pirazzini et al. (2006, hereafter referred to as PI06) for the Baltic land-fast sea ice were tested.

Table 2.2: Statistics of ice thickness residuals for the control simulations.

	Calibration parameters		Ice thickness residuals (observations-model results in m)					
site	albedo	$Fw\ (W\,m^{-2})$	mean	variance	correlation	RMSE	kurtosis	skewness
Ajos	FB96	6	-0.0010	0.01440	0.8812	0.1114	3.9337	0.2407
Kummelgrund	FB96	0	-0.0393	0.0105	0.9012	0.1022	5.4249	-0.2206
Jussarö	FB96	7	-0.0002	0.0093	0.8738	0.0965	4.9824	-0.4331
Kotka	FB96	9	0.0061	0.0189	0.7375	0.1109	4.3011	-0.6862

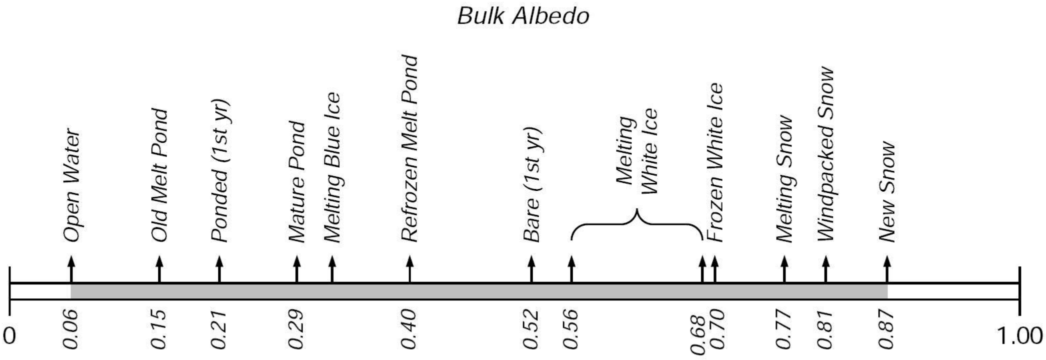

Figure 2.5: Range of observed values of total albedo for sea ice (From Perovich, 1996).

Sea ice also receives a certain amount of heat from the underneath ocean, which is function of the seawater temperature and contributes to the melting of sea ice from the bottom. In our model system, the slab ocean only computes the seawater temperature when the surface is ice/snow-free, while otherwise the seawater temperature is fixed at the freezing point of seawater and the ocean heat flux is kept constant. When the oceanic heat flux is large or highly variable, a proper determination of F_w may require a fully-coupled sea ice-ocean model (e.g. Maykut and McPhee, 1995). However, in marginal seas the vertical stratification beneath the ice tends to be stable and F_w remains small or not very variable. Thus the oceanic heat flux may be considered constant (Cheng and Launiainen, 1998). The Baltic Sea is an extreme example, being permanently stratified throughout the year and the heat contribution from below very limited.

First, ESIM1 was run using the three different parametrizations of the albedo (PE96, FB96 and PI06) and 4 different oceanic heat flux values (0, 3, 6, 9 $W\,m^{-2}$). Therefore, 12 simulations for every station are produced. Total ice thickness was chosen as a target variable for the model calibration and the residuals, that is the difference between the observed ice thickness and the model ice thickness, are analyzed. The mean, variance, kurtosis and skewness indexes of the residuals for every simulation are computed. Finally, the albedo parametrization and the oceanic heat flux value that produced the best statistical results and the best fit of the residuals were chosen as reference (Table 2.2).

Table 2.3: Ice thickness residuals for model calibration to albedo.

parametrization	site	$F_w (W\,m^{-2})$	mean (m)	variance (m)	kurtosis index	skewness index
PE96	Ajos	6	0.0046	0.0163	4.3264	0.5273
PE96	Kummelgrund	0	-0.0238	0.0159	8.4157	1.3988
PE96	Jussarö	7	0.0396	0.0091	4.9674	0.6154
PE96	Kotka	9	0.0245	0.0241	4.9458	-0.7115
FB96	Ajos	6	-0.0010	0.0144	3.9337	0.2407
FB96	Kummelgrund	0	-0.0393	0.0105	5.4249	-0.2206
FB96	Jussarö	7	-0.0002	0.0093	4.9824	-0.4331
FB96	Kotka	9	0.0061	0.0189	4.3011	-0.6862
PI06	Ajos	6	0.0037	0.0152	4.2283	0.4555
PI06	Kummelgrund	0	-0.0315	0.0126	6.7599	0.5772
PI06	Jussarö	7	0.0195	0.0081	5.0251	0.4473
PI06	Kotka	9	0.0227	0.0194	4.4513	-0.6770

At every station, the albedo parametrization of FB96 showed to produce the best results (Table 2.3), followed by the PI06 and PE96, whose parametrizations, instead, tend to slightly overestimate the total ice thickness. Looking forward to more general applications and coupling of ESIM in the future and also to the fact that the FB96 parametrization reduced the numbers of albedo parameters from 7 to 5 compared to the one of PE96, the FB96 parametrization was chosen as the best one for landfast sea ice. About the oceanic heat flux, the chosen values were 0 $W\,m^{-2}$ in Kummelgrund to 6 $W\,m^{-2}$ in Ajos, to 7 $W\,m^{-2}$ in Jussarö and to 9 $W\,m^{-2}$ in Kotka (Table 2.2 and Table2.3).

In order to understand the sensitivity of ESIM1 to the choice of the albedo parametrization of FB96 and to the value of the oceanic fluxes assumed, a sensitivity analysis was performed by using the S index (Eq. 8) for one of the test-case stations (Ajos).

The assumed value of the oceanic heat flux F_w at Ajos is 6 W m^{-2}. The model was thus run also with F_w of 5.4 W m^{-2} (-10%) and F_w of 6.6 W m^{-2} (+10%). The S index was 0.5460, a high value.

The FB96 albedo parametrization assumes two different snow albedos in freezing (“winter”) and non-freezing (“summer”) conditions, while the sea ice albedo depends on the snow and sea ice thickness. Since the FB96 algorithm does not include any parametrization of the snow ice and superimposed ice albedos, those formulated by Perovich (1996) for compacted snow and melting white ice were used. At each of those albedos 10% of their values was added and subtracted for totally 12 simulations at Ajos. The S index results are shown in Table 2.4. Even the highest sensitivity of the model to

Table 2.4: Model sensitivity S to albedo (Ajos).

Albedo	S
Winter snow	0.0994
Winter meteoric ice	0.0193
Winter sea ice	0.0024
Summer snow	0.0788
Summer meteoric ice	0.0529
Summer sea ice	0.0500

the snow “winter” albedo is very small (0.0994), showing that ESIM1 is very robust to small variations of albedo (±10%) in our simulations.

2.2.6 Sensitivity to physical processes

ESIM1 is a very comprehensive sea ice thermodynamic model, in terms of number of physical processes included. Thus, the sensitivity of ESIM1 to 3 important dynamical processes was analyzed:

i. Coupling with a simple ocean mixed-layer

ii. Superimposed ice

iii. Snow ice

ESIM1 was made more similar to a simple Semtner 0-layer sea ice model (hereafter referred to as SIMPLE1), that is with only one layer of sea ice and one layer of snow on top of it, without considering any snow metamorphism. In Fig. 2.6a the results of ESIM1 for snow and ice thickness plotted together with the results of SIMPLE1 for the same two variables are shown. SIMPLE1 overestimates the snow thickness of about 27 cm and, consequently, the ice thickness is underestimated of about 17 cm.

In SIMPLE2 (Fig. 2.6b) a simple ocean mixed-layer 10 m thick underneath sea ice is added to SIMPLE1. Comparing SIMPLE2 to SIMPLE1 a slightly better estimation of snow thickness (23.6 cm overestimation) and ice thickness (16.3 cm underestimation) is obtained. The inclusion of a slab ocean underneath sea ice produced a better agreement with the date of freezing/melting. Thus, the coupled configuration with the slab ocean was kept in all the other simulations.

SIMPLE3 also includes the superimposed ice formation process (Eq. 2.14). Simulation results are shown in Fig. 2.6c where thicknesses of ESIM1 are plotted together with

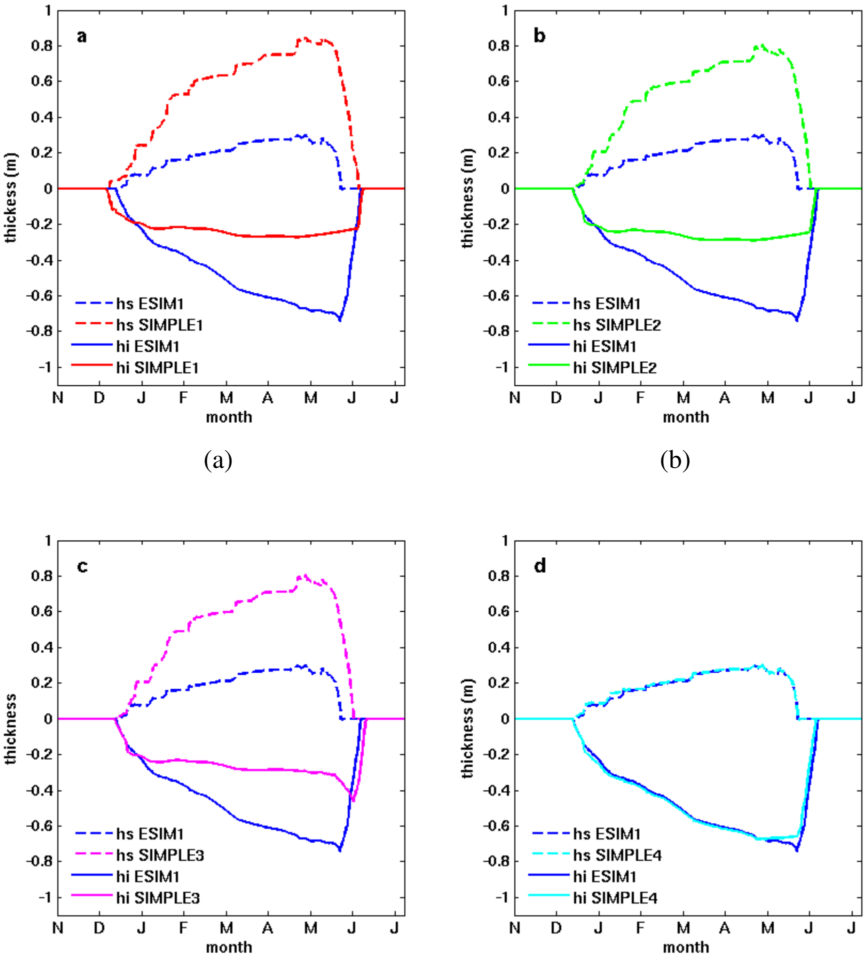

(a) (b)

(c) (d)

Figure 2.6: Comparisons among ESIM1 and SIMPLE (1: no slab ocean, no meteoric ice; 2: slab ocean; 3 slab ocean and superimposed ice; 4: slab ocean and snow ice. hs: total snow in positive ordinate, hi: total ice in negative ordinate).

the thicknesses of SIMPLE3. The snow overestimation slightly decreases to 23.1 cm, while the ice underestimation decreases to 14.5 cm. Therefore, superimposed ice shows to give a rather small contribution, in terms of thickness, to the total ice mass balance.

Snow ice formation (Eq. 2.12) is added to SIMPLE2 in SIMPLE4 and the simulation results of ESIM1 together with SIMPLE4 are plotted in Fig. 2.6d. In this last case, it is very clear the role and the contribution of the snow ice to the total ice mass. The discrepancy between ESIM1 and SIMPLE4 snow thickness is reduced to 0.4 cm, while the difference between ESIM1 and SIMPLE4 ice thickness is now 0.2 cm.

2.2.7 Scenario analyzes for atmospheric forcing

The model was forced by the ECMWF ERA-15 and NCEP 6h Reanalysis data at 2.5 degrees resolution (Sect. 2.2.3). The choice of such a coarse resolution database was driven by the plans of using this model also in coupled configurations with low-resolution climate models.

In order to assess the robustness of the model to the used forcing data, a scenario analysis for one of the test-case site (Ajos) was performed. 10% of the value of each forcing at every time step was added/removed , one-by-one for all the 7 meteorological data. Totally, 14 “perturbed” simulations were produced to be compared with the control simulation and with the observations of total ice thickness. The model results were analyzed by means of a Taylor diagram; a way of graphically summarizing how closely a pattern (or set of pattern) matches observations (Taylor, 2001). The similarity between patterns is quantified in terms of their linear correlation coefficient, their centered root-mean-square difference and the amplitude of their variations (represented by standard deviations).

The Taylor diagram (Fig. 2.7) presents the observations on the x-axis as a black dot, while the perturbed simulations are represented by color squares and circles and the control simulation is plotted as a blue star. All of the simulations have a relative high correlation with observations (0.87-0.89) and their root mean square errors stay constant from 0.11 to 0.12 m. The only slight difference among simulations is their standard deviation, which ranges from 0.22 to 0.25 m, but it always stays smaller than the observations standard deviation (bit higher than 0.25 m). Consequently, there is no significant difference among the control and the perturbed simulations.

2.3 Summary

In this chapter, the basic concept of sea ice thermodynamics and the Enhanced Sea Ice Model 1 (ESIM1) are presented.

ESIM1 is a comprehensive – in terms of the number of physical processes included – sea ice thermodynamic model, which was developed and applied to the Baltic landfast sea ice.

ESIM1 reasonably reproduces the inter-annual variability of the sea ice season in the ice-covered Baltic Sea. Some of the main physical features of the sea ice and snow evolution are rather well reproduced. Particularly, the thickness of the ice layers and the timing of growing/melting are generally in good agreement with the observed data.

The sensitivity test to the physical processes shows that the ESIM1 does a good job whenever the snow layer is well simulated and one layer of sea ice is sufficient to sim-

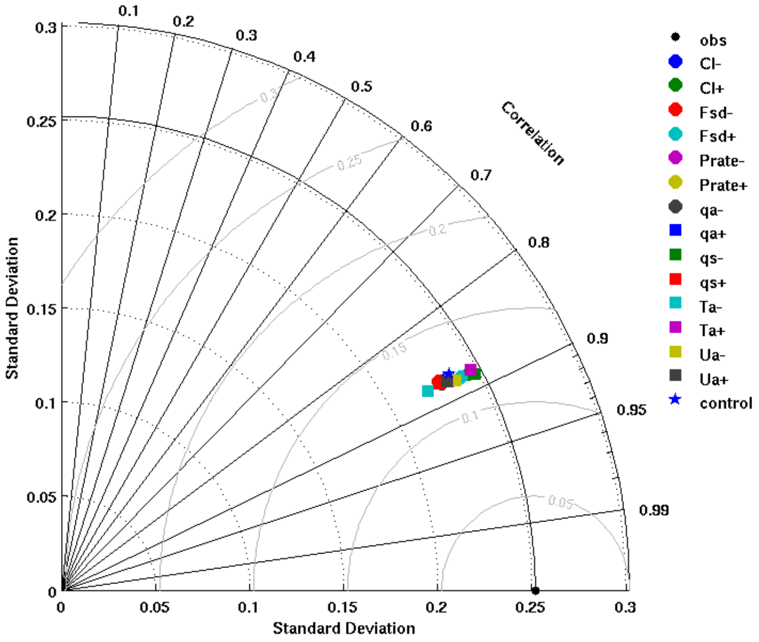

Figure 2.7: Taylor diagram presenting standard deviations, root mean square errors (grey contours) and correlations for the ice thickness control simulation (blue star symbol) and 14 perturbed simulations (Cl: total cloud cover, Fsd: irradiance, Prate: precipitation rate, qa: specific humidity at 2 m height, qs: specific humidity at the surface, Ta: air temperature at 2 m height, Ua: wind speed at 10 m height) at Ajos.

ulate the total ice thickness. The model is, instead, very sensitive to the meteoric ice dynamics and snow is the key variable in sea ice modelling because of its peculiar thermal properties. Thus, more attention should be paid to snow accumulation, compaction and metamorphoses to further improve ESIM1 results.

The calibration and the related sensitivity test to some model parameters stress the relevant role of the oceanic heat flux in sea ice modelling, while ESIM1 does not result to be very sensitive to small variations of the surface albedo. The Taylor diagram for scenarios analysis shows that small perturbations in large-scale forcing do not significantly affect model results when compared to the control run and such coarse resolution can thus be acceptable for long term simulations of sea ice thermodynamics.

Model results are sufficiently robust for an appropriate simulation of the ice characteristics functional to the Baltic Sea biota, where sea ice salinity plays a minor role, being close to 0 ‰, and usually characterized by constant in time vertical profile. Further improvements, which may render the model more suitable for application in other polar and sub-polar regions, concern the inclusion of a halodynamic component (ESIM2), which will be described in the next chapter.

Chapter 3

Modelling sea ice physics: halodynamics

The colour of snow.
The taste of tears.
The enormity of oceans.

(salt packets on SAS flights)

3.1 Sea ice halodynamics

While salinity variations in the brackish waters of the Baltic Sea are of small entity, a more general sea ice physical model requires a proper treatment of the salt dynamics in sea ice. The thermodynamic component of ESIM (Sect. 2.2) was sufficient for adequate simulations of the Baltic sea ice season: the assumption of constant salinity in the Baltic sea ice did not affect simulation results. However, in order to generalize the potential spatial application of ESIM, a new halodynamic component is required, which takes into consideration all the physical processes that are responsible of the changes in sea ice bulk and brine salinities and the dependencies of some of the parameters upon both temperature and salinity.

Large-scale sea ice models mostly assumed constant ice salinity, thus depriving the simulated ice cover of an important response mechanism to changes in atmospheric or oceanic boundary conditions (Eicken, 2003). Moreover, as mentioned above, sea ice microorganisms may be limited by high salinities in cold brines as well as by almost zero-salinity water during flushing. Organic and inorganic matter move internally to sea ice along with brine movements. Salt ice becomes thus a necessary element to study both in sea ice physics and biogeochemistry.

In the Baltic Sea, Granskog et al. (2006b) reported that quantitative information on desalination processes is virtually non-existent. Granskog et al. (2006a) also mentioned that such information would be vital towards the development of a Baltic Sea ice temperature-salinity model that could also be used for development of an ecological sea ice model to resolve the potential consequences of changes in ambient conditions in the sea ice habitat. Obviously, their considerations can be easily generalized and applied to the whole of ice-covered oceans.

During formation, growth and decay, sea ice remains a mushy layer (Feltham et al., 2006), made of two-phases and two-components. Salt dissolved in the ocean cannot be incorporated into ice crystals and is expelled into the liquid solution between the crystals. Boundaries between the liquid brine and the freshwater ice must always remain in phase equilibrium: ice temperature must always be equal to liquidus temperature. The liquidus temperature is a function of salt concentrations, thus is a function of salinity. The approximate freezing temperature T_{fr} of a saline solution such as sea ice may thus be represented by a linear function of its brine salinity S_{br} . Since brines are considered always at their freezing point and in thermal equilibrium, their temperature is obtained by:

$$T = -\mu S_{br} \tag{3.1}$$

as determined by Assur (1958) and where μ is 0.054°C $^{-1}$and T refers to either ice or brine temperature.

The bulk salinity S_{bk} of sea ice is then determined by:

$$S_{bk} = V_{br} S_{br} \tag{3.2}$$

resulting in brine volume V_{br} to be only function of temperature and salinity:

$$V_{br} = -\mu \frac{S_{bk}}{T} \tag{3.3}$$

When temperature falls, some water from brines freezes to form pure ice, thus increasing brine salinity and re-establishing phase equilibrium at the new lower temperature. Knowing the mass of liquid brines and the mass of solid ice, it is thus possible to know the sea ice bulk salinity, which is the salinity of a molten sea ice sample.

Untersteiner (1964) and Maykut and Untersteiner (1971) studied numerically the effects of snow cover, ice salinity, and internal heating due to penetration of solar radiation. The incoming radiative and turbulent fluxes, oceanic heat flux, ice salinity, snow accumulation, and surface albedo were specified as functions of time. They specified some ice properties, such as the heat capacity c and the thermal conductivity k as function of temperature and salinity, i.e.:

$$\rho c = \rho c_0 + \frac{\gamma S_{bk}}{T^2} \tag{3.4}$$

$$k = k_0 + \frac{\beta S_{bk}}{T} \tag{3.5}$$

where c_0 is the constant heat capacity of solid fresh ice, γ is a constant (17.2 kJ $K^{-1}kg^{-1}$), k_0 is the heat conductivity of the solid ice (2.03 W m^{-1} K^{-1}) and β (0.17 W m^{-1} salinity^{-1}) is another constant.

Cox and Weeks (1983) derived an useful set of equations describing the brine volume fraction as function of ice temperature and salinity:

$$V_{br} = (1 - V_{po}) \frac{\rho_i S_{bk}}{F_1(T) - \rho_i S_{bk} F_2(T)} \tag{3.6}$$

where V_{po} is the pore volume fraction and $F_1(T)$ and $F_2(T)$ are empirical polynomial functions based on the phase relations:

$$F_i(T) = a_i + b_i T + c_i T^2 + d_i T^3. \tag{3.7}$$

The coefficients for functions F1 and F2 are listed in Table 3.1 together with the addi-

Table 3.1: Coefficients for functions F1(T) and F2(T) for different temperature intervals (Cox and Weeks, 1983; Leppäranta and Manninen, 1983)

T (°C)	a_1	b_1	c_1	d_1
$0.0 \geq T > -2.0$	-0.041221	-18.407	0.58402	0.21454
$-2.0 \geq T > -22.9$	-4.732	-22.45	-0.6397	-0.0174
$-22.9 \geq T \geq -30.0$	9899	1309	55.27	0.7160

T (°C)	a_2	b_2	c_2	d_2
$0.0 \geq T > -2.0$	0.090312	-0.016111	$1.2291\ 10^{-4}$	$1.3603\ 10^{-4}$
$-2.0 \geq T > -22.9$	0.08903	-0.01763	$-5.330\ 10^{-4}$	$-8.801\ 10^{-6}$
$-22.9 \geq T \geq -30.0$	8.547	1.089	0.04518	$5.819\ 10^{-4}$

tion of those ones for temperatures lower than -2 °C (Leppäranta and Manninen, 1983).

Later, Weeks and Ackley (1986) and Cox and Weeks (1988) studied the thermal role of brines. Their model considers the dependence of the initial ice salinity on ice growth velocity υ_i and seawater salinity:

$$\left(\frac{dS}{dt}\right)_{en} = k_{eff}\left(\frac{dS}{dt}\right)_{w} \tag{3.8}$$

where k_{eff} represent the so-called distribution (or salt segregation or partition) coefficient for the initial salt entrapment. Nearly no salt can be incorporated in the ice crystal lattice, but as the freezing process can be quite rapid, some salt can be trapped inside the ice and placed in brines. In their salinity-evolution model, Cox and Weeks (1988) found 3 distinct regimes for the distribution coefficient k_{eff} :

$$k_{eff} = \frac{0.26}{0.26 + 0.74e^{-7243\upsilon_i}} \quad for\ \upsilon_i > 3.6 \cdot 10^{-5}\ cm\,s^{-1} \tag{3.9}$$

$$k_{eff} = 0.8925 + 0.0568 \ln \upsilon_i \quad for\ 2.0 \cdot 10^{-6} < \upsilon_i < 3.6 \cdot 10^{-5}\ cm\,s^{-1} \tag{3.10}$$

$$k_{eff} = 0.12 \quad for \quad \upsilon_i \quad < 2.0 \cdot 10^{-6}\ cm\,s^{-1}. \tag{3.11}$$

Granskog et al. (2006b) determined a new effective salt segregation coefficient for low-salinity seawater using a time-series dataset of low-salinity Baltic Sea ice salinity profiles and modeled growth rates using a 1-D thermodynamic sea ice model:

$$k_{eff} = \frac{0.113}{0.113 + 0.887\,\exp\left(-2.66 \cdot 10^{4}\, \upsilon_i\right)} \quad for\, 0.2 \cdot 10^{-4} < \upsilon_i < 4.5 \cdot 10^{-4}\, mm\, s^{-1}. \tag{3.12}$$

It has been argued that the salt segregation coefficient does not describe the actual physical process, as stated by the mushy layer theory (Feltham et al., 2006). However, the concept remains very useful to approximate sea ice salinities, especially for numerical studies of salt in sea ice.

After the initial ice formation and salt entrapment, sea ice is also desalinated by several other physical processes. During the cold season in which sea ice continues growing, gravity drainage, brines-pocket diffusion and brine expulsion are of importance. During the warm season, flushing is the main process responsible of sea ice desalination.

Brines-pocket diffusion stands for the molecular diffusion of salt downwards in brines. In cold ice, any brine pocket has a colder upper and a warmer lower part. This temperature gradient must correspond to a salinity gradient in order to maintain phase equilibrium. Thus, a slow motion of salt in the lower part of brines leads to a decrease in the salinity of the top part and to the freezing of some of the liquidus in there to maintain phase equilibrium. At the same time, excess of salt at the bottom part brings to dissolution of salt. Beginning with the pioneer work of Whitman (1926) who first proposed it, this process was believed to be the main explanation of sea ice winter desalination until the 1960s, when both experimental and theoretical work estimated the velocity of this process (e.g., Untersteiner, 1968), which is very slow due to the very small diffusivity of salt in seawater. Even though brine-pocket diffusion may be an important process at microscopic level, it is currently recognized that it does not play any significant role in sea ice desalination under natural conditions.

Brine expulsion is the process due to the pressure gradient which drives brines upward and downward and eventually to expulsion when changes in local temperature caused by internal phase changes lead to brine volume changes. This process was first studied by Bennington (1963) and later revised by several others (e.g., Cox and Weeks, 1988). More recently, Notz and Worster (2006) showed analytically, numerically and experimentally that brine expulsion does not lead to any loss of brines from sea ice, but only to a brine slow motion downward, whose velocity is irrelevant compared to ice growth velocity.

Gravity drainage is considered the most relevant physical process responsible of winter sea ice desalination. In the cold season, sea ice is warmer at its base and this creates an unstable brine density profile, with the highest densities on top. If the ice is porous enough, this can result in convective overturning of brine, causing net downward salt transport and a local decrease in salinity; cold saline brines are replaced by warmer, less saline sea water or brines from lower layers. Cox and Weeks (1988) derived an empirical formula which relates gravity drainage to local brine temperature and volume:

$$\left(\frac{dS}{dt}\right)_{gr} = \delta\frac{\partial T}{\partial z} - \delta\eta V_{br}\frac{\partial T}{\partial z} \tag{3.13}$$

where δ and η are empirical coefficients. η is 20 (non dimensional) and it represents the fact that for brine volume fraction less than 5 % gravity drainage stops. δ is responsible for the magnitude of the desalination. Cox and Weeks (1988) proposed δ to be 1.68 10^{-7} °C^{-1}m s^{-1} based on laboratory observations. Vancoppenolle et al. (2007), instead, suggested 5.88 10^{-8}°C^{-1}m s^{-1} , which was more suitable for their modelling study.

Flushing is the only physical process which takes place in warm sea ice and it is also the most effective in terms of total sea ice desalination. It is similar to gravity drainage, but with the pressure exerted cause of zero or low-salinity melt water, which moves brines downward. Since the work by Untersteiner (1968), little studies on this process have improved our knowledge. Flushing seems to be a very fast and time-fluctuating process with an also significant horizontal velocity (Eicken et al., 2002). However, some simplification may be done and a simple 1-D mathematical formulation which considers the vertical component of the melt water flow through ice is possible. Eicken et al. (2002) showed in his field experiments that, once the permeability threshold of brine connection is reached, any available melt water is almost instantly transferred through the ice matrix. Consequently, it is assumed that brine drainage processes are much more rapid than the thermal requilibrium processes and brines do not enlarge through advection of heat (Vancoppenolle et al., 2007). Thus, flushing occurs whenever the permeability threshold is reached and the surface is at the melting temperature. A fraction of the meltwater flows through brines, replacing salty brine by almost fresh meltwater coming from the top of the ice. The mass of melt water which flows through the ice matrix is:

$$M_{i,s} = (1-\theta)\rho_{i,s}\frac{dh_{i,s}}{dt} \tag{3.14}$$

where θ is the fraction of melt water which percolates vertically. The salinity of melt water depends on the salinity of the melting layer. Once flushing takes place, the process is much faster than any thermal equilibrium and it moves brines downward modifying their salinity, as in Vancoppenolle et al. (2007):

$$\left(\frac{dS_{br}}{dt}\right)_{fl} = -\frac{M_{i,s}}{V_{br}\rho_{br}}\frac{\partial S_{br}}{\partial z} \tag{3.15}$$

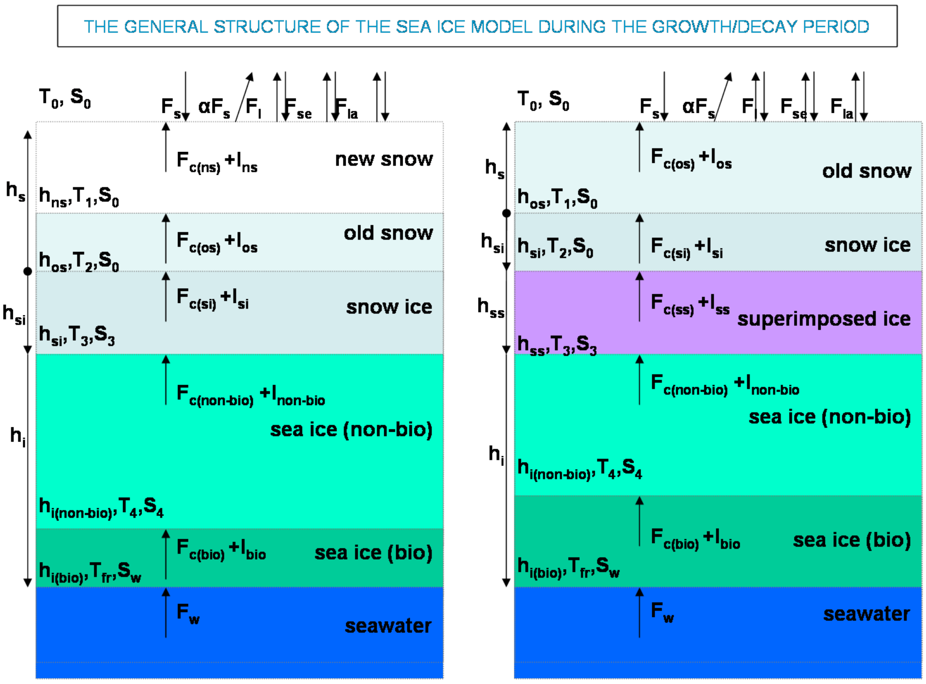

Figure 3.1: General structure of the ESIM2 (heat fluxes, temperatures, salinities snow and ice layers) during growth (left) and melting (right) periods.

3.2 Enhanced Sea Ice Model version 2 (ESIM2)[1]

3.2.1 Description of ESIM2

ESIM2 is a direct improvement of ESIM1. It is made of the same thermodynamic component than ESIM1 - to which some improvements has been made - and of a new halodynamic component which simulates the salinity evolution in sea ice and the salinity dependence of some of the physical parameters which previously were considered constant. A schematic drawing of ESIM2 is presented in Fig. 3.1. Comparing to ESIM1 (Fig. 2.1), ESIM2 includes 2 layers of sea ice, namely the biological layer and the non-biological layer, which are further described in this chapter and later in the next chapter.

---

[1] This section is partially based on Tedesco et al. (2009b)

Table 3.2: ESIM2 parameters (in addition or substitution to ESIM1 parameters, Table 2.1).

Symbol	Description	Value	Unit	Reference
$(\rho_s)_y$	Density of “cold” new snow	250	kg m^{-3}	
$(\rho_s)_y$	Density of “warm” new snow	300	kg m^{-3}	
ρ_s	Density of “cold”snow	300	kg m^{-3}	
ρ_s	Density of “warm”snow	350	kg m^{-3}	
$(\rho_s)_{cp}$	Density of “cold”compacted snow	300	kg m^{-3}	
$(\rho_s)_{cp}$	Density of “warm”compacted snow	350	kg m^{-3}	
$(k_s)_y$	Thermal conductivity of new snow	f of $(\rho_s)_y$	W m^{-1} K^{-1}	(Abels, 1892)
k_s	Thermal conductivity of snow	f of ρ_s	W m^{-1} K^{-1}	(Abels, 1892)
$(k_s)_{cp}$	Thermal conductivity of compacted snow	f of $(\rho_s)_{cp}$	W m^{-1} K^{-1}	(Abels, 1892)
κ_s	Extinction coefficient of snow	15–25 (min, max)	m^{-1}	
κ_{si}	Extinction coefficient of meteoric ice	9.8–21.05 (min, max, f of T and cloudiness)	m^{-1}	
$\kappa_{i,10}$	Extinction coefficient of sea ice (top 0.1 m)	4.6–17.1 (min, max, f of T and cloudiness)	m^{-1}	
κ_i	Extinction coefficient of snow (below top 0.1 m)	1.4–1.6 (min, max, f of T and cloudiness)	m^{-1}	

3.2.1.1 Thermodynamics improvements

One of the main outcome of Sect. 2.2 and Tedesco et al. (2009a) was the relevant role that the snow cover plays in sea ice models. In fact, ESIM1 revealed to be very sensitive to the meteoric ice dynamics (Sect. 2.2.6) and the snow cover to be the key variable because of its different metamorphoses, high albedo and strong insulating effect (Sect. 2.3). In same cases, ESIM1 underestimated the maximum thickness of the snow layer, especially in areas of greater snow accumulation (Sect. 2.2.4). This was explained by the fact the snow compaction is immediately initiated in ESIM1 when new precipitation falls on old snow. In order to improve model results, a new description of the snow compaction in ESIM2, using a bucket model for solid precipitation, is added. When snow falls, it first accumulates in a virtual bucket, whose thickness can be adequately chosen if necessary. Once the bucket is full-filled, it is immediately emptied and snow is compacted in the same way as in Eq. 2.7, changing its thermal properties. Thus in ESIM2 the snow layers becomes three: fresh solid precipitation $(h_s)_y$, bucket snow $(h_s)_{bk}$ and compacted snow $(h_s)_{cp}$ (see Table 3.2 for snow properties):

$$\frac{dh_s}{dt} = \frac{d\,(h_s)_y}{dt} + \frac{d\,(h_s)_{bk}}{dt} + \frac{d\,(h_s)_{cp}}{dt}. \tag{3.16}$$

Besides, in ESIM1 snow density was different only for newly fallen snow and older snow. Instead, in ESIM2, snow density also depends on temperature: if the surface temperature is at the melting point, snow is “warmer” and its density increases (see Table 3.2 for snow densities values). Density of snow collected in the bucket is computed as the weighted mean between the older snow layer and the new fresh snow deposition. The same is applied for the computation of the thermal conductivity of the snow in the bucket, following the work of Abels (1892):

$$k_{sx} = 2.85\rho_{sx}^2 \tag{3.17}$$

where the subscript sx refers to either fresh snow, older snow, snow in the bucket or compacted snow.

The heat conduction equation in ESIM2 implements the penetration of solar radiation for every sea ice/meteoric ice/snow layer instead of just sea ice as in ESIM1 (Eq. 2.4):

$$(\rho c)_{i,s}\frac{\partial T_{i,s}}{\partial t}k_{i,s}\frac{\partial T_{i,s}}{\partial z} = \frac{\partial}{\partial z}\left(k_{i,s}\frac{\partial T_{i,s}}{\partial z}\right) + (1-\alpha_{i,s})F_{s,i}e^{-\kappa_{i,s}z} \tag{3.18}$$

where $\kappa_{i,s}$ is the extinction coefficient which varies depending on the medium. In snow, the penetrating solar radiation is very consistent with the Bouguer-Lambert law and the extinction coefficient is 25 m^{-1} for "cold" snow and 15 m^{-1} for "warm snow". In meteoric ice, the extinction coefficient is parametrized also considering sky conditions. In sea ice, the Bouguer -Lambert law is less consistent, since in the very top 10 cm κ_i can be much larger. Consequently, ESIM2 uses two different parametrization, also embedding the dependence on sky conditions, for the top 10 cm of the ice layer and for the remaining part (see Table 3.2 for $\kappa_{i,s}$ values and parametrization).

Another important upshot of Sect. 2.2 (Tedesco et al., 2009a) was the unnecessariness to add more sea ice layers to better reproduce the total ice-thickness, since ESIM1 did a good job whenever the snow layer was well simulated. Thus the standard configuration of ESIM2 still includes only one sea ice layer. However, as mentioned earlier, the aim of the development of ESIM is the building of sea ice model suitable for studies of sea ice biogeochemistry. The core of the coupling structure between ESIM and a biogeochemical flux model is the layer which is biologically-active (namely BAL), as further described in Sect. 4.3. For now, it is important to mention that this layer is the part of sea ice which continuously maintains a brine volume fraction larger than 5 %. Hence, differently from any other existing sea ice model, ESIM2 computes two sea ice layer - $(h_s)_{bio}$, biologically active and $(h_i)_{abio}$, non-biologically-active -, which have a time-varying thickness:

$$\frac{dh_i}{dt} = \frac{d(h_i)_{abio}}{dt} + \frac{d(h_i)_{bio}}{dt}. \tag{3.19}$$

Among several parametrization of the snow/ice albedo that were tested in Sect. 2.2, the one from Flato and Brown (1996) showed to produce the best results and the sensitivity test of ESIM1 to small perturbations (±10%) revealed that the model was very robust to small changes (Sect. 2.2.5). Since those applications were limited to Baltic Sea ice, the same test (S index, Eq. 2.16) was repeated here (not shown) to understand if the model is generally robust also in non-brackish waters. Results suggest the robustness of the Flato and Brown (1996) parametrization in the Arctic test-case as well. Consequently the same parametrization of the albedo is used in ESIM2.

Also, in Sect. 2.2 ESIM1 was forced by large-scale atmospheric forcing, which were linearly interpolated on the exact location of model simulation. The scenario analysis showed that, even perturbing the forcing, adding/removing (±10%) of their value, model results did not significantly differed from the control run . Thus, also for ESIM2 simulations, such coarse-resolution forcings are used.

3.2.1.2 The halodynamic component

The new halodynamic component of ESIM2 derives the brine salinity using Eq. 3.1 after computing the temperature of every layer. The instantaneous brine volume and bulk salinity are consequently derived by applying Eq. 3.2 and Eq. 3.3. Sea ice heat capacity is computed as in Eq. 3.4, while sea ice thermal conductivity as in Eq. 3.5. ESIM2 uses the F1(T) and F2(T) functions (Eq. 3.7) to calculate sea ice density. First, the pure ice and brine densities ρ_{0i} and ρ_{br} are computed as:

$$\rho_{0i} = 0.917 - 1.403 \cdot 10^{-4} T_i \tag{3.20}$$

$$\rho_{br} = 1 + 8 \cdot 10^{-4} S_{br}. \tag{3.21}$$

The bulk sea ice density ρ_i is derived from Eq. 3.6.

ESIM2 takes in consideration the initial salt entrapment, gravity drainage and flushing in order to simulate sea ice bulk salinity evolution:

$$\frac{dS}{dt} = \left(\frac{dS}{dt}\right)_{en} + \left(\frac{dS}{dt}\right)_{gr} + \left(\frac{dS}{dt}\right)_{fl} \tag{3.22}$$

For the initial salt entrapment, ESIM2 uses Eq. 3.8 with the partition coefficient of Eq. 3.9, Eq. 3.10, Eq. 3.11 and Eq. 3.12. . Once the bulk salinity of the newly formed sea ice is computed, the new bulk salinity of the whole sea ice layer is computed by a weighted mean. Gravity drainage is calculated as in Eq. 3.13. Both empirical coefficients from Cox and Weeks (1988), based on laboratory observations, and from Vancoppenolle et al. (2007) from modeling studies, are used for every simulation. Flushing is calculated according to Eq. 3.14 and Eq. 3.15. Differently from Vancoppenolle et al. (2007), ESIM2 also accounts for meteoric ice flushing, thus also including an eventual melting snow ice layer, which has a non-zero salinity. After the new brine salinity is computed, ESIM2 calculates the new brine volume and consequently the new bulk salinity of sea ice.

A sensitivity analysis is applied to desalination processes and a new empirical coefficient is derived for gravity drainage, which results to better fit observations at every test-case location and is thus considered more general than the previous ones available from the literature .

3.2.2 ESIM2 results and comparison

ESIM2 results in terms of thickness of snow and ice and in terms of ice temperatures and brine and bulk salinity were compared with observations - when available - for an Arctic site and two Baltic sites. The focus is on the thermodynamic improvements with respect to ESIM1 and on effect of the new halodynamic component in both regions. The main aim of the new halodynamic component added to ESIM1 was to generalize its application in also non-brackish waters and to understand how much of the temporal evolution of the ice thickness and ice temperature may be explained by considering the effect of salinity.

The meteorological data were taken from NCEP 6h Reanalysis data at 2.5 degrees resolution (Kalnay et al., 1994) considering air temperature at 2 m height, total cloud cover, wind speed at 10 m height, precipitation rate, irradiance and specific humidity at the surface and at 2 m height. The model time step is 1.5 hours in all cases.

3.2.2.1 The Arctic test-case

The chosen site for model comparison is Kobbefjord, a fjord near Nuuk, West Greenland (64° 09.69’ N, 51° 27.17’ W, Fig. 3.2). The fjord is about 17 km long, and 0.8 to 2.0 km wide, while the innermost part is 100 m deep. The chosen ice season is from 27 of November 2005 to 27 of June 2006, based on observations taken about every 3 weeks on sea ice physical properties (Mikkelsen et al., 2008).

Model results of thickness, ice temperature, brine salinity and ice bulk salinity are shown in Fig. 3.3.

The upper panel (Fig. 3.3) shows the simulated ice and snow thicknesses in comparison to observations. In general, there is a good agreement, except that the model starts forming ice a bit earlier than the observed date of ice forming. However, the reached equilibrium thickness well-agrees with observations. Good agreement is also found for the date of complete melting.

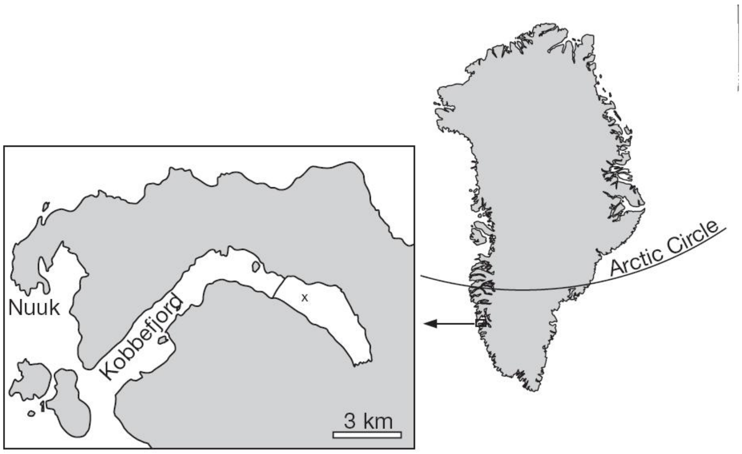

Fig. 1. Kobbefjord/Kangerluarssunguaq, West Greenland. Line marks maximum sea ice extent. x: sea ice station (64° 09.69′ N, 51° 27.17′ W)

Figure 3.2: Location of Kobbefjord: the test-case simulation of ESIM2 in non-brackish waters (Mikkelsen et al., 2008).

The second upper panel (Fig. 3.3) shows the simulated mean ice temperature in comparison with the observed one. The model tends to slightly underestimate the ice temperature, especially at the end of the season. This is likely due to the fact that the freezing point of seawater is fixed by the model (271.45 K) throughout the season, while the effect of flushing during the melt season lowers the ice salinity and consequently the freezing point of brines.

This is also confirmed by the simulated brine salinity (Fig. 3.3, lower second panel). The model tends to overestimate brine salinity during wintertime, while underestimates it during the melting season, when brine salinity approaches zero.

Finally, the first lower panel of Fig. 3.3 shows the temporal evolution of the mean ice bulk salinity in comparison with observations. At the beginning of the season the initial ice salinity values are lowered by the salt entrapment since the ice growth rate slackens (Fig .3.3, upper panel). From January on, the gravity drainage effect starts playing the major role, increasing the ice bulk salinities for the next two months. In the middle of March, ice starts melting and flushing is the main physical process responsible for ice desalination until the end of the ice season.

Even though ice and brine salinities slightly diverge from observations, the temporal evolution of ice bulk salinity is still in good agreement indicating a compensation between the two model variables.

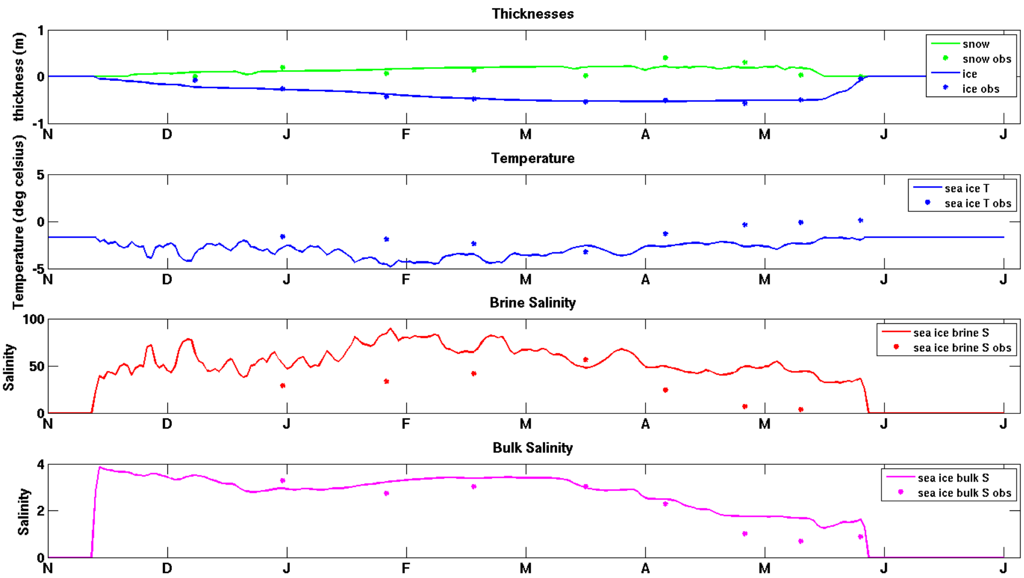

Figure 3.3: ESIM2 simulation of ice/snow thickness (above), ice temperature (second from above), brine salinity (second from below) and bulk salinity (below), in comparison with observations at Kobbefjord site.

3.2.2.2 The Baltic test-case

Even though salinity is meant to play a major role in more salty ice-covered oceans, the effect of ESIM2 on Baltic ice dynamics is also tested, also to analyze any improvement due to the new thermodynamic component of the model.

The chosen site is Santala Bay, a coastal location of the Gulf of Finland (59°55' N, 23°03' E, Fig. 3.4) where salinity data are available. The water depth is about 6 m. The chosen ice season is from 1 of January to 30 of April 2000 - a very mild ice season - based on weekly observations on sea ice physical properties (Granskog et al., 2003a; Kaartokallio, 2004).

As for Kobbefjord, Fig. 3.5 shows ESIM2 results for ice/snow thickness, ice temperature, brine salinity and bulk salinity.

There is a general good agreement between the simulated temporal evolution of the snow cover and ice thickness with observations (Fig. 3.5, upper panel). Especially the snow cover is well-reproduced, considering that values are very small.

The observed ice temperature is available only from the end of February to the end of March and is compared to model simulations in Fig. 3.5 (second upper panel). There

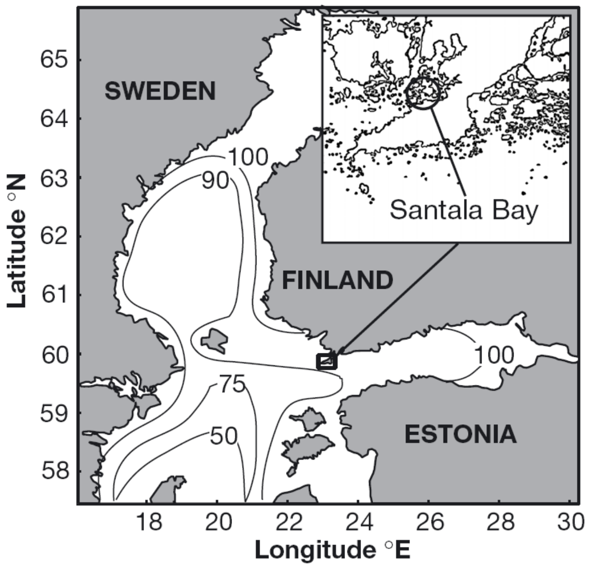

Fig. 1. Northern Baltic Sea, showing sampling location. Contour lines denote percentage of annual ice occurrence probability (contours redrawn from Mälkki & Tamsalu 1985)

Figure 3.4: Location of Santala Bay: the test-case simulation of ESIM2 in brackish waters (Kaartokallio, 2004).

is a general good agreement for the considered short period. The sudden decrease of temperature around 10th of March is due to the sea ice exposure to the colder atmosphere when snow cover almost completely disappears on it (Fig. 3.5, upper panel).

Knowing ice temperature, brine salinity was directly derived from Eq. 3.1 (Fig. 3.5, second lower panel). Also in this case, there is a general good agreement between model results and observation for the short period. A sudden increase in brine salinity is also due to the dropping of ice temperature when snow cover is highly reduced around 10th of March.

In the lower panel of Fig. 3.5, the simulated ice bulk salinity is compared with the observed one. Even though the observed variations are very small, ranging from 0.2 to 1.2, the model seems to not respond to any of the physical processes included (salt entrapment, gravity drainage and flushing) and ice stay isosaline (about 0.5-0.6) during all the ice season.

The salinity component of the model in brackish water will be further analyzed and discussed in Sect. 3.2.3.

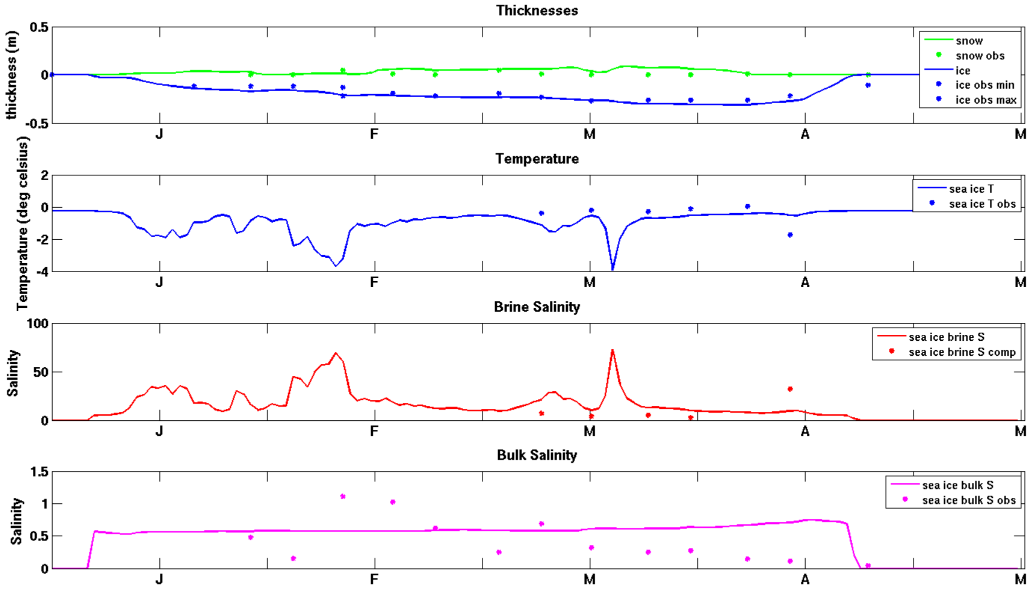

Figure 3.5: ESIM2 simulation of ice/snow thickness (above), ice temperature (second from above), brine salinity (second lower panel) and bulk salinity (below), in comparison with observations at Santala Bay site.

3.2.3 ESIM2 sensitivity to desalination processes

This section aims to analyze if there are, and what are the improvements that ESIM2 produces compared to ESIM1 (Sect. 3.2.3.1). It also analyzes in more details the effect of some of the physical processes responsible of the ice desalination (salt entrapment and gravity drainage) on the temporal evolution of ice salinity in both the Arctic and the Baltic sites (Sect. 3.2.3.2 and Sect. 3.2.3.3).

3.2.3.1 ESIM1 vs. ESIM2

The first analysis in terms of model performance is done comparing ESIM1 and ESIM2 simulations at the same sites, for both the Arctic and the Baltic case.

Fig. 3.6 (upper panel) shows the modeled thicknesses of snow and ice of both models compared to observations.

The new bucket model for precipitation of ESIM2 improves model results: the snow thickness of ESIM2, in fact, agrees better with the observed one, especially during March, when a sudden melting of the snow cover is not captured by ESIM1. Even though there is no consequent mismatch between model and observed ice thickness, the ability of the model to reproduce well the thickness of the snow cover is an essential prerequisite for

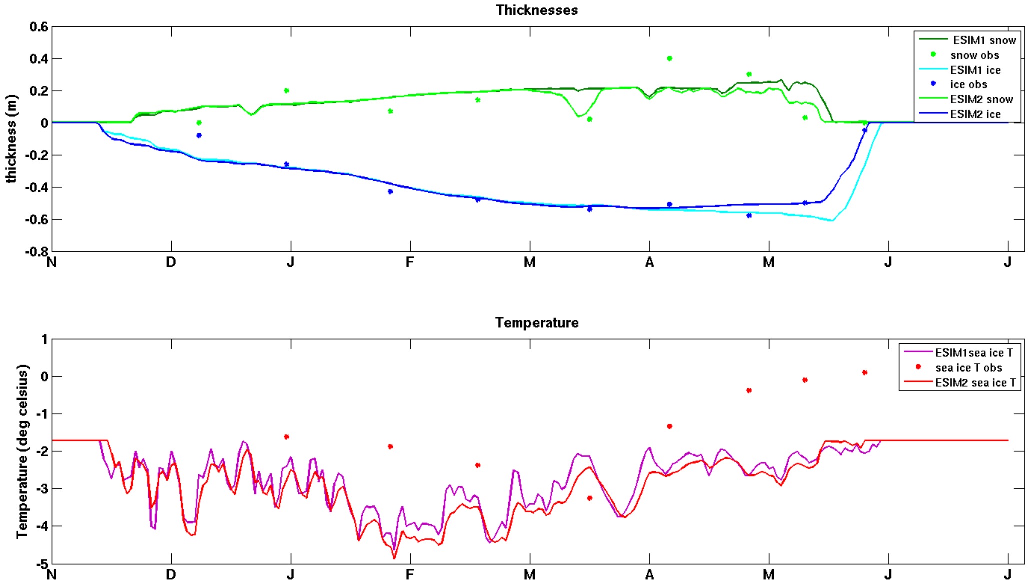

Figure 3.6: ESIM1 and ESIM2 results at Kobbefjord site for thicknesses (above) and ice temperature (below).

biogeochemical applications, as it will be discussed in Sect. 5.2.3. Different snow covers, in terms of thickness but also in terms of insulating properties, control the amount of incident light which penetrates through snow and consequently sea ice, until reaching the bottom of the ice where biology is found (see Sect. 4.3).

Besides, ESIM2 better simulates the date of complete melting comparing to ESIM1, which slightly postpones it of a few days compared to observations. This is again due to the snow cover, which disappears later in ESIM1 simulations.

The comparison between ice temperatures computed by ESIM1 and ESIM2 does not reveal any significant difference between the two models (Fig. 3.6, lower panel). As discussed earlier for ESIM2, also ESIM1 tends to slightly underestimate the sea ice temperature compared to observations.

The same comparison between ESIM1 and ESIM2 is repeated for Santala Bay site (Fig. 3.7).

Since the snow cover is characterized by smaller thicknesses at this site, it is even more evident the benefit of the bucket model for precipitation of ESIM2 (Fig. 3.7, upper panel). ESIM1 underestimates the evolution of the snow cover during almost all of the ice season. Consequently, ice thickness is overestimated during the growth period, reaching

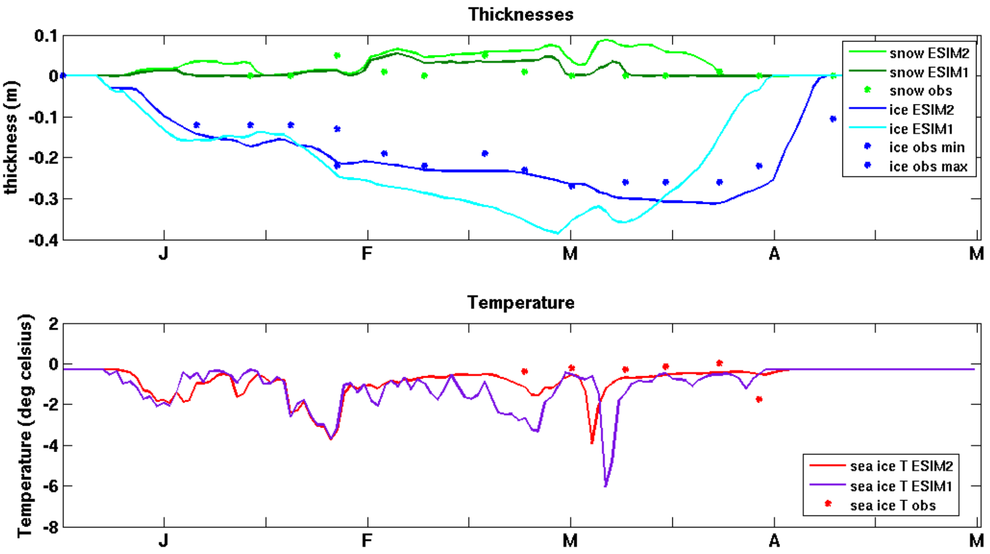

Figure 3.7: ESIM1 and ESIM2 results at Santala Bay site for thicknesses (above) and ice temperature (below).

a larger maximum thickness, and it is underestimated in the melt period, that is ice melts faster than in observations.

This is also very evident from the comparison between the ice temperature simulated by ESIM1 and ESIM2 (Fig. 3.7, lower panel). Throughout the ice season, ESIM1 ice temperatures are almost constantly lower than ESIM2 ice temperatures, which agree better with the observations.

At both sites and in both cases, ESIM2 simulations better agree with observations, especially due to a better reproduction of the temporal evolution of the snow thickness. The inclusion of the bucket model for precipitation is thus definitely improving model skills.

3.2.3.2 Salt entrapment

Salt entrapment is the physical process described in Sect. 3.1, which was first studied by Weeks and Ackley (1986) and Cox and Weeks (1988). It explains the initial entrapment of salt in sea ice during ice formation and it is thus a function of ice growth velocity and seawater salinity, as in Eq. 3.8. Cox and Weeks (1988) proposed the parametrization of the process of Eq. 3.9, Eq. 3.10 and Eq. 3.11. Later, Granskog et al. (2006b) studied the physical process also for low-salinity seawater (Eq. 3.12).

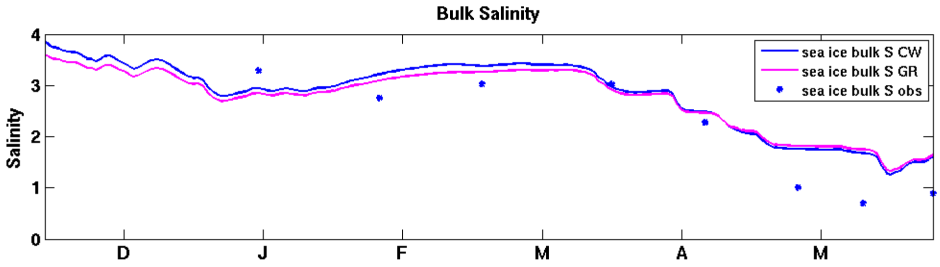

Figure 3.8: Ice bulk salinity at Kobbefjord site using different parametrization for initial salt entrapment.

Here, it is tested how both parametrizations affect model performances in terms of ice salinity results at both sites, even though the parametrization of Granskog et al. (2006b) is meant for only brackish waters.

Fig. 3.8 shows the model results using the Cox and Weeks parametrization of salt entrapment (Cox and Weeks, 1988, hereafter referred to as CW) and the parametrization from Granskog et al. (2006b, hereafter referred to as GR). There are slight differences, the GR parametrization showing more variability than the CW once. However, it is possible to conclude that both of them are suitable for the Arctic test site.

The same comparison is repeated for the Baltic test case, Santala Bay (Fig. 3.9). At this site, none of the parametrization is able to capture the salinity evolution of sea ice. Since sea ice salinity stay almost constant throughout the season, this cannot only be due to the initial salt entrapment, but also to the other physical processes which desalinate sea ice, as it will discussed in next section.

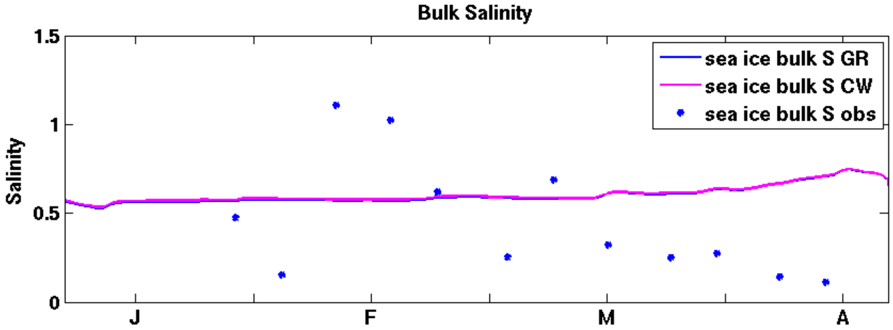

Figure 3.9: Ice bulk salinity at Santala Bay site using different parametrization for initial salt entrapment.

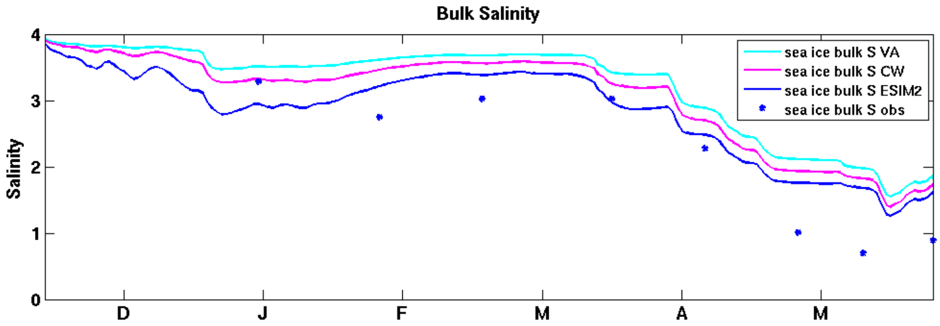

Figure 3.10: Ice bulk salinity at Kobbefjord site using different parametrization for gravity drainage.

3.2.3.3 Gravity drainage

Gravity drainage is the physical process described in Sect. 3.1, which was also studied by Cox and Weeks (1988), and later revisited by Vancoppenolle et al. (2007).

It is due to the unstable brine density profiles of growing sea ice, which result in convective overturning of brines and a local decrease in salinity. Cox and Weeks (1988) described it mathematically as in Eq. 3.13. In particular, they used a value of $1.68 \cdot 10^{-7}\,°C^{-1} m\, s^{-1}$ (hereafter referred to as CW) for the empirical coefficient δ, while Vancoppenolle et al. (2007) suggested a smaller value ($5.88 \cdot 10^{-8}\,°C^{-1} m\, s^{-1}$, hereafter referred to as VA).

Both parametrizations of gravity drainage (CW and VA) were used in ESIM2 simulations of sea ice bulk salinity. Both were found to underestimate the magnitude of the effect of gravity drainage at Kobbefjord site (Fig. 3.10), that is both values of δ were too small. Thus the need of a bigger value was necessary. Based on several attempts (also at the Baltic test case, see further), a new value of $5.88 \cdot 10^{-7}\,°C^{-1} m\, s^{-1}$ was assigned to δ, which is bigger than the one of CW and, exactly, an order of magnitude larger than that of VA.

Surprisingly, the new value assigned to δ revealed to be very important also for ESIM2 simulations at the Baltic test-case.

Similarly to what ESIM1 did in comparison to ESIM2 (Fig. 3.7), both parametrizations of CW and VA not only do not explain the temporal evolution of the sea ice bulk salinity at Santala Bay site, but negatively affect the ice temperature (March), which is higher than the one simulated by ESIM2. The lower temperature in turn affects the ice melt rate and sea ice has totally melted away by about 20th of March.

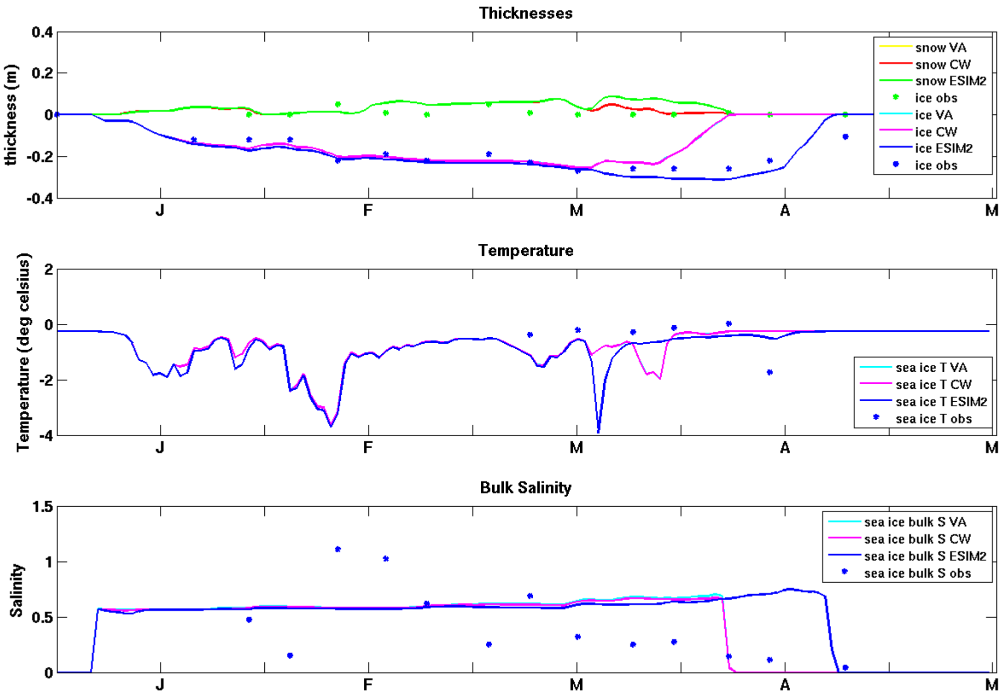

Figure 3.11: Thicknesses (above), ice temperature (middle) and ice bulk salinity (below) at Santala Bay site using different parametrization for gravity drainage.

However, despite the ability of the new parametrization of gravity drainage to produce better results in terms of ice thickness, it still does not produce the higher variability of salt in sea ice as the observations show (Fig. 3.7, below).

This is further tested in another Baltic site, Hailuoto, which is located futher north than Santala Bay, in the northern Bothnian Bay (Fig. 2.2). Hailuoto site is characterized by even smaller seawater salinity (average 2.0) and the considered ice season is from 1st of December 1999 to 31th of May 2000, based on weekly observations of ice bulk salinity and ice/snow thicknesses (Granskog et al., 2006b).

ESIM1 and ESIM2 results at Hailuoto site are again compared (Fig. 3.12, upper panel). Also in this case, ESIM2 better reproduces the thickness evolution of snow and sea ice.

As found at Santala bay site, ESIM2 halodynamics does not reproduce the small observed variations in ice bulk salinity (0.4-0.7), but stays almost constant throughout the season.

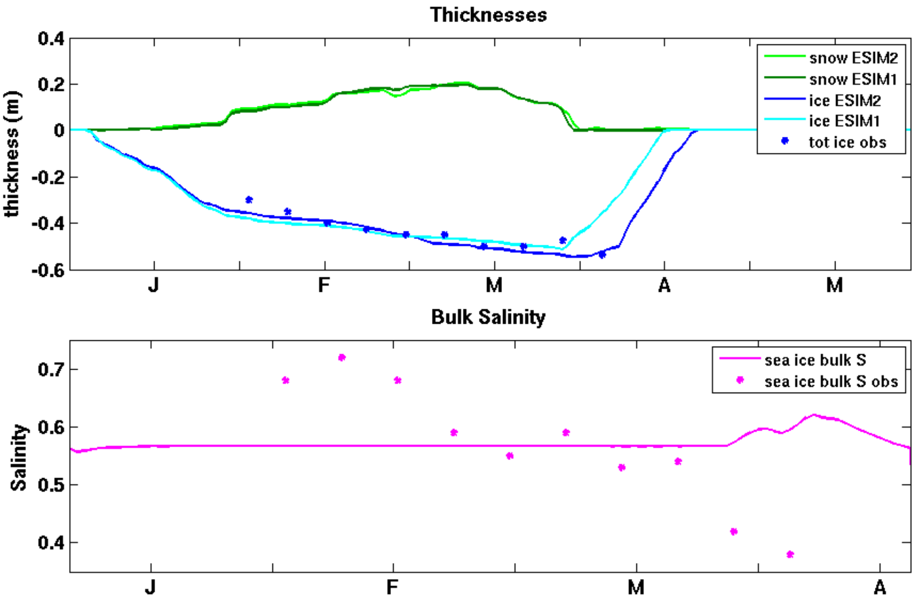

Figure 3.12: ESIM1 and ESIM2 ice and snow thicknesses (above) and ESIM2 ice bulk salinity (below), compared to observations

Even though such small variations in ice bulk salinity cannot have any consequence in terms of model performance for the applications of ESIM2 to biological studies, it is likely that gravity drainage and flushing physical processes require a more detailed analysis and new parametrizations of desalination processes.

3.3 Summary

In Chapter 3, the basic formulations of sea ice halodynamics have been revisited and the new version of ESIM1 (ESIM2), which includes some thermodynamic improvements and a new halodynamic component, is presented. ESIM2 performance is tested at two different sites, one in the Arctic (Kobbefjord) and one in the Baltic (Santala Bay).

At both sites, ESIM2 better agrees with observations in terms of snow/ice thicknesses. This is mostly due to better simulations of the snow cover, which in turn depends on the new bucket model for precipitation added in ESIM2.

Both parametrizations available from literature of the initial salt entrapment in brackish (Granskog et al., 2006b) and non-brackish waters (Cox and Weeks, 1988) worked well at the Arctic site.

At both sites it was needed an empirical coefficient to adjust the value responsible of the magnitude of gravity drainage in order to produce better results in terms of ice thickness

The halodynamic component of ESIM2 captures the ice salinity evolution at the Arctic site, with initial salt entrapment responsible of the initial ice salinity, followed by gravity drainage that first desalinates sea ice and later, when ice gets thicker, slightly increases its salinity, finally followed by the flushing effect which freshens sea ice until the end of the ice season.

Surprisingly, the new halodynamic component added to ESIM1, not only generalizes its applications, but it is shown to improve the ice simulations in the Baltic, where salinity is supposed to play a minor role. However, the halodynamic component is not able to explain the small variations of sea ice bulk salinity at the tested two Baltic sites (Santala Bay and Hailuoto). Hence, there is the need of a more detailed analysis of the parametrizations of the desalination processes, and in particular of gravity drainage and flushing, not yet studied for instance in the Baltic Sea, which may also be used for some other low-salinity ice-covered waters of the Arctic.

Chapter 4

Biogeochemistry of ice-covered oceans: theory[1]

In physics, you don't have to go around
making trouble for yourself
- nature does it for you.

(Frank Wilczek)

---

[1] This chapter is partially based on Tedesco et al. (2009b) and Tedesco and Vichi (2009)

This chapter presents the theory of the new biogeochemical flux model implemented in a sea ice system derived from the Biogeochemical Flux Model (BFM, Vichi et al., 2007b). First, the chapter describes the sea ice habitat (Sect. 4.1) and the previous attempts at the modelling of the sea ice ecosystem (Sect. 4.2). Then, the novel concept of Biologically-Active-Layer is introduced and described (4.3). It allows a direct coupling between the physics of ESIM2 (Section 3.2) and the new biogeochemistry of sea ice (BFM-SI). BFM-SI is directly constructed from the theoretical background of the BFM which is briefly outlined in Sect. 4.5. The sea ice biogeochemistry is also coupled to the pelagic biogeochemistry of ice-covered areas and the strategy of coupling is also described (Sect. 4.4). The new biogeochemical flux model in sea ice (BFM-SI, Sect. 4.6) is presented, together with some equations representing some important biological processes, such as primary production and chlorophyll synthesis.

4.1 Sea ice habitat

From the earliest observations of sea ice to the present, one of the most remarkable features that has been routinely noted by all that have ventured into sea ice covered regions is the presence of ice discoloration; while sediment and mineral inclusions can discolor ice, the most common cause is the growth of pigmented algae (Lizotte, 2003). Sea ice provides a platform for sea ice algae to remain suspended in the upper ocean where light is sufficient for net growth (Arrigo, 2003). Except for those areas where snow cover is extremely thick, light is usually sufficient for net photosynthesis during the polar spring and summer (Grossi et al., 1987). Typically, the amount of light regulates the onset of ice algal bloom whereas availability of nutrients set constraints for the magnitude of the bloom in polar areas (Kirst and Wiencke, 1995). However, as observed for instance during the mild winter of 2000 in the Gulf of Finland, high chl-*a* concentrations already in mid-January suggest that ice algal community was not light-limited at any stage of the ice season due to the thin ice sheet without snow cover (Granskog et al., 2003a).

Microorganisms are not homogeneously distributed in the sea ice depth. Sea ice as a habitat is often characterized by strong gradients of temperature, salinity, light and nutrient availability.

Sea ice biology assemblages may be found (see Fig. 4.1):

- at the sea ice surface. Surface communities form in regions of the pack that become flooded with seawater, either as a result of rafting or snow loading, and are more common in the Arctic due to the larger amount of drifting ice, which eventually draft (Arrigo, 2003). They often have adequate light levels for growth, but have restricted availability of nutrients. Surface flooding is a major source of nutrients, occurring over 15–30% of the ice pack in Antarctica (Wadhams et al., 1987).

- in the internal layers, where they are often subject to large environmental fluctuations (Lizotte and Sullivan, 1991) and are thus particularly dependent upon nutrient availability and salinity. Arrigo and Sullivan (1992) found brines with salinity as high as 173 and temperature as low as as - 16°C in the upper 1.0-1.5m of sea ice at McMurdo Sound (Antarctica). On the contrary, flushing of relatively fresh melt water can expose algal community to very low-salinity environment. In both cases, internal communities are more common in the Antarctic than the Arctic (Arrigo, 2003).
- at the ice bottom. Bottom communities can extend upward, typically as far as 0.2m from the bottom of the ice sheet, depending upon nutrient availability and salinity (e.g., Arrigo and Sullivan, 1992). Bottom communities in the Antarctic are more productive than surface communities, which are themselves more productive than internal communities; the same may be true for the Arctic as well, but data are more sparse and differences between communities are not as obvious (Arrigo, 2003).
- in a "strand" layer just beneath the sea ice, where algae are loosely attached to the underside of the sea ice and extend well into the water column. Typically, those are found in the Arctic regions (Melnikov and Bounderchuk, 1987; Johnsen and Hegseth, 1991).
- in the platelet, a habitat exclusive to Antarctic regions. It is, in fact, associated with floating ice shelves, which are relatively rare in the Arctic. The platelet ice is a porous and isothermal environment with salinity similar to seawater. If enough light is provided, it is an ideal habitat for algal growth: peaks of chl-*a* greater than 1000 mg m^{-2} have been reported (Arrigo et al., 1993; Bunt and Lee, 1970).

4.2 Models of sea ice ecosystem: state-of-the-art

To date, very few studies have dealt with modelling of coupled sea ice algae with phytoplankton production, while most of the studies usually concerns one or the other subject.

Arrigo et al. (1993, and following developments) are the only one, to date, that have developed a comprehensive fast-ice ecosystem model and applied it to the Antarctic sea

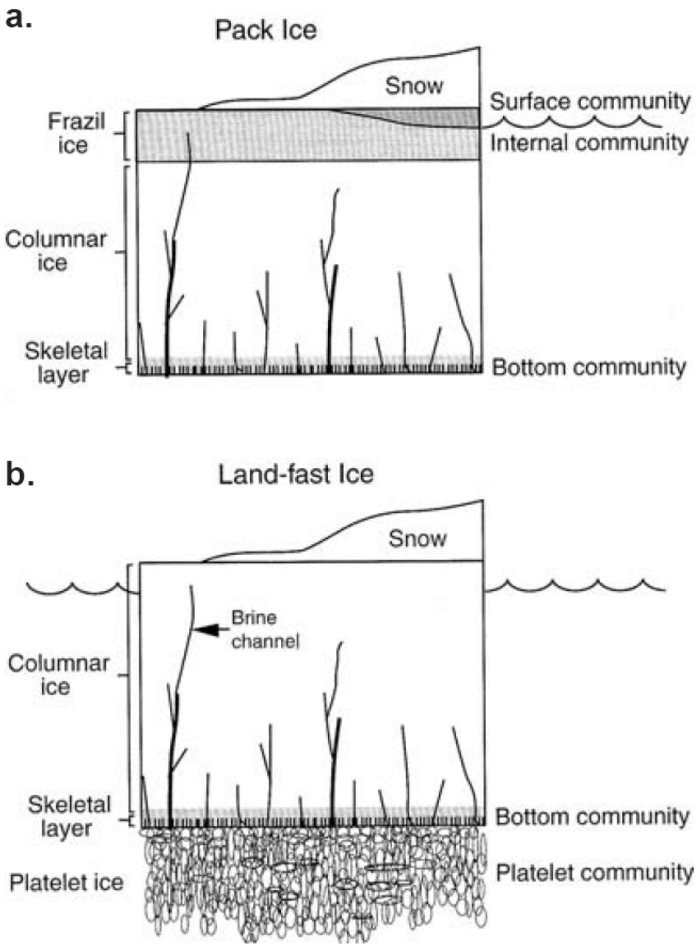

Figure 4.1: Schematic illustration of pack ice and landfast ice showing the major physical features and locations of microbial habitats (Arrigo and Thomas, 2004).

ice. They coupled a simple first-year sea ice thermodynamic model with an intermediate complexity model of microalgal growth. The biological component was based on a maximum temperature-dependent algal growth rate, which was reduced by light or nutrient insufficiency or suboptimal salinity. They demonstrated that sea ice algae are able to maintain their vertical position at the bottom of the congelation ice during ice growth. In the early stages of the spring bloom, high brine salinity inhibited algal growth throughout the congelation ice, except in the skeletal/platelet layer where light was the limiting factor. Later in the bloom, when environmental condition were more favorable for growth, biomass accumulation in the upper congelation ice was regulated by microzooplankton grazing, while in the platelet and skeletal layer, nutrients may have been the limiting factors, due to the decreased flux between sea ice and seawater and the increased nutrient demand. The platelet/skeletal layers, where 76% of the total algal biomass was concentrated with replete nutrients conditions, were light-limited during each bloom stage.

However, they applied the model in a landfast sea ice region that differs in many aspects from pack ice areas, where internal communities are generally relict of the previous year bottom communities and can strongly contribute to the overall biomass. They also did not consider the presence of surface communities, locally common in Antarctic where heavy snow loads cause seawater flooding at the snow-ice interface.

Nishi and Tabeta (2005) developed an ice-ocean ecosystem model and applied it to Lake Saroma. They used a 10-layer Maykut-Untersteiner thermodynamic sea ice model, 1-D vertical equations for heat, salinity and momentum with the turbulent closure scheme of Kantha and Klaison (1994) and an intermediate complexity ecosystem model, made of two submodels: a pelagic one with 13 compartments and an ice one with 12 compartments. Their objective was to develop a system representing the exchange of organic matter between the ice and water components, including both the vertical and the lateral variations. Vertically, they estimated the brine convection, the freezing flux and the diffusive flux at the bottom of the ice. Laterally, they included the melting flux. Since Lake Saroma is very shallow (max depth 15 m), they assumed a logarithmic law for the re-suspended materials that contributed to the organic matter budget of the pelagic ecosystem. Their results were comparable with the observations. Their model predicted that ice algae are efficiently grazed by copepods before being released in the water and this grazing is the most important food source during the period of ice coverage. However, the sinking speed of those algae down to the water was too high (100 mm day^{-1}) to be the algae efficiently exploited for secondary production. They also noticed a strong correlation between the speed of sinking of sea ice algae and the magnitude of the phytoplankton bloom. Some sensitive experiments showed that a fast sinking results in a late increasing of the zooplankton biomass and thus a lower grazing pressure that resulted in a more intense phytoplankton bloom. They clearly demonstrated that the released algae strongly influence the timing of the onset of active secondary production and the magnitude of the phytoplankton spring bloom.

Jin et al. (2006) developed a 1-D ice-ocean ecosystem model to determine the factors controlling the bottom-ice algal community (0.02 m) of the landfast ice off Barrow, Alaska. Snow and ice data were provided from observations. Their 1-D model (physical-biological) revealed a 3-stage bloom: an early and slow light-limited growth, a fast growth with sufficient light and nutrients and a declining stage when algae are flushed out of the ice bottom and are nutrient-limited. They found that the net primary production increased almost proportionally to the initial nutrient concentrations in the water column, despite other factors (initial ice algae concentration, water-ice interface transport). The onset of an under-ice phytoplankton bloom was also limiting the nutrient availability for sea ice algae. They finally estimated that 45% of the NPP was exported to the benthic system.

4.3 The Biologically-Active-Layer (BAL)

As mentioned in Sect. 4.1, the greatest fraction of sea ice microalgae typically resides in the bottom 0.2 m of the ice sheet, where environmental conditions are generally stable and more favorable for growth (e.g., Arrigo, 2003). Upward distribution of bottom communities is generally limited by nutrient availability (brine interconnection, Fig. 4.2, left panel) and high brine salinity (Arrigo and Sullivan, 1992). In the Antarctic, bottom ice communities exhibited the highest algal biomass accumulation of any sea ice habitat, up to more than 500 mg chl-a m^{-2} (Riaux Goben et al., 2000), with the exception of the platelet ice (Arrigo, 2003). Besides, landfast ice accumulates more algal biomass than pack ice in both Arctic and Antarctic regions: the reported peak biomass accumulation in pack ice has been less than 100 mg chl-*a* m^{-2} in both polar regions, while in landfast has been greater than 200 mg chl-*a* m^{-2} in the Antarctic and in the Arctic as well (Arrigo, 2003).

From a more theoretical point of view, the sea ice layer where any biological process occurs can be considered as biologically-active. The term biological process means the presence in the liquid fraction of sea ice (brine pockets and channels) of both organic and inorganic matter dynamics. After sea ice formation, this matter is entrapped in sea ice and moves within it following the salinity and temperature gradients which regulate its vertical distribution. Brines can be further isolated or interconnected. Interconnected brines have the potentialities for biomass accumulation whenever environmental conditions (temperature, salinity and light) are favorable. Theoretical (Golden et al., 1998) and experimental studies (Eicken et al., 2004) have showed that the permeability threshold is a brine volume of 5%. Over it, the brine network connects and sea ice is permeable to fluid transport. Thus, a brine volume larger than 5 % is the criteria that distinguishes between productive and non-productive sea ice layers (Fig. 4.2, right panel).

In order to apply these theoretical considerations into a mathematical formulation, the novel concept of Biologically-Active-Layer (BAL) is formulated in this thesis. Considering the temporal evolution of sea ice from the formation to the growth and decay, it is relevant for the purpose of simulation of sea ice biogeochemistry to know the fraction of sea ice which is potentially productive. ESIM2 (Sect. 3.2) does so. While computing the salination and desalination processes which affect sea ice, ESIM2 computes the thickness of the sea ice layer where the brine volume is always larger than 5 %. This is defined as BAL (Fig. 4.2, right panel). An important assumption is thus that the BAL includes only the bottom communities which extend upwards until sea ice is permeable. It does not

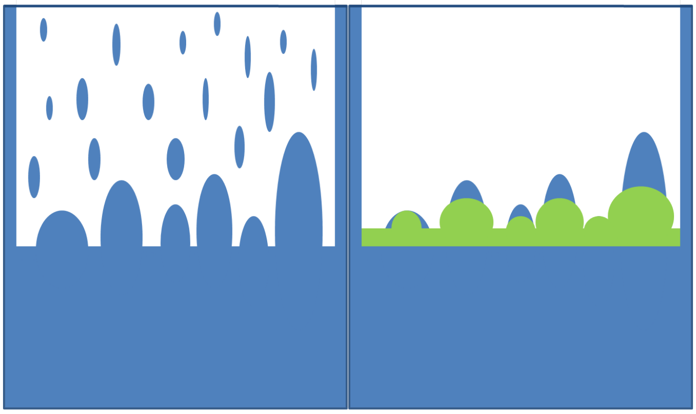

Figure 4.2: General scheme of the partitioning of the liquid (blue) and solid (white) fraction of sea ice (left panel) and model representation of the Biologically-Active-Layer (right panel, in green color).

currently include the surface and internal communities, which can be eventually added later using the same kind of mathematical approach.

Temperature, salinity, space, nutrients and light availability are the key environmental factors that affect the growth, distribution and abundance of sea ice algae. ESIM2 (Sect. 3.2) computes the mean key physical properties of the sea ice BAL, which are: thickness, temperature, bulk salinity, irradiance ,brine volume, brine salinity and growth/melt rate. Those are currently passed to BFM-SI as an off-line coupling (Fig. 4.3).

Those are the necessary requirements for simulating the physiological and ecological response of the biological community to the physical environment, which will be further analyzed in the next chapter.

4.4 Coupling sea ice biogeochemistry to pelagic biogeochemistry

The construction of a biological model in the BAL implies the coupling with the underlying pelagic system (see also Fig. 4.3). The coupling between the two systems (Fig. 4.3 and Fig. 4.4, right panel) has been done using the same strategy that was used to originally couple the pelagic Biogeochemical Flux Model to the benthic Biogeochemical Flux Model (Fig. 4.4, left panel). The benthic BFM is a layer model: it is, in fact, characterized by three different layers of the benthic habitat (oxic, denitrification and anoxic), which are described by different chemical and biological processes (Fig. 4.3, left).

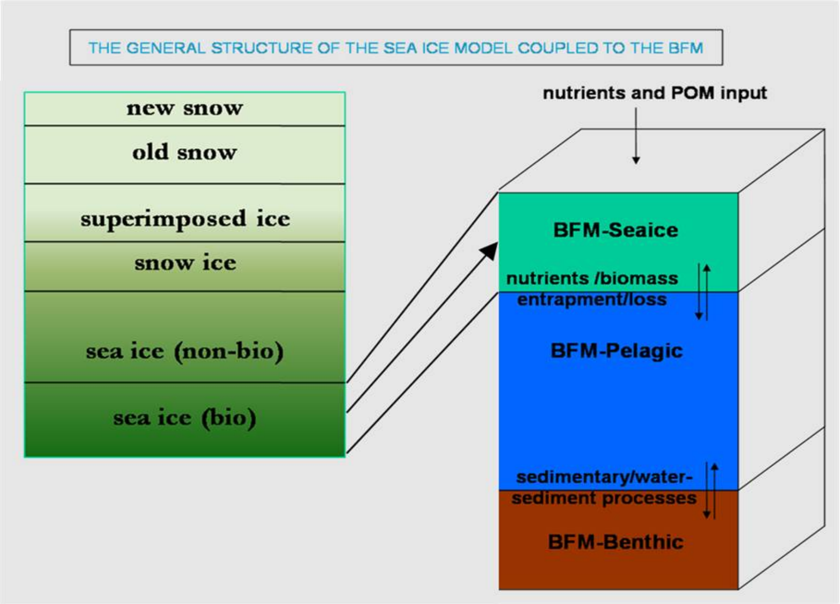

Figure 4.3: Scheme of the coupling structure between physics and biogeochemistry of sea ice and between different BFM systems: sea ice (upper right box), pelagic (middle right box), benthic (lower right box).

Also ESIM1 and ESIM2 are layer models. In particular, ESIM2 is made of 2 to 7 different layers : 2 sea ice layers (biologically-active and non-biologically active, grouped as “Sea ice” layer in Fig. 4.4, right panel), 3 layers of snow (fresh, bucket and compacted, grouped ad “Snow” layer in Fig. 4.4, right panel) and 2 layers of meteoric ice (snow ice and superimposed ice, grouped as an intermediate layer in Fig. 4.4, right panel). In principle, as for the benthic model, it may be possible to model the biogeochemistry in every layer of ESIM2. However, as a first implementation of a model of biogeochemistry in sea ice, the focus is on the layer where the majority of the biomass is generally present, that is the Biologically-Active Layer (BAL) described in Sect. 4.3. Thus the coupling between the sea ice system and the ocean system is made in the same way as it was made the coupling of the ocean with the benthic system. Further developments may also include the coupling with other layers of the sea ice model, such as the snow-ice layer for surface communities.

While constituents of the pelagic system are expressed in terms of concentration per cubic meters, the layer variables are expressed in terms of concentration per square meters. The same applies for BFM-SI. At the boundaries the exchange of particulate and organic matter is done by considering several fluxes, which will be further described in Sect. 4.8.

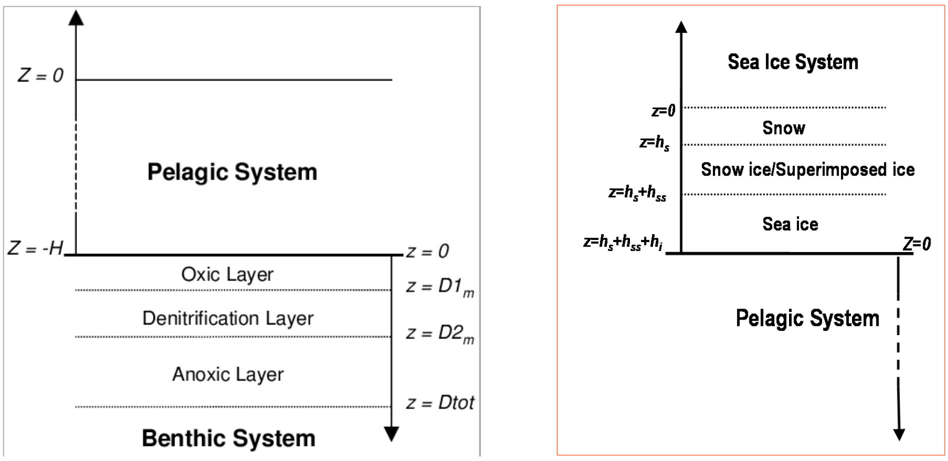

Figure 4.4: Structure of the coupling between pelagic BFM and benthic BFM (left, from M. Vichi) and between pelagic BFM and sea ice BFM (right).

4.5 The pelagic Biogeochemical Flux Model

The Biogeochemical Flux Model (BFM, Vichi et al., 2007b,a, http://bfm.cmcc.it) is a direct descendant of the European Regional Seas Ecosystem Model (Baretta et al., 1995; Baretta-Bekker, 1997, , ERSEM I and ERSEM II), which was the first comprehensive model to include physiological considerations in the definition of the divergence of material fluxes. The model has been widely used by the scientific community in coastal and regional seas (Ruardij et al., 1997; Allen et al., 1998; Vichi et al., 1998; Zavatarelli et al., 2000; Obernosterer et al., 2001; Allen et al., 2001; Petihakis et al., 2002; Vichi et al., 2003c; Raick et al., 2005) as well as in climate studies (Taylor et al., 2002; Vichi et al., 2003a) and in a global ocean coupled physical–biogeochemical numerical application (PELAGOS, PELAgic biogeochemistry model for Global Ocean Simulations, Vichi et al., 2007a). The BFM (Vichi et al., 2007b) generalizes the biogeochemical concepts developed in ERSEM, elucidating the basic constituent, introducing a clear definitions of the ecosystem state variables and adding new important biogeochemical constituents such as iron and chlorophyll.

The ERSEM view of the marine ecosystem was based upon the recognition that the major ecological functions of producers, decomposers and consumers and their specific trophic interactions can be expressed in terms of material flows of basic elements (C, N, P, etc.). The concentration and characteristics of organic and inorganic compounds in the water were thus seen under a stoichiometrical perspective as the final result of the direct uptake and release by producers, decomposers, heterotrophic consumers of these constituents. The central role was thus not played by single species but by the total biomass of a collection of species sharing the same functional behavior. This functional approach

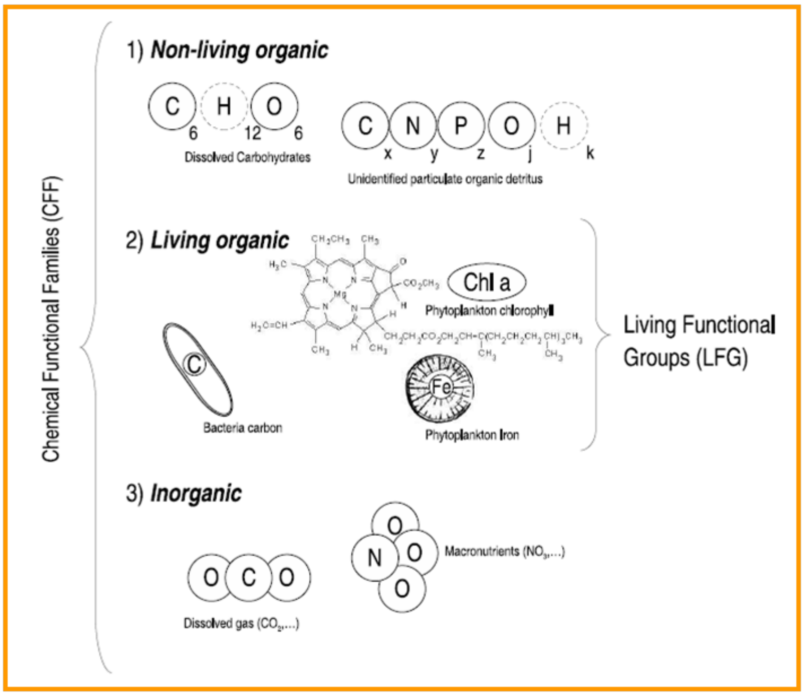

Figure 4.5: Scheme of the various types of Chemical Functional Families (CFF) expressed in terms of basic biogeochemical elements (Vichi et al., 2007b).

is rewritten in the BFM (Vichi et al., 2007b) with a new formalism which is based on the definition of Chemical Functional Families (CFF) and Living Functional Groups (LFG). The core components of the formalism are the CFFs (Fig. 4.5) which are theoretical constructs that are useful to describe the way materials are exchanged in marine biogeochemistry. CFFs can be sometimes identified as specific compounds such as dissolved inorganic nutrients, but in most of the cases are defined as the inventory of a certain biogeochemical element contained in more complex living and nonliving components of marine biogeochemical cycles. CFFs can be described in terms of concentrations and the choice of CFFs as the basic state variables is natural since they are measurable quantities in the limits of laboratory or in situ experiments. CFFs are divided in inorganic, non-living organic and living organic compounds (Fig. 4.5) and they are measured in equivalents of major chemical elements (C, N, P, Si, O, Fe) or in molecular weight units as in the case of chlorophyll.

Members of one LFG are represented by the prototype of a standard organism as in Fig. 4.6. As well as CFFs, also the standard organism is a theoretical construct, which should not be identified with the real organism. The standard organism is thus the model of the LFGs, whose total biomass is composed of living CFFs and interacts with other (liv-

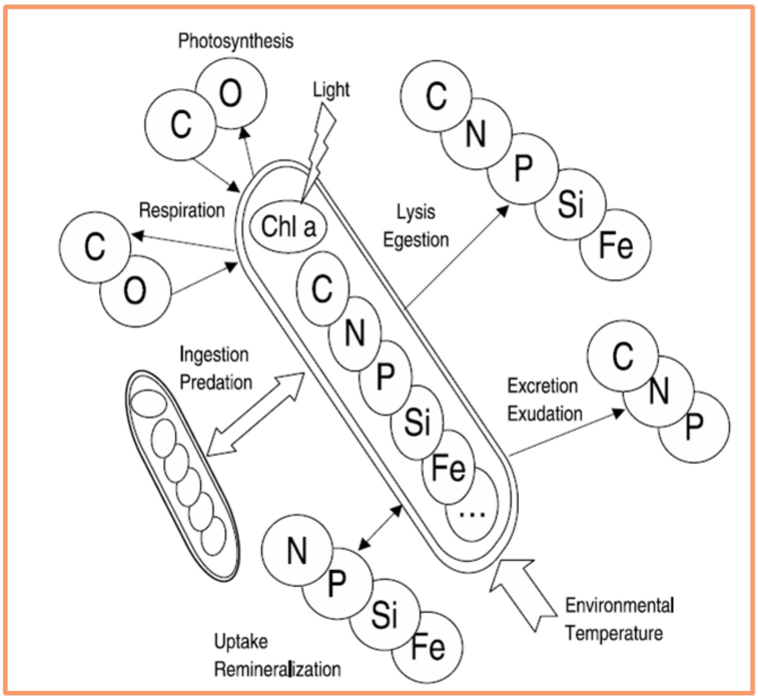

Figure 4.6: Scheme of the standard organism of BFM, which is the prototype of any Living Functional Group (LFG), and the physiological/trophic relationships among the Chemical Functional Families and major environmental forcing (Vichi et al., 2007b).

ing and non-living) CFFs by means of universal physiological and ecological processes such as photosynthesis, excretion, grazing, etc. The parametrization of the physiological and trophic dynamics considered are generally limited to interactions at the membrane level, which also implies neglecting the details of ingestion mechanisms in metazoans. It is important to notice that this approach does not exclude the further implementation of more detailed formulations which mechanistically resolve the intracellular transport of nutrients and carbon or parametrizations of the feeding behavior of zooplankton.

The mathematical relationships between the CFFs and the LFG functionalities are defined following the stoichiometrical requirements of basic elements. These requirements can be both dynamically varying between given maximum and minimum values of element ratios or constant. This makes the definition of LFGs very general and can be also applied, for instance, to other existing biogeochemical models which use one single nutrient as currency. If it is assumed that the standard organism has fixed stoichiometry (e.g., Redfield ratios in phytoplankton), then the dynamics of the LFG can be formulated with one single CFF, and the time rate of change of the others are derived from the constant ratios.

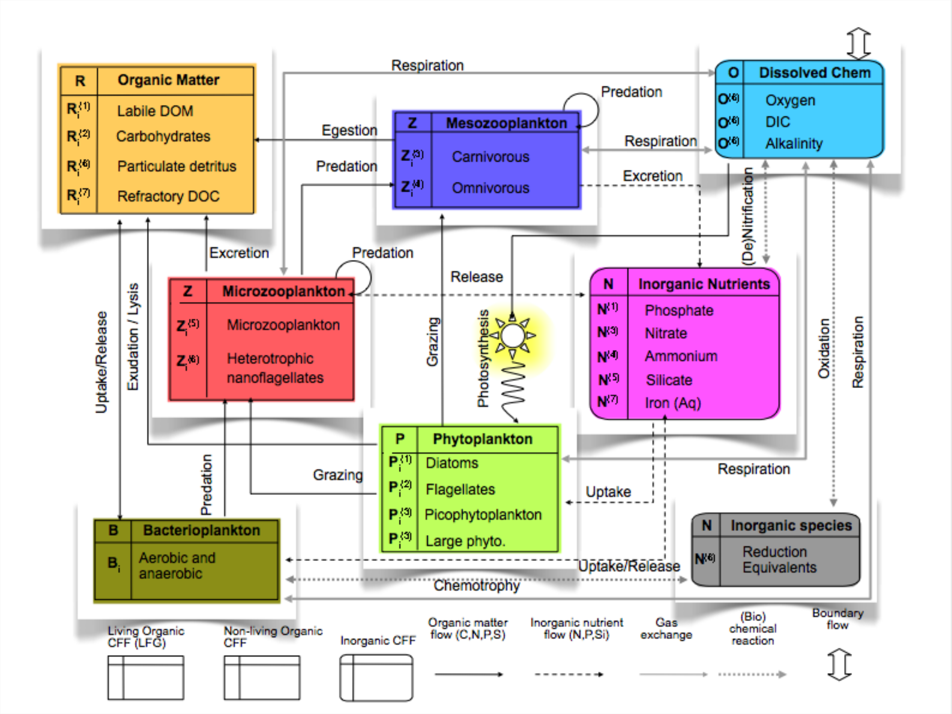

Figure 4.7: Scheme of the state variables and pelagic interactions of BFM (Image from M. Vichi).

The structure of BFM is shown in Fig. 4.7. The model resolves totally 54 state variables derived from:

- 4 different LFGs for phytoplankton (diatoms, autotrophic nanoflagellates, picophytoplankton and large phytoplankton)
- 4 LFGs for zooplankton (omnivorous and carnivorous mesozooplankton, microzooplankton and heterotrophic nanoflagellates)
- 1 LFG for bacteria
- 9 inorganic CFFs for nutrients and gases (phosphate, nitrate, ammonium, silicate, dissolved iron, reduction equivalents, oxygen, carbon dioxide and dissolved inorganic carbon)
- 4 organic non-living CFFs for dissolved and particulate detritus.

The state variable nitrate is assumed to be the sum of both nitrate and nitrite. Reduction equivalents represent all the reduced ions produced under anaerobic conditions.

4.6 The BFM implementation in Sea Ice: BFM-SI

The new implementation of a sea ice system in the framework of BFM is directly derived from its theoretical basis. As a first implementation, the system is highly semplified and the chosen CFFs and LFGs are reduced. However, more subgroups may be easily included in future developments.

The new impelmentation (BFM-SI, Fig. 4.8) takes advantage of the same biological processes of the pelagic BFM. The focus is here on primary producers, which are assumed to differently adapt and acclimatize to the new physical enevironment and whose dynamics will be further described in the Sect. 4.7. For a complete review of the dynamics of other groups, see Vichi et al. (2007b).

The main differences between BFM and BFM-SI stand in the type and number of CFFs and LFGs, in the parameters assigned to several physiological and ecological processes (see Table 5.1) and in the dimensional form they represent. While pelagic state variables are expressed in terms of their constituent per cubic meters, the BFM-SI state variables are expressed in terms of constituent per square meters, due to the strategy of coupling described in Sect. 4.4.

BFM-SI totally resolves 28 state variables (Fig. 4.8 and Table 4.1) which are derived from new LFG and CFF:

- 2 different LFGs for sea ice algae (adapted diatoms and surviving sea ice algae, mostly represented by autotrophic nanoflagellates)
- 1 LFG for zooplankton
- 1 LFG for bacteria (aerobic and anaerobic)
- 6 inorganic CFFs for nutrients and gases (phosphate, nitrate, ammonium, silicate, oxygen and carbon dioxide)
- 2 organic non-living CFFs for dissolved and particulate detritus

As for BFM, nitrate is assumed here to be the sum of both nitrite and nitrate. All the nutrient:carbon ratios in chemical organic and LFGs are allowed to vary within their given range and each component has a distinct biological time rate of change. This kind of parametrizations are meant to mimic the adaptation of organisms to the diverse availability of nutrients and light observed in nature, and also allow to recycle organic matter depending on the actual nutrient content (Baretta et al., 1995; Vichi et al., 2003b).

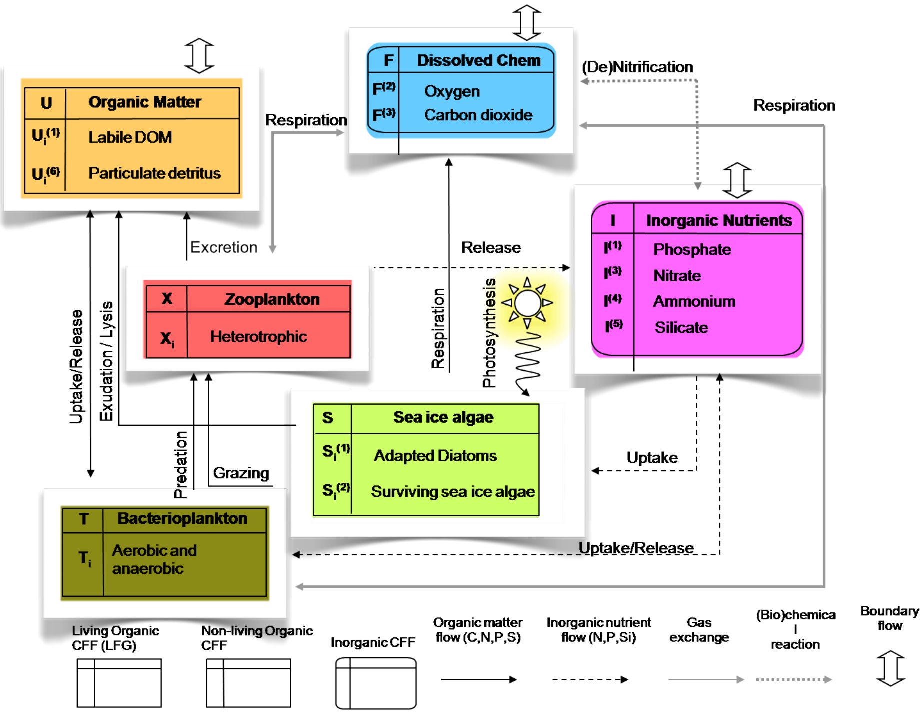

Figure 4.8: Scheme of the state variables and sea ice interactions of BFM-SI.

Each state variable interacts with the others through the universal physiological and ecological processes depicted in Fig. 4.8. Any biological reaction term is generally written in ecological modelling as an ordinary differential equation, holding the primitive biogeochemical processes on the right hand side. For instance, for a generic sea ice algae state variable S, the biological reaction term is literally written as:

$$\frac{dS}{dt} = Uptake - Exudation - Lysis - Respiration - Grazing \tag{4.1}$$

4.7 BFM-SI dynamics

As mentioned earlier, the focus is here on primary producers, while other LFG such as bacteria and zooplankton are currently only controlling and closing the sea ice food web and will not be described here. Hence, in this section the aim is to give an updated formulation of sea ice algae dynamics and, particularly, on some important reaction terms such as the gross primary production and chlorophyll rates of change. For a complete review of the other CFFs and LFGs dynamics in the pelagic system, see Vichi et al. (2007b).

Table 4.1: List of the Chemical Functional Family state variables (CFF, for a total of 28 prognostic equations) for BFM-SI.

Variable	Type	Components	# of CFFs	Description
$I^{(1)}$	IO	P	1	Phosphate (mmol P m^{-2})
$I^{(3)}$	IO	N	1	Nitrate (mmol N m^{-2})
$I^{(4)}$	IO	N	1	Ammonium (mmol N m^{-2})
$I^{(5)}$	IO	Si	1	Silicate (mmol Si m^{-2})
$F^{(2)}$	IO	O	1	Dissolved oxygen (mg C m^{-2})
$F^{(3)}$	IO	C	1	Carbon dioxide (mg C m^{-2})
$S_i^{(1)}$	LO	C N P Si Chl	5	Adapted diatoms (mg C m^{-2}, mmol N-P-Si m^{-2}, mg Chl-a m^{-2})
$S_i^{(2)}$	LO	C N P Chl	4	Surviving sea ice algae (mg C m^{-2}, mmol N-P m^{-2}, mg Chl-a m^{-2})
T_i	LO	C N P	3	Heterotrophic zooplankton (mg C m^{-2} , mmol N-P m^{-2})
X_i	LO	C N P	3	Bacteria (mg C m^{-2}, mmol N-P m^{-2})
$U_i^{(1)}$	NO	C N P	3	Dissolved organic detritus (mg C m^{-2}, mmol N-P m^{-2})
$U_i^{(6)}$	NO	C N P Si	4	Particulate organic detritus (mg C m^{-2}, mmol N-P-Si m^{-2})

Legend: IO = Inorganic; LO = Living organic; NO = Non-living organic. The subscript i indicates the basic components of the CFF, e.g. $S_i^{(1)} \equiv (S_c^{(1)}; S_n^{(1)}; S_p^{(1)}; S_s^{(1)}; S_l^{(1)})$.

4.7.1 Sea ice Algae

As a first implementation of the BFM in sea ice, 2 distinct subgroups have been chosen as representative of sea ice primary producers:

- Adapted diatoms, which are meant to be highly adapted to the environment and also show distinct skills in acclimatize. They are supposed to be first light-limited and, later in the bloom, dependent on nutrient availability. They have an Equivalent Spherical Diameter (ESD) of 20-200 μm and preyed by adult mesozooplankton (> 200 μm), which is not currently present in the sea ice system, but it acts externally in the pelagic BFM when sea ice melts and algae are released in the water column. They are also partially preyed by microzooplankton of larger dimensions (20-200 μm), which is instead present in BFM-SI as part of the sea ice zooplankton. Sea ice diatoms are the main source of biogenic silica and differ from the other subgroup being their growth limited by dissolved silicate.

- Surviving sea ice algae, which may be mostly represented by autotrophic nanoflagellates, are meant to only survive in the sea ice environment, being less adapted to it and showing less possibilities of acclimatization. However, they may be able to grow in sea ice if the diatoms bloom is quickly exhausted - for instance, for depletion of silicate - and a sufficient amount of nutrients is still available for their growth. Their ESD is 2-20 μm and are mainly preyed by sea ice microzooplankton.

Sea ice algae are involved in several processes: gross primary production (gpp), respiration (rsp), exudation (exu), cell lysis (lys), nutrient uptake (upt), predation (prd) and biochemical synthesis (syn). Both subgroups share the same form of primitive equations, but are differentiated in terms of the values of the physiological parameters (see further Table 5.1). There are 5 living CFFs that describe the constituents of sea ice algae (C, N, P, Si and Chl) and thus for each group we have 4 or 5 equations:

$$\frac{dS}{dt} = \left.\frac{dS}{dt}\right|^{gpp}_{F^{(3)}} - \left.\frac{dS_c}{dt}\right|^{exu}_{U_c^{(1)}} - \left.\frac{dS_c}{dt}\right|^{rsp}_{F^{(3)}} - \sum_{j=1,5} \left.\frac{dS_c}{dt}\right|^{lys}_{U_c^{(6)}} - \sum_{k=4,5} \left.\frac{dS_c}{dt}\right|^{prd}_{X_c^{(k)}} \tag{4.2}$$

$$\frac{dS_n}{dt} = \sum_{i=3,4} \left.\frac{dS_n}{dt}\right|^{upt}_{I^{(i)}} - \sum_{j=1,5} \left.\frac{dS_n}{dt}\right|^{lys}_{U_n^{(j)}} - \frac{S_n}{S_c} \sum_{k=4,5} \left.\frac{dS_c}{dt}\right|^{prd}_{X_c^{(k)}} \tag{4.3}$$

$$\frac{dS_p}{dt} = \left.\frac{dS_p}{dt}\right|^{upt}_{I^{(1)}} - \sum_{j=1,5} \left.\frac{dS_p}{dt}\right|^{lys}_{U_p^{(j)}} - \frac{S_n}{S_c} \sum_{k=4,5} \left.\frac{dS_c}{dt}\right|^{prd}_{X_c^{(k)}} \tag{4.4}$$

$$\frac{dS_s}{dt} = \left.\frac{dS_s}{dt}\right|^{upt}_{I^{(5)}} - \left.\frac{dS_s}{dt}\right|^{lys}_{U_s^{(6)}} - \frac{S_s}{S_c} \sum_{k=4,5} \left.\frac{dS_c}{dt}\right|^{prd}_{X_c^{(k)}} \tag{4.5}$$

$$\frac{dS_l}{dt} = \left.\frac{dS_l}{dt}\right|^{syn} - \frac{S_l}{S_c} \sum_{j} \left.\frac{dS_c}{dt}\right|^{prd}_{X_c^{(j)}} \tag{4.6}$$

4.7.2 Gross primary production and chlorophyll synthesis

The rate of change of carbon in sea ice algae depends on gross primary production, exudation, respiration, lysis and predation (Eq. 4.2). Here, the mathematical formulation of gross primary production is described, while the other terms are explained in Vichi et al. (2007b), replacing the names of the corresponding variables.

Gross primary production in Eq. 4.2 is the rate of change of sea ice algae carbon S_c due to photosynthesis, which involves an uptake of dissolved carbon dioxide $F^{(3)}$. It is written as:

$$\left.\frac{dS_c}{dt}\right|^{gpp}_{F^{(3)}} = f_S^T f_S^E f_S^s r_S^0 S_c \tag{4.7}$$

where the r_S^0 is the maximum specific photosynthetic rate under nutrient-replete, light saturated conditions. The f functions are multiplicative, non-dimensional regulating factors for temperature, light and silicate, which vary from 0 to 1.

Temperature is regulating several physiological processes. Its effect is expressed in a non-dimensional form by f_S^T:

$$f_S^T = Q_{10}^{\frac{T-10}{10}} \tag{4.8}$$

where Q_{10} is the characteristic doubling temperature parameter.

Many relevant biological processes, such as potential photosynthesis, are also affected by the non-dimensional light regulating factor f_S^E:

$$f_S^E = 1 - exp\left(-\frac{E_{PAR}}{E_K}\right) \tag{4.9}$$

where E_{PAR} is the Photosynthetic Available Radiation (PAR).

E_{PAR} is parametrized according to the Lambert-Beer formulation with depth-dependent extinction coefficients:

$$E_{PAR}(z) = \varepsilon_{PAR} F_{sw} e^{\lambda_{s,i} z + \int_z^0 \lambda_{bio} z' dz'} \tag{4.10}$$

where F_{sw} is the short-wave surface irradiance flux, which is computed by the physical model (ESIM2, Sect. 3.2) and it is converted from W m^{-2} to the units of μE m^{-2} s^{-1} with the constant factor 1/0.215 (Reinart et al., 1998). ε_{PAR} is the coefficient determining the portion of PAR in F_{sw}. Light propagation takes into account the extinction due to the background extinction of snow/sea ice $\lambda_{s,i}$ and due to suspended particles λ_{bio}, where:

$$\lambda_{bio} = \sum_j^2 c_S S_l^{(j)} + c_{U^{(6)}} U_c^{(6)}. \tag{4.11}$$

Thus, λ_{bio} takes into consideration the extinction due to sea ice algae chlorophyll and to particulate detritus, while dissolved substances and inorganic suspended matter are not currently taken into account. The c_S and c_U constants are the specific absorption coefficients of each suspended substance.

E_K is the light saturation parameter, that is the ratio between the maximum chl-*a* specific photosynthetic rate and the maximum light utilization coefficient, i.e.:

$$E_K = \frac{S_m^*}{\alpha^*} \tag{4.12}$$

where * stands for instantaneous values. As for pelagic phytoplankton of BFM:

$$S_m^* = f_S^T f_S^s r_S^0 \frac{S_c}{S_l} \tag{4.13}$$

$$\alpha^* = f_S^T f_S^s \alpha_{chl}^0 \tag{4.14}$$

where f_S^T is the regulating factor for temperature, f_S^s is the regulating factor for silicate, r_S^0 is the maximum specific photosynthetic rate under nutrient-replete, light-saturated conditions and α_{chl}^0 is the maximum slope of the production-irradiance curve at optimal conditions.

The f_S^s is parametrized as an external limiting factor with a Michaelis-Menten form:

$$f_S^s = \frac{I^{(5)}}{I^{(5)} + d_s} \tag{4.15}$$

where d_s is the Michaelis-Menten constant for SiO_2 uptake inhibition.

The chlorophyll rate of change of Eq. 4.6 is due to chlorophyll photosynthesis and losses due to grazing.

The net chlorophyll photosynthesis is a complicated function of acclimatisation to light conditions, nutrient availability and turnover rate. As in BFM, it is assumed here that nutrient-stressed cells that release substantial amount of dissolved organic matter tend to regulate their internal chl:C ratio as well.

Net photosynthesis is thus a direct function of gross carbon assimilation (excluded exudation) and chlorophyll losses due to mortality and total respiration:

$$\left.\frac{dS_l}{dt}\right|^{syn} = \theta_{chl}\left(\left.\frac{dS_c}{dt}\right|^{gpp}_{F^{(3)}} - \left.\frac{dS_c}{dt}\right|^{exu}_{U_c^{(i)}}\right) - \left(\left.\frac{dS_c}{dt}\right|^{rsp}_{F^{(3)}} + \left.\frac{dS_c}{dt}\right|^{lys}_{U_c^{(i)}}\right)\frac{S_l}{S_c} \tag{4.16}$$

The rate of change of net photosynthesis is thus primarily controlled by the dynamical chl:C ratio θ_{chl} proposed by Geider et al. (1998), which regulates the amount of chl-*a* in the cell according to a non-dimensional ratio between the realized photosynthetic rate in Eq. 4.2 and the maximum potential photosynthesis, i.e.:

$$\theta_{chl} = \theta_{chl}^0 \frac{f_S^E r_S^0 S_c}{\alpha_{chl}^0 E_{PAR} S_l} \tag{4.17}$$

where θ_{chl}^0 is the maximum quotum chl-*a*:C and $\alpha_{chl}^0$is the maximum slope of the production-irradiance curve at optimal growth conditions.

The ratio is down-regulated when the rate of light absorption (governed by the quantum efficiency and the amount of pigments themselves) exceeds the rate of utilization of photons for carbon fixation. The losses of chlorophyll are not explicitly taken into account in the model since currently there is not a chlorophyll component in detritus and dissolved organic matter. The same consideration applies to the ingested chlorophyll fraction in zooplankton.

4.8 The pelagic-sea ice interface

BFM-SI is also coupled to a simplified version of the BFM representing pelagic lower trophic levels in ice-covered oceans (Fig. 4.9). The living and nonliving organic and inorganic matter is exchanged between the ocean system and the sea ice system. In order to have a full mass conservation, the pelagic BFM described in Sect. 4.5 has been simplified in a way that every sea ice LFG and CFF has its own pelagic counterpart and there is no loss term between the two systems. The number of CFF and LFG is reduced and the total number of state variables computed are 34. The included groups and subgroups are:

- 2 LFGs for phytoplankton (diatoms and autotrophic nanoflagellates)
- 3 LFGs for zooplankton (omnivorous mesozooplankton, microzooplankton and heterotrophic nanoflagellates)
- 1 LFG for bacteria
- 9 inorganic CFFs for nutrients and gases (phosphate, nitrate, ammonium, silicate,oxygen, carbon dioxide)
- 2 organic non-living CFFs for dissolved and particulate detritus.

Differently to BFM-SI, the pelagic zooplankton includes 3 different subgroups. It is assumed that zooplankton accessibility to sea ice is reduced by their dimensions. Hence, only one group of generic microzooplankton is included in BFM-SI. However, zooplankton diversity is not limited in seawater and mesozooplankton may effectively control the fate of the sea ice algae release to water and the magnitude of the phytoplankton bloom. Consequently, the diversity of feeding behaviors of zooplankton is maintained and it is assumed that the sea ice zooplankton has its own counterpart in the pelagic heterotrophic nanoflagellates, while pelagic micro- and mesozooplankton are not able to be entrapped in the sea ice system.

The major communications between the sea ice and the pelagic systems are the fluxes of organic and inorganic matter at the interface. It is assumed that the entrapment of dissolved matter follows the same partitioning of salt in sea ice, that is the dynamics

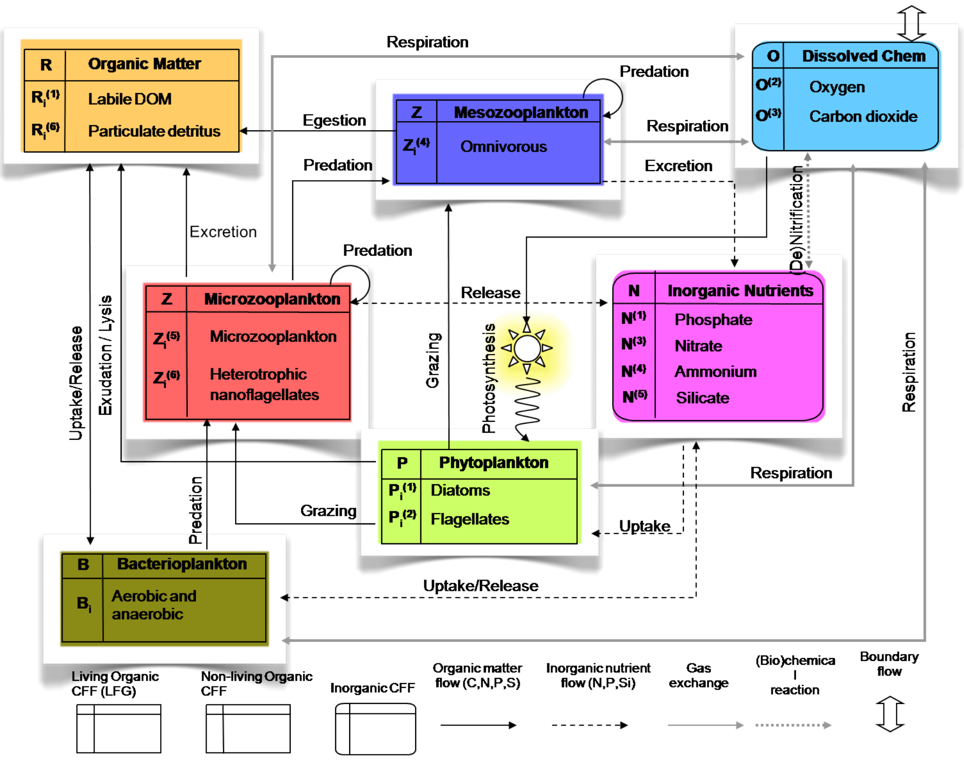

Figure 4.9: Scheme of the state variables and sea ice interactions of the pelagic BFM in the ice-covered ocean.

of dissolved matter is treated as the salinity dynamics (Sect. 3.2.1.2), considering the concentration of dissolved matter in seawater and sea ice growth rate.

The boundary fluxes are currently added as additional source terms to the biogeochemical equations and solved explicitly. For instance, in the case of an inorganic nutrient in sea ice (e.g. nitrate, $I^{(3)}$), the complete equation is written as

$$\frac{dI^{(3)}}{dt} = \left.\frac{dS_n^{(1)}}{dt}\right|_{I^{(3)}}^{upt} + \left.\frac{dS_n^{(2)}}{dt}\right|_{I^{(3)}}^{upt} + \left.\frac{dI^{(3)}}{dt}\right|_{N^{(3)}}^{flux} \tag{4.18}$$

where the first two terms on the right hand side represent the uptake from sea ice algae and the last one is the flux of nutrient at the boundary with pelagic nitrate.

Fluxes are defined positive towards the sea ice according to the convention of Fig. 4.3). The nitrate flux is described here as an example of inorganic component. The flux is composed of a positive part (entrapment) during sea ice formation when sea ice growth (Eq. 2.10) is positive, and of a negative part during the melting phase:

$$\left.\frac{dI^{(3)}}{dt}\right|_{N^{(3)}}^{flux} = \max\left(0,\frac{\partial h_i}{\partial t}\right)\max\left(0, N^{(3)}h_{bio} - I^{(3)}\right) + \min\left(0,\frac{\partial h_i}{\partial t}\right) I^{(3)} \tag{4.19}$$

where $N^{(3)}$ is the nitrate concentration in seawater, h_i is the ice thickness and h_{bio} is the thickness of the BAL. The same flux, converted into units of volume concentration, is added to the dynamical equation for pelagic nutrients. When ice starts melting, the release to the water column depends only on the sea ice melting rate and on the sea ice concentration.

The entrapment of particulate matter is assumed to be only a function of the seawater concentration, the sea ice growth rate and the actual available space (BAL brine volume, V_{bio}, Sect. 4.3). For instance, the flux of the chlorophyll component of sea ice algae $S_l^{(1)}$, from the pelagic variable $P_l^{(1)}$ to sea ice is defined as:

$$\left.\frac{dS_l^{(1)}}{dt}\right|_{P^{(1)}}^{flux} = \max\left(0, \frac{\partial h_i}{\partial t}\right) P_l^{(1)} V_{bio} + \min\left(0, \frac{\partial h_i}{\partial t}\right) S_l^{(1)}. \tag{4.20}$$

where the release during the melting phase is parametrized as in (4.19).

4.9 Summary

As a first approximation, bottom communities represent the largest biomass found in sea ice. Despite the low-light availability, bottom communities experience environmental conditions similar to those of seawater (temperature and salinity) and the availability of nutrients and gases is ensured by the continuous physical connection of brines with seawater. Those considerations have brought to the development of the novel concept of Biologically-Active-Layer (BAL). While the previous attempts of modelling sea ice biogeochemistry prescribed the fraction of sea ice where biology was computed, the BAL is instead time-varying, its thickness depending on the ice permeability. This ensures a more realistic approach and a useful tool for the coupling of sea ice physical and biological processes.

A novel implementation of a sea ice ecosystem in the frame of an already existing and comprehensive biogeochemical flux model (BFM) has been presented. The new biogeochemical flux model in sea ice (BFM-SI) is directly derived from it and takes the advantage to include the same, already developed and tested, dynamics. BFM is a biomass-based model, which includes several Chemical Functional Families (CFF) and Living Functional Groups (LFG), together with several biological processes which relate every constituent to the others in the system.

The new BFM in sea ice is coupled to a pelagic counterpart in the ocean holding the same functional groups, except for zooplankton, which is size-limited in sea ice, but not in seawater, where larger zooplankton live.

This is the first sea ice biomass-based ecosystem model of higher complexity. Its skills will be further analyzed in the next chapter.

Chapter 5

Biogeochemistry of ice-covered oceans: numerical simulations[1]

The real voyage of discovery consists
not in seeking new landscapes
but in having new eyes.

(Marcel Proust)

---

[1] This chapter is partially based on Tedesco et al. (2009b) and Tedesco and Vichi (2009)

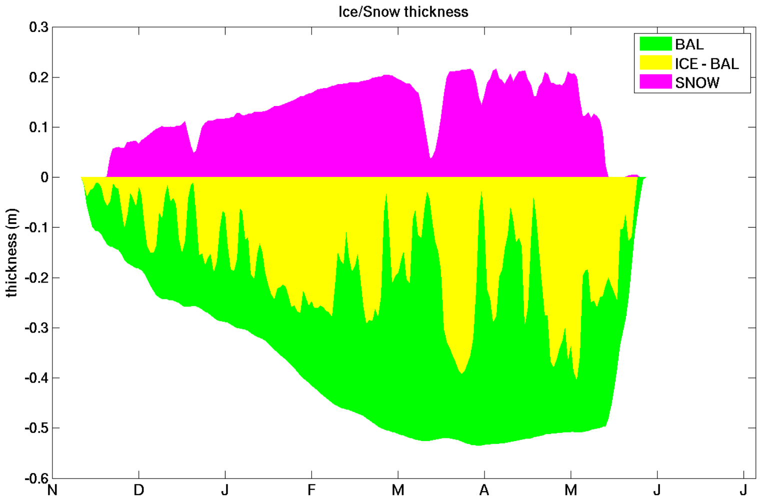

Figure 5.1: ESIM2 thicknesses during the ice season 2005-2006 at Kobbefjord (magenta, snow; green, BAL; yellow, ice non-BAL).

5.1 BFM-SI set-up

Numerical simulations of sea ice biogeochemistry were done at two different sites during two different ice seasons where ESIM2 physical model results are good (Sect.3.2).

The first chosen site for model calibration and comparison represents a less rich and productive Arctic site, Kobbefjord (Mikkelsen et al., 2008). The second test-case site is a typical rich and productive coastal site, Santala Bay in the Baltic (Kaartokallio, 2004; Granskog et al., 2003a). These regions represent two possible cases found in ice-covered regions and the model applications presented in this section demonstrate the generality of the parametrizations.

5.1.1 BAL environmental variables

As mentioned earlier in Sect. 4.3, the strategy of coupling stays in the ability of ESIM2 (Sect. 3.2) to compute the mean key physical properties of the sea ice BAL (thickness, temperature, bulk salinity, irradiance, brine volume and salinity), which are passed to BFM-SI. This is currently done as an off-line coupling. However, the system is set up to run with a complete on-line coupling.

An overview of the physical properties at the Kobbefjord site during the ice season 2005-2006 is given in Fig. 5.1 (see also Sect. 3.2). All the BAL environmental variables relevant to the biogeochemical processes are presented in Fig. 5.2.

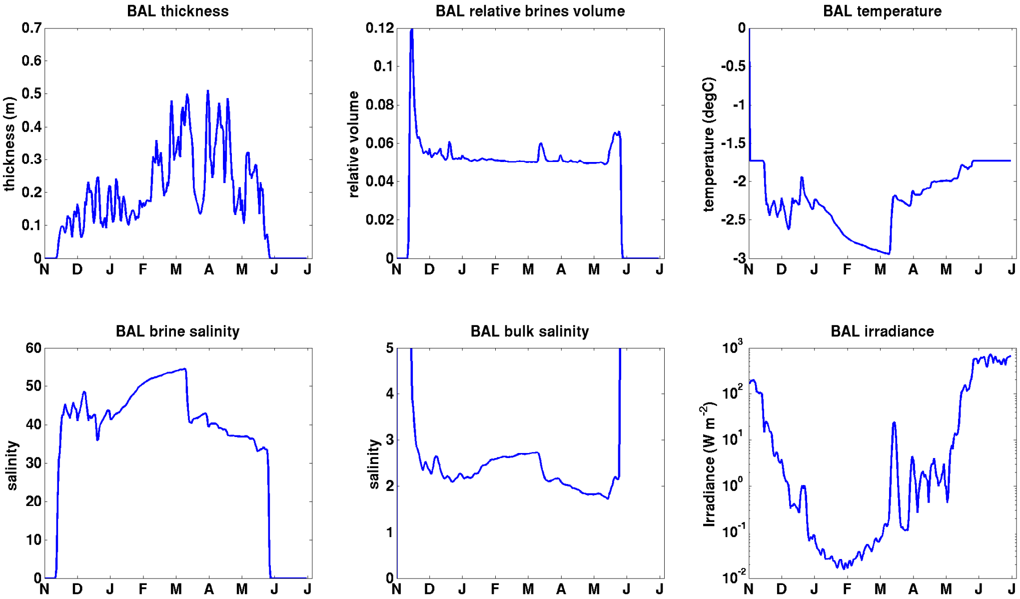

Figure 5.2: BAL environmental variables at Kobbefjord during the ice season 2005-2006. From left above, clockwise: thickness, brine volume, temperature, irradiance, bulk salinity and brine salinity.

The thickness of the BAL (upper left panel of Fig. 5.2) increases during the ice season reaching a maximum of about 0.5 m at the beginning of March, when sea ice becomes almost completely permeable from top to bottom (Fig. 5.1). After this period, a sudden melting of snow (Fig. 5.1) causes a large flushing of zero-salinity water, which dramatically reduces the thickness of the BAL at the end of March. Later, the BAL thickness increases again in April. Sea ice starts melting in May and the BAL thickness is reduced until the end of the sea ice season.

The average brine volume of the BAL always stays larger than 5% (upper middle panel of Fig. 5.2), as this is the major assumption for the existence of the BAL. When ice starts forming in November and the BAL thickness is still small, the mean brine volume is large, greater than 10% of total ice volume. A slightly increase is also noticed at the end of the ice season, in May, when the BAL thickness is again small and ice is warmer.

The temporal evolution of the BAL temperature is also shown (Fig, 5.2, upper right panel). There is an initial steep drop of the BAL temperature, due to thin layers of snow and sea ice, which mitigates the atmospheric cooling. After a thick slab of snow covers sea ice, the temperature continues to decrease, though more slowly, until reaching a minimum

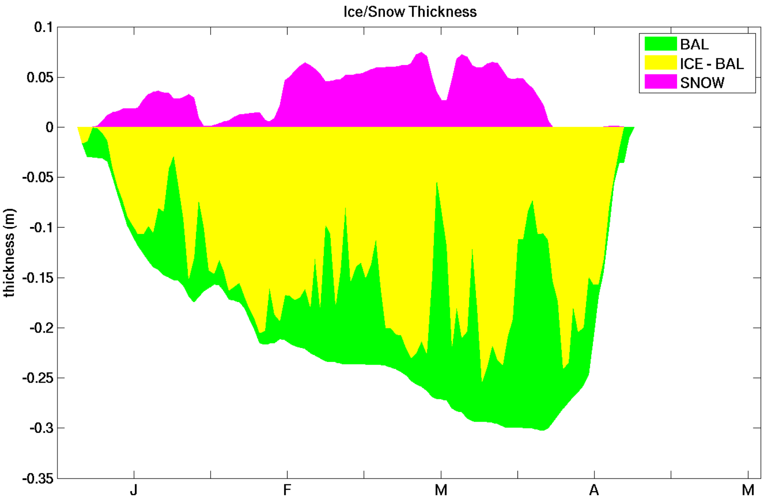

Figure 5.3: ESIM2 thicknesses during the ice season 1999-2000 at Santala Bay (magenta, snow; green, BAL; yellow, ice non-BAL).

temperature of about -3 °C in March, when snow has almost completely melted away. Afterward, the BAL temperature increases, first more rapidly when snow covers sea ice, later more slowly when ice starts melting and until the end of the ice season.

Brine salinity is a linear function of ice temperature in the model (Eq. 3.1). Consequently, the temporal evolution of the BAL brine salinity (lower left panel of Fig. 5.2) is a direct consequence of the temporal evolution of the BAL temperature. Initially, the BAL brine salinity is about 40 and when the BAL gets colder, brine salinity increases till reaching a maximum salinity of 57 in March. It is followed by a fast decrease due to flushing and a slow decrease until the end of the ice season.

The BAL bulk salinity ranges between 2 and 3 (Fig. 5.2, lower middle panel). The BAL salinity is higher at the beginning of the season when the salt entrapment plays a major role. Later, when BAL thickness has increased, gravity drainage causes a decrease in salinity. During March, lower salinity values are also enhanced by the sudden flushing of snow. The flushing effect during the melting season (from April to May) is balanced by the increase in temperature, which has the opposite effect of increasing salinity. Consequently, the BAL salinity continues to increase until late May. When the BAL temperature is almost stabilized at the freezing temperature, bulk salinity continues to decrease owing to the desalination effect of flushing, which is the only important physical process left.

The mean irradiance of the BAL (Fig. 5.2, lower right panel , logarithmic scale) represents a typical pattern of the polar winter irradiance. There is a decrease of irradiance

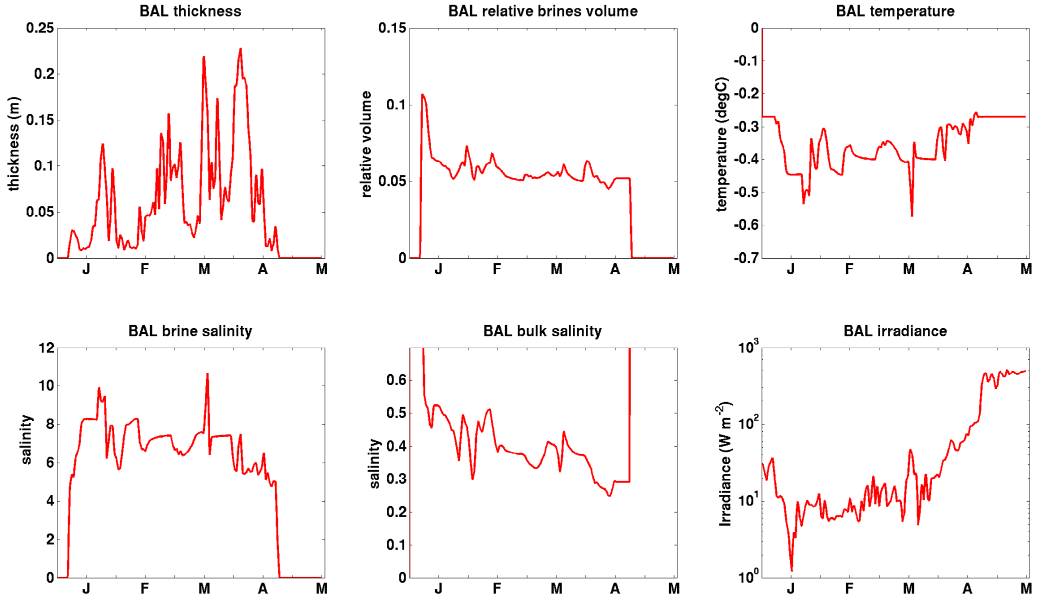

Figure 5.4: BAL environmental variables at Santala Bay during the ice season 1999-2000. From left above, clockwise: thickness, brine volume, temperature, irradiance, bulk salinity and brine salinity.

since the beginning of the ice season, due to the reduced incident short-wave radiation and also to the thickening of the BAL. The increase of available light occurs in March, when a sudden melt of the snow cover allows more incident light to penetrate sea ice. After that, the BAL irradiance continues increasing until the end of the ice season.

The temporal evolution of the snow and ice layers at Santala Bay during the ice season 1999-2000 is shown in Fig. 5.3 (Sect. 3.2). The BAL environmental variables of Santala Bay are presented in Fig. 5.4.

The thickness of the BAL is more variable (upper left panel of Fig. 5.4) with respect to Kobbefjord (Fig. 5.3), due to the very mild winter of 1999-2000 which caused air temperature to often exceed 0°C and consequently snow and ice melted and refreezed several times. The BAL reaches its maximum thickness at the end of February, and again at the end of March.

As in Kobbefjord, at the beginning of the ice season, the mean brine volume (Fig. 5.4, upper middle panel) is large, due to warmer ice and reduced thickness of the BAL. Then, the mean brine volume is about 6 % throughout all the ice season.

BAL temperature was also highly variable (Fig. 5.4, upper right panel), ranging between -0.27 and -0.50 °C during all the season. Ice got colder when snow cover was reduced (Fig. 5.3) and sea ice was more exposed to the atmosphere temperature.

The BAL brine salinity (lower left panel of Fig. 5.4) follows a similar pattern as temperature, oscillating throughout the season between 5 and 10. Higher brine salinity values are also found during periods when ice is almost snow-free and colder, as at the beginning of March.

The BAL bulk salinity (lower middle panel of Fig. 5.4) shows, instead, peculiar patterns. Initial ice growth is low, and consequently the effect of the salt entrapment is small, keeping BAL bulk salinity around 0.4-0.5. Later, also the effect of gravity drainage is not very evident. Even though gravity drainage is meant to desalinate sea ice, the thickness of the BAL starts increasing at the same time, that is more salt is redistributed in the BAL layer. Snow flushing is almost irrelevant in this case and sea ice flushing is low owing to the small thickness of sea ice. Even the small increase in the BAL temperature since March does not significantly affect mean bulk salinity. Consequently, the BAL bulk salinity increases throughout the season, following the increase and decrease of the BAL thickness.

The BAL irradiance (Fig. 5.4, lower right panel, logarithmic scale) is much higher than found at Kobbefjord, due to the smaller thickness of the snow and ice layers. The minimum of irradiance is reached in January. Afterward, mean irradiance slowly increases until the end of the ice season.

5.1.2 Model comparison and calibration

Model calibration has been based on the visual comparison between chlorophyll values obtained by sampled ice cores at Kobbefjord and Santala Bay (Mikkelsen et al., 2008; Kaartokallio, 2004) and model simulations of total chlorophyll content in sea ice algae at both sites. Chlorophyll was chosen as the target CFF for model calibration since its synthesis is the final result of several biological processes (see Eq. 4.16).

The comparison between model results and ice core values needs to be carefully addressed. BFM-SI computes biological processes of a time-varying sea ice layer (BAL). Biological samples are instead measured in ice core sections, whose thickness is typically 0.1 m. The BAL concept assumes that all the active sea ice biology is placed within it, excluding internal and surface communities. Thus, model outputs in terms of concentration and biomass should give results ranging from values of the last section of the ice core (bottom section) and values of the total ice core. In the following analysis, both information will be given: model results will be compared with values of the lowest ice section and values of the total ice core.

The main attention for calibration purposes has been put on the adaptation of sea ice

Table 5.1: Values and description of the sea ice algae parameters used in the reference simulation of BFM-SI after visual calibration.

Symbol	$S^{(1)}$	$S^{(2)}$	Description
$r0_S$	1.5	2.0	Maximum specific photosynthetic rate (d^{-1})
$Q10_S$	2.0	2.0	Characteristic Q10 coefficient (-)
θ^0_{chl}	0.035	0.03	Optimal quotum chl-a:C (mg chl mg C^{-1})
α^0_{chl}	5.8 e^{-4}	3.8 e^{-6}	Maximum light utilization coefficient (mg C (mg chl)$^{-1}$ $\mu E^{-1} m^2 s$)
Q^s_{S1}	0.1	-	Half saturation value for Si-limitation (mmolSi m^{-2})
b_S	0.05	0.1	Basal specific respiration rate (d^{-1})
γ_S	0.1	0.1	Activity respiration fraction (-)
α_S	0.05	0.2	Excreted fraction of primary production (-)
$d_S^{p,n,s}$	0.1	0.1	Nutrient stress threshold (-)
d_{0S}	0.5	0.5	Specific lysis rate (d^{-1})
λ_1	2.5 10^{-3}	5.0 10^{-3}	Specific affinity for P (mgC^{-1} d^{-1})
λ_3	2.5 10^{-3}	2.5 10^{-3}	Specific affinity for N-NO3 (mgC^{-1} d^{-1})
λ_4	2.5 10^{-2}	2.5 10^{-2}	Specific affinity for N-NH4 (mgC^{-1} d^{-1})
s_{S1}^{max}	0.03	-	Standard Si:C ratio in diatoms (mmol Si mg C^{-1})
Rr_c^n	1.26 10^{-2}	1.26 10^{-2}	Reference nutrient quota for N (Redfield, mmol N mg C^{-1})
Rr_c^p	7.86 10^{-4}	7.86 10^{-4}	Reference nutrient quota for P (Redfield, mmol P mg C^{-1})
n_S^{min}	0.5 Rr_c^n	0.5 Rr_c^n	Minimum nutrient quota for N (mmol N mg C^{-1})
p_S^{min}	$0.5Rr_c^p$	$0.5Rr_c^p$	Minimum nutrient quota for P (mmol P mg C^{-1})
n_S^{max}	2 Rr_c^n	2 Rr_c^n	Maximum nutrient quota for N (mmol N mg C^{-1})
p_S^{max}	$2Rr_c^p$	$2Rr_c^p$	Maximum nutrient quota for P (mmol P mg C^{-1})

algae to a low-light environment. In fact, bottom communities experience environmental conditions similar to those of seawater in terms of salinity and temperature (e.g., Arrigo, 2003). However, the availability of PAR is highly reduced comparing to non-ice-covered regions. Main differences between different groups of sea ice algae in terms of their adaptation concern their regulation of productivity, light harvesting mechanisms and chl:C ratio. Those are represented in BFM-SI by the following parameters: maximum specific growth rate, maximum light utilization coefficient and optimal chl:C quotum, respectively (see Eq. 4.17).

Several experiments were performed for both sites and the outcome of the calibration is a new set of parameters for sea ice algae (Table 5.1) and two reference simulations (Fig. 5.5 and Fig. 5.6). The sensitivity of biological rates to environmental parameters is analyzed in Sect. 5.2.

At Kobbefjord total chlorophyll stays low during all winter season as also found in the observations (Fig. 5.5, lower panel). The first increase occurs in March, coincident with

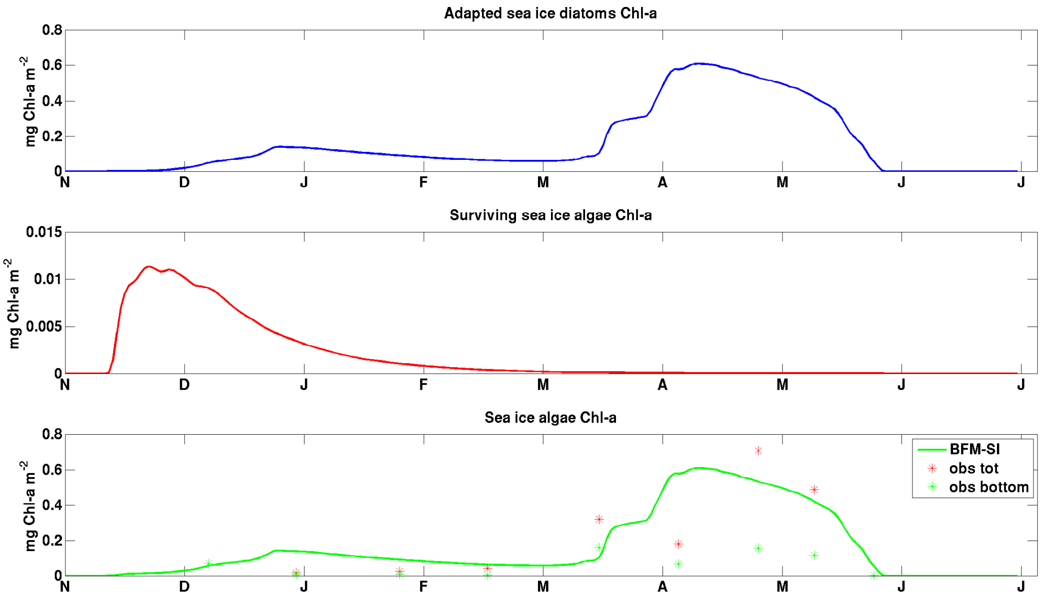

Figure 5.5: BFM-SI chlorophyll of sea ice algae (from above: diatoms, survivors and total chlorophyll) compared with observations at Kobbefjord during the ice season 2005-2006.

an increase in irradiance due to snow melt (see Fig. 5.1 for snow thickness and Fig. 5.2, lower right panel for irradiance levels). A second and higher peak occurs later in April, when sea ice is very thin and the penetrating light is almost at the same level as later on when sea ice has totally melted away. Adapted sea ice diatoms (Fig. 5.5, upper panel) shows low concentration of chlorophyll during wintertime. Later, they respond to the increase in light availability and are the main responsible of both blooms. Surviving sea ice algae (Fig. 5.5, middle panel) experience a high initial mortality rate once entrapped in sea ice, and do not show any form of acclimation, that is their chlorophyll content remains at the minimum throughout the season.

The temporal evolution of chlorophyll at Santala Bay during the specific ice season is a less typical pattern for polar biology in winter sea ice. Light is never limiting since the beginning of the sea ice season and throughout all winter, due to thin layers of snow and ice, as also stated by Granskog et al. (2003a) and Kaartokallio (2004). Total chlorophyll content (Fig. 5.6, lower panel) increases since the beginning of ice formation. The first increase is already reached in January, followed by a second one at the beginning of February and a last peak at the beginning of March. Mainly sea ice diatoms are responsible for the chlorophyll blooms (Fig. 5.6, upper panel). However, also surviving sea ice

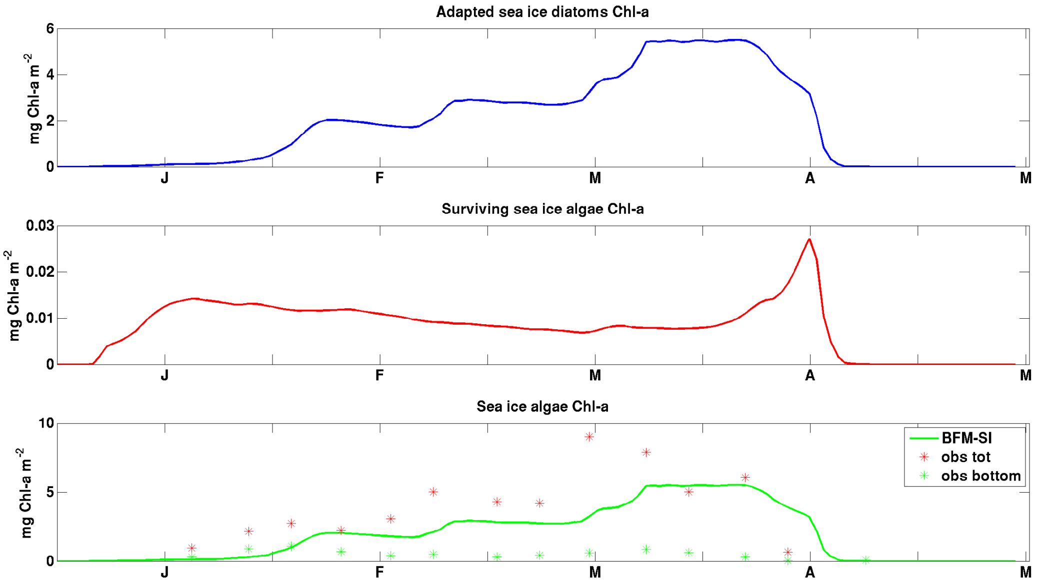

Figure 5.6: BFM-SI chlorophyll of sea ice algae (from above: diatoms, survivors and total chlorophyll) compared with observations at Santala Bay during the ice season 1999-2000.

algae (Fig. 5.6, middle panel) contributes, even though at a lesser degree, in late March when the diatom abundance is lowering. This clearly shows that all sea ice algae, which are able to survive the polar winter in sea ice, have the potentiality of blooming. The starting and the magnitude of the bloom depend on environmental conditions, nutrient availability and competition with other groups. Flagellates require higher light intensities compared to adapted diatoms and may take advantage, as in this case, of the fact that diatom abundance is lowering to start competing with them.

5.2 Physical controlling factors

In next subsections the most important features of the BAL environmental variables and their influence on the biological community will be analyzed. The Kobbefjord reference experiment (Fig. 5.5), whose physical properties of the BAL were shown in Sect. 5.1.1, will be used for analyzing the sensitivity to relevant physical controlling factors of BFM-SI. There is currently no feedback of the biogeochemistry on the physics, such as the contribution of the biomass of the sea ice community to the melting process. This may be added in future developments when a full two-way coupling is implemented between the physics and the biogeochemistry of sea ice.

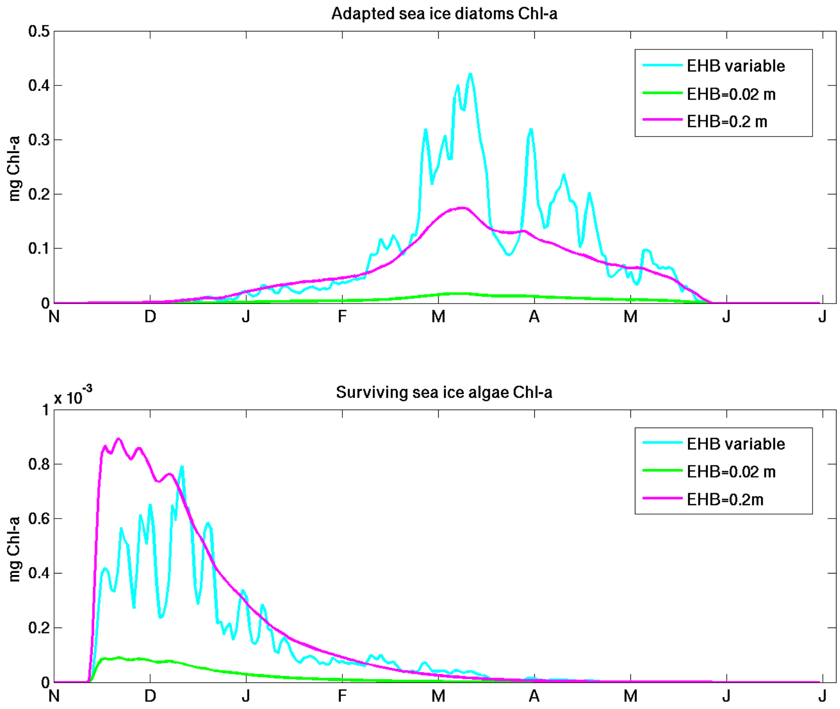

Figure 5.7: Comparison among the chlorophyll content of diatoms (above) and survivors (below) in a time-varying sea ice layer (BAL) with prescribed fractions of sea ice (0.02 and 0.2 m).

5.2.1 Space

Sea ice algae need to be in continuous connection with seawater in order to receive a sufficient amount of dissolved gases and nutrients to sustain grow. It is assumed that a brine volume smaller than 5% prevents brine pockets and channels to be interconnected, and thus the survival of any living organism. From this considerations, it evolved the concept of Biologically-Active Layer (BAL). During the growth period, ice gets thicker and colder and brine volume stays smaller. When sea ice starts melting, sea ice becomes warmer and brines larger. However, the flushing from above of quasi-zero salt water, desalinates sea ice, also reducing the brine volume.

In some previous attempts to model sea ice biogeochemistry the fraction of sea ice where biological processes were considered was prescribed (e.g. 0.02 m for the studies of Jin et al., 2006 at Point Barrow, Alaska). Arrigo (2003) also reported that the highest algal biomass is found in the bottom 0.2 m of Antarctic sea ice. Without any information on the physical properties of sea ice at different latitudes and under different forcing conditions, it would be very hard to realistically prescribe the fraction of sea ice which is biologically-active. The concept of the BAL not only allows to study the temporal evolution of the BAL thickness, but it also ensures a more realistic approach, which is based on physical formulations. Moreover, the melting of ice at the ice-water interface cause an irreversible loss of habitat (biological loss) and immediate termination of the bloom, since algae are released to the water column (Lizotte, 2003), where they may eventually seed the following phytoplankton bloom (e.g., Smith and Nelson, 1985) or sink rapidly down to the bottom of the ocean (e.g., Riebesell et al., 1991).

Fig. 5.7 shows the differences between the vertically integrated mass of chl-*a* of the two subgroups of sea ice algae (diatoms and survivors) computed by considering a time-varying thickness (the BAL, Fig. 5.2, upper left panel) and two different prescribed thicknesses (0.02 m and 0.2 m). The variable BAL results are taken as reference since they were compared with observations (Sect. 5.1).

Assuming a BAL thickness of 0.02 m, biomass is highly underestimated, while in the second case (BAL thickness of 0.2 m) is slightly overestimated. Besides, a prescribed thickness of 0.2 m would highly underestimate the total chl-*a* content of diatoms during the period when the BAL thickness is at its maximum (March, Fig. 5.7, upper panel) and would overestimate the chl-*a* content of survivors at the beginning of the sea ice season (December, Fig. 5.7, lower panel).

5.2.2 Salinity and Temperature

The concept of BAL assumes that the distribution of living and non living matter extends from the bottom of sea ice upward till ice is permeable. The first implementation, in fact, does not include surface and internal communities. No salinity dependence is thus currently assumed, while temperature is regulating several physiological processes. Its effect is expressed by the non-dimensional f_S^T factor (Eq. 4.8).

The characteristic Q_{10} parameter (Eq. 4.8 and Table 5.1) affects several biological processes: primary production, respiration and uptake of nutrients. In order to understand the sensitivity of the model to different Q_{10} values, Fig. 5.8 shows how the chlorophyll content in primary producers at Kobbefjord site would be affected by a Q_{10} value, half and double the reference one (2.0, Table 5.1).

A Q_{10} value of 1.0 causes higher production in both algae groups, but also an earlier bloom followed by an earlier decrease. On the other hand, a Q_{10} value of 3.0 would cause a later bloom and a later decrease for both diatoms and survivors. As expected, temperature is a sensitive parameter and a proper estimation of Q_{10} values from natural

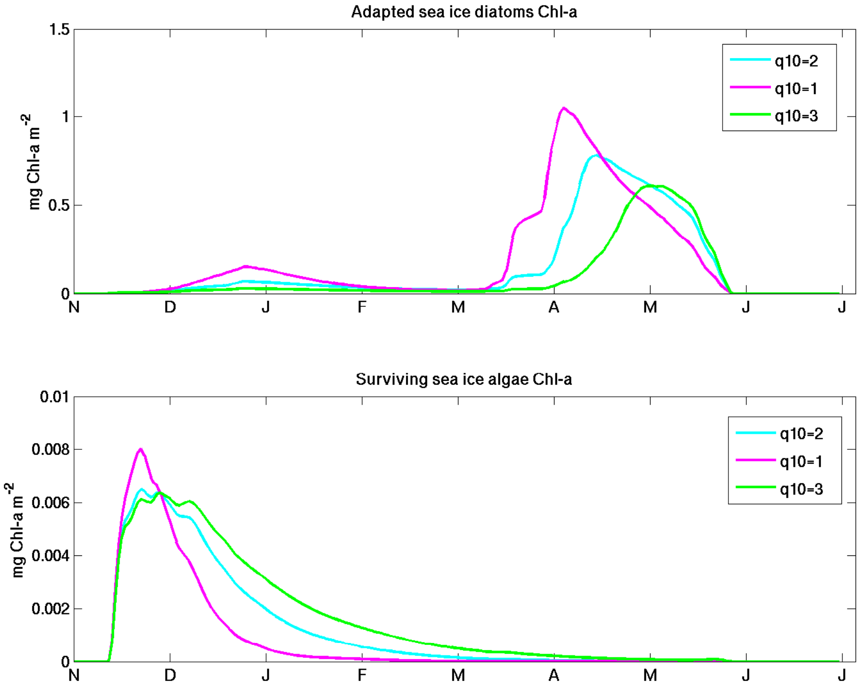

Figure 5.8: Sensitivity of BFM-SI diatoms (above) and survivors (below) to temperature dependence.

sea ice algae populations is important.

5.2.3 Light

Light is fundamental for primary producers and the energy source for photosynthesis is the under-ice transmitted amount of the incident solar radiation reaching the sea surface, penetrating the snow cover, if present, and sea ice. Phytoplankton and sea ice algae can adapt to low light intensity by increasing the size and/or the number of photosynthetic subunits. Sensitivity experiments have shown that manipulating the amount of snow cover result in different species composition in the bottom algae communities (Grossi et al., 1987). In general, small cells are present in surface communities, while larger cells reside in the internal and bottom communities (Arrigo et al., 1993) since higher intracellular pigment concentrations are present. An additional adaptation has been found in diatoms that inhabit the platelet ice layer of McMurdo Sound ice and release an “ice-active substance” that pits on the surface of ice crystals and thus increases the light scattering (Raymond et al., 1994).

Respect to other sea ice parameters, α^0_{chl} (Eq. 4.17 and Table 5.1) has been found to be the most important. While bottom communities experience environmental conditions similar to those of seawater in terms of temperature and salinity, the light availability is highly constrained by the thickness of the snow and ice cover. The α^0_{chl} value represents the initial primary producers response to the increase in light availability. A large value indicates (genotypic) adaptation to low-light intensities, while algae characterized by a small value require more photons and tend to grow later in the season. In BFM-SI, adapted sea ice diatoms are meant to grow at low-light intensities, while surviving sea ice algae need a bigger amount of available light to start photosynthesis.

Fig. 5.9 shows how the chlorophyll content in primary producers at Kobbefjord site would be affected by α^0_{chl} values which are an order of magnitude bigger and an order of magnitude smaller than the calibrated values for every subgroup (Table 5.1). Beside the fact that bigger values causes an earlier and more extensive bloom in both groups, it is interesting to notice the different behavior of diatoms and flagellates in their response to the availability of light. While nanoflagellates would be better competitors at the beginning of the sea ice season if they were as much adapted as diatoms to low light intensities (α^0_{chl}= 3.8 e-5 mg C (mg chl)$^{-1}$ μE^{-1}m^{2}s), diatoms would react later to the increasing light availability in the season, indicating slower response but higher photosynthetic efficiency.

5.2.3.1 The role of snow

Snow on sea ice plays many relevant roles. From a biological point of view, the higher light extinction coefficient (15-25 m^{-1}) with respect to sea ice (1-4-1.6 m^{-1}) leads to stronger light-limitation.

ESIM2 is capable to properly simulate the thickness of the snow layer and the amount of light reaching the BAL thanks to the parametrization of snow accumulation, compaction and transformation. In comparison with ESIM1, ESIM2 embeds more complex snow dynamics (Sect. 3.1).

This section presents the comparison between the results of BFM-SI forced with the snow physics of ESIM1 (Sect. 2.2 and Tedesco et al., 2009a) and with the snow physics of ESIM2 (Sect. 3.1) at Kobbefjord. The aim of this experiment is to understand the role of snow on sea ice biology and also to test if there is any improvement in terms of biological results.

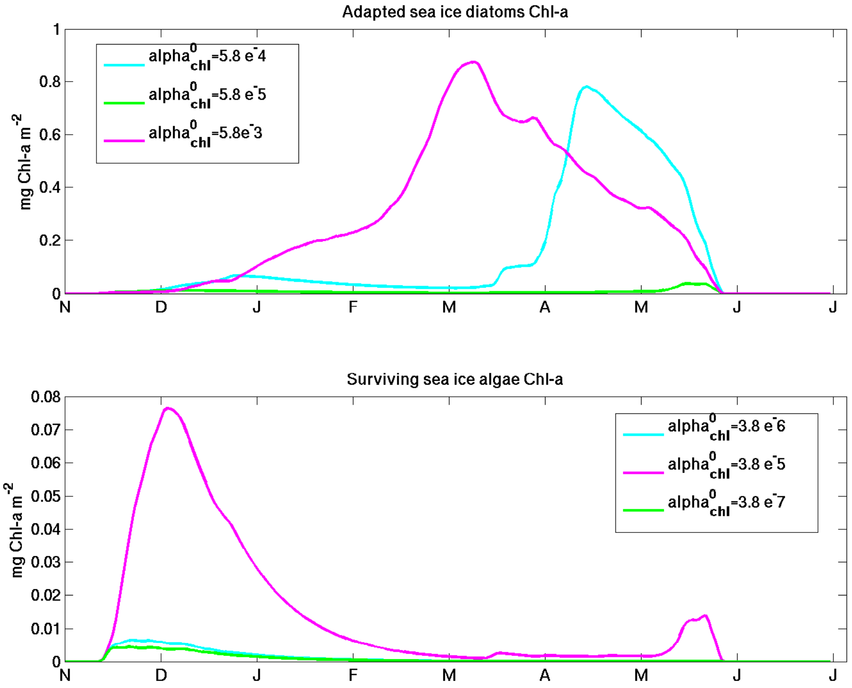

Figure 5.9: Sensitivity of BFM-SI diatoms (above) and survivors (below) to α^{0}_{chl} (maximum light utilization coefficient) values.

The temporal evolution of the snow layer (Fig. 5.10, upper panel) shows that ESIM2 better fits with the observations. In particular, ESIM2 is able to well simulate the fast snow melting during March, while with ESIM1 snow melts later and to a minor extent.

From a biological point of view, the capability of the physical model to properly reproduce the snow cover is important, especially when the snow layer is very thin. An experimental study from Grossi et al. (1987) showed that under-ice irradiance is strongly attenuated when the snow cover exceeds 0.1 m. They also noticed that algae blooms occur later and total production is more than halved when snow covers are thicker.

Similar results are obtained in this experiment. BFM-SI total chlorophyll coupled to the snow physics of ESIM1 and ESIM2 (Fig. 5.10, lower panel) is of the same order of magnitude for both simulations (about 0.6 mg chl-*a* m^{-2}). However, sea ice algae starts growing about 1 month earlier if the physical forcing of the model is provided by ESIM2 and BFM-SI results better fit with the timing of the bloom found in the observations. Afterward, the timing of the end of the bloom is similar in both simulations (end of May). In summary, the visual comparison of the integrated chlorophyll over time tells us that sea ice algae of BFM-SI coupled to ESIM1 have about half of the chlorophyll content with respect to the coupling with ESIM2.

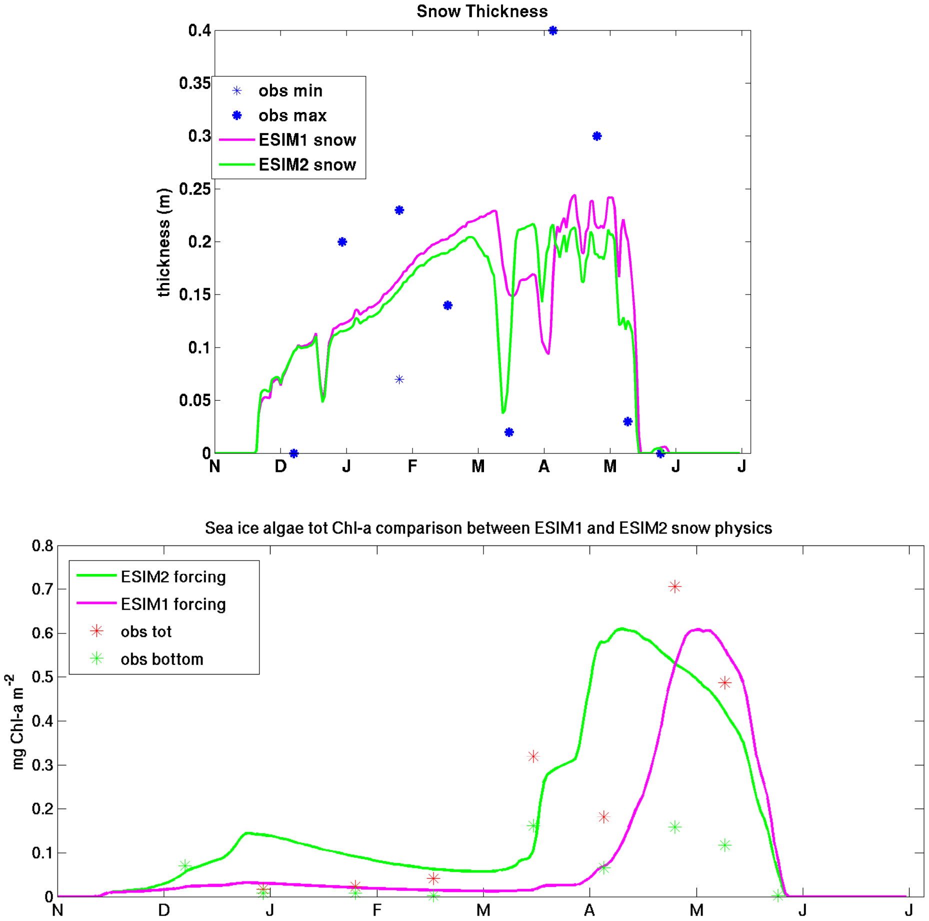

Figure 5.10: Comparison between ESIM1 (magenta) and ESIM2 (green) snow physics (above) and consequent sea ice algae chlorophyll simulations of BFM-SI (below).

5.3 Biological controlling factors

The most important biological controlling factors for sea ice algae to grow are the nutrient supply and grazing pressure.

Ice algae can potentially be grazed in the ice matrix by large protozoa, such as ciliates and flagellates, metazoa, such as nematodes, and amphipods especially in shallow water areas (Welch and Bergmann, 1989). Copepods also feed on cells sloughed off the ice. Reasonable assessment of grazing rate is, to date, not yet achieved; consequently, the grazing rate is usually considered a constant fraction of the ice algal growth rate (e.g. 10%). Better parametrization includes a smaller grazing rate in the first half part of the bloom and a bigger grazing rate in the later part, when enlargement of brine channels allow larger animals to graze in the ice matrix (Lavoie et al., 2005).

One of the LFG of BFM-SI is zooplankton. Currently this group has characteristics similar to those that of microzooplankton. It feeds mostly on small cells, such as flagellates, while only in absence of available smaller-size food, it may partially feed on larger cells, such as diatoms. Hence, there is no currently a strong control of zooplankton on sea ice algae, also due to insufficient knowledge on the space required by zooplankton to access sea ice at different stages of the ice season. However, an important role is played by pelagic zooplankton on controlling the phytoplankton bloom but also viable sea ice algae in the water column (see also Sect. 5.5 on the fate of the sea ice biomass).

In the rest of the section the second important biological controlling factor - nutrients supply - will be analyzed in detail.

5.3.1 Nutrients supply

Nutrients supply for algal growth are coming from the mixed layer up to the ice sheet for sustaining bottom communities, but also from snow deposition through brine drainage for surface communities and from *in situ* regeneration processes.

Even in isolated brine pockets bacteria, heterotrophic protozoa and small metazoans have shown to regenerate the mayor nutrients (Arrigo et al., 1995), but not silicate. Silicate dissolution and regeneration may be slower than demand and can be the major limiting factor for diatoms growth (Lizotte and Sullivan, 1991), shifting the community from being diatom-dominated to flagellates-dominated (Dieckmann et al., 1991). The slow regeneration of silicate in sea ice is parametrized in BFM-SI as a smaller value for the half saturation of silica and a larger value for the standard Si:C quotum in adapted diatoms (Table 5.1). The other two mechanisms of nutrients replenishment (exchange with the ocean and atmospheric deposition) will be analyzed in the next two subsections.

5.3.1.1 Flux of entrapment from the ocean

Ice structure determines the porosity and therefore the rate of exchange of nutrients: frazil ice is less porous than congelation ice and algae may experience nutrient depletion in the former.

The rates of advection and diffusion of nutrients from seawater into the porous bottom layer of ice may also depend on under-ice current velocities, tides and atmospheric pressure cycles (Cota et al., 1991). High algal biomass in the platelet layer has been found to reduce the flux of nutrients to algae communities of the upper congelation layer in Antarctica (Lizotte and Sullivan, 1991).

High biomass is usually found in area of slow ice growth rate (Legendre et al., 1992). During the growth season, convection in the skeletal layer enhances nutrient fluxes (Cota et al., 1991). During the melting season, the supply of freshwater increases the stratification just below the ice and reduces the flux of nutrients upward by reducing mixing

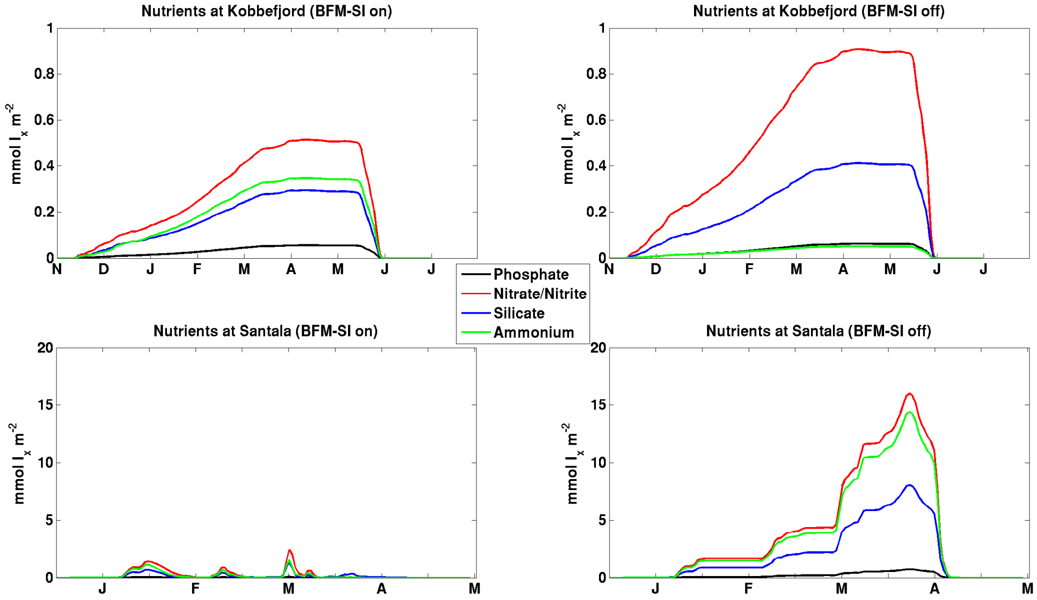

Figure 5.11: BFM-SI nutrients dynamics at Kobbefjord (above) and Santala Bay (below) with (left) and without (right) biological processes.

and friction velocity (Gosselin et al., 1985). Even if the enlargement and interconnections of the brine channels allows a greater biomass accumulation and nutrient supply, it also leads to an increase in the biological loss by cells sinking in the water column.

The model parametrization for the entrapment into sea ice and the release to the ocean of dissolved and particulate organic matter has been presented in Sect. 4.8. The coupling between the ocean and sea ice is modeled as a function of ice growth/melt rate, brine volume and concentration of nutrients in seawater.

The temporal evolution of nutrients in sea ice is shown at both sites in Fig. 5.11. Left panels represent the nutrients dynamics at Kobbefjord (above) and Santala Bay (below). The temporal evolution of each nutrient is the result of the exchange with the ocean (and the atmosphere at Santala Bay, cfr. Sect. 5.3.1.2) and of nutrient uptake by algae. The comparison allows to understand how efficient are the transport and sea ice algae utilization of nutrients, and which one may be the process controlling the actual nutrient concentrations.

Nutrients concentrations in sea ice are small at Kobbefjord (Fig. 5.11, above) compared to concentrations at Santala Bay (5.11, below). Chlorophyll concentrations are also smaller at Kobbefjord, as seen in the reference simulations (Fig. 5.5 and Fig. 5.6). Sea ice algae start growing at the beginning of the ice season at Santala Bay (Fig. 5.6), likely consuming nutrients earlier than at Kobbefjord. This is in fact the case: the algal upatke of nutrients is continuous throughout the season at Santala, while at Kobbefjord the uptake is very small (Fig. 5.11, left panels). The temporal evolution of nutrients at Kobbefjord matches well the temporal evolution of the ice growth (Fig. 5.1), showing that the concentration is controlled by transport processes than by algal uptake. Also at Santala Bay nutrients are not exhausted. The declining of the bloom at Santala is thus possibly associated with the loss of algae only.

In order to understand what is the actual supply of nutrients from external sources, the right panels of Fig. 5.11 show BFM-SI simulations of nutrients when no biological process is computed (Kobbefjord, above and Santala Bay, below). Nutrient concentrations at Kobbefjord remain low, also showing that seawater concentrations are small. At Santala Bay, melting of snow and sea ice flooding additionally contribute to nutrients supply (see also Sect. 5.3.1.2). The nutrient transport in the absence of biology matches well the temporal evolution of the ice growth, but it is also enhanced in periods of snow melts and sea ice flooding (especially during March, Fig. 5.3). This will be further analyzed in the next subsection.

5.3.1.2 Atmospheric depositions and sea ice flooding

Nutrient content in snow and liquid precipitation may lead to additional nutrient availability for surface communities, but also for bottom communities if nutrients accumulate and are made available through flushing and snow ice formation. In this last case, flooding of sea ice is also necessary for proper environmental conditions (temperature, salinity).

In the Baltic Sea, 5% of the total annual flux of N and P and 20 - 40% of lead and cadmium are deposited as snow: due to the intense stratification of most of the Baltic waters, sea ice is the major source of nutrients and trace elements to the surface Baltic waters during the melting season (Granskog et al., 2006a).

This is the case found at Santala Bay, as also stated by Granskog et al. (2003a). The evolution of nutrients and chlorophyll dynamics as simulated by the BFM-SI at Santala Bay was studied considering the nutrient supply processes separately: the exchange with the ocean (Fig. 5.12), the contribution of atmospheric deposition (Fig. 5.13) and the supply from atmospheric deposition and sea ice flooding together (Fig. 5.14). Observations of bottom ice concentration and total ice concentrations of nutrients are also plotted and reveal that concentrations found in the full ice core are much higher than those one found at the bottom. Thus the exchange with the ocean cannot be the only source of dissolved inorganic nutrient for the sea ice biological community.

In the first experiment (Fig. 5.12) nutrients supply is provided only by the ocean, considering the fluxes described in Sect. 4.8. Nutrient concentrations are lower than the ones found in the sampled ice cores, but similar to the magnitude found in the bottom section of the ice core. Chlorophyll is lower than in data, although the pattern is similar to the reference simulation (Fig. 5.6). Sea ice diatoms start growing at the beginning of the ice season, reaching a peak in February followed by a decrease likely due to nitrogen depletion. Flagellates start growing only at the end of the ice season, just prior to the complete ice melting.

In the second experiment (Fig. 5.13), the contribution due to phosphate and nitrogen in snow precipitation is added to the ocean fluxes. The prescribed concentrations of phosphate and nitrogen in the snow are derived from direct observations (Granskog et al., 2003a). The flux of nutrients due to precipitation is a linear function of the snow melting rate. Phosphate and nitrogen concentrations in sea ice increase (Fig. 5.13, upper panel). However, sea ice diatoms become silicate-limited and their chlorophyll content (Fig. 5.13, lower panel) is only slightly higher than in the previous experiment (Fig. 5.12). Flagellate chlorophyll stays low, being mostly light- and not nutrient-limited.

In the last experiment (Fig. 5.14), the effect of sea ice flooding on nutrients is added to the processes described above. Snow ice formation is parametrized by ESIM as the physical process that brings seawater to percolate trough brines and until reaching the sea ice surface in a very short time period (Sect. 2.2). The flux of nutrients from seawater to brines caused by sea ice flooding is thus a function of snow ice growth rate and the thickness of the BAL. Nutrients percolate trough all the ice matrix. However, only the fraction which stays in the BAL is of interest here. Nutrient concentrations are higher with respect to the previous experiment (Fig. 5.13), even though still underestimated comparing to observations (Fig. 5.14, upper panel). Nutrients are not limiting anymore and chlorophyll concentrations fits better with the data (Fig. 5.14, lower panel). There is a clear decrease of nutrients due to diatom uptake in periods of high biomass (late January, late February and late March). Flagellates are instead not affected by these processes.

The analysis of different mechanisms of nutrient supply analyzed here suggests the importance of considering solid precipitation as an important vector for nutrients transport. Chlorophyll results obtained from the first experiment (Fig. 5.12) are comparable

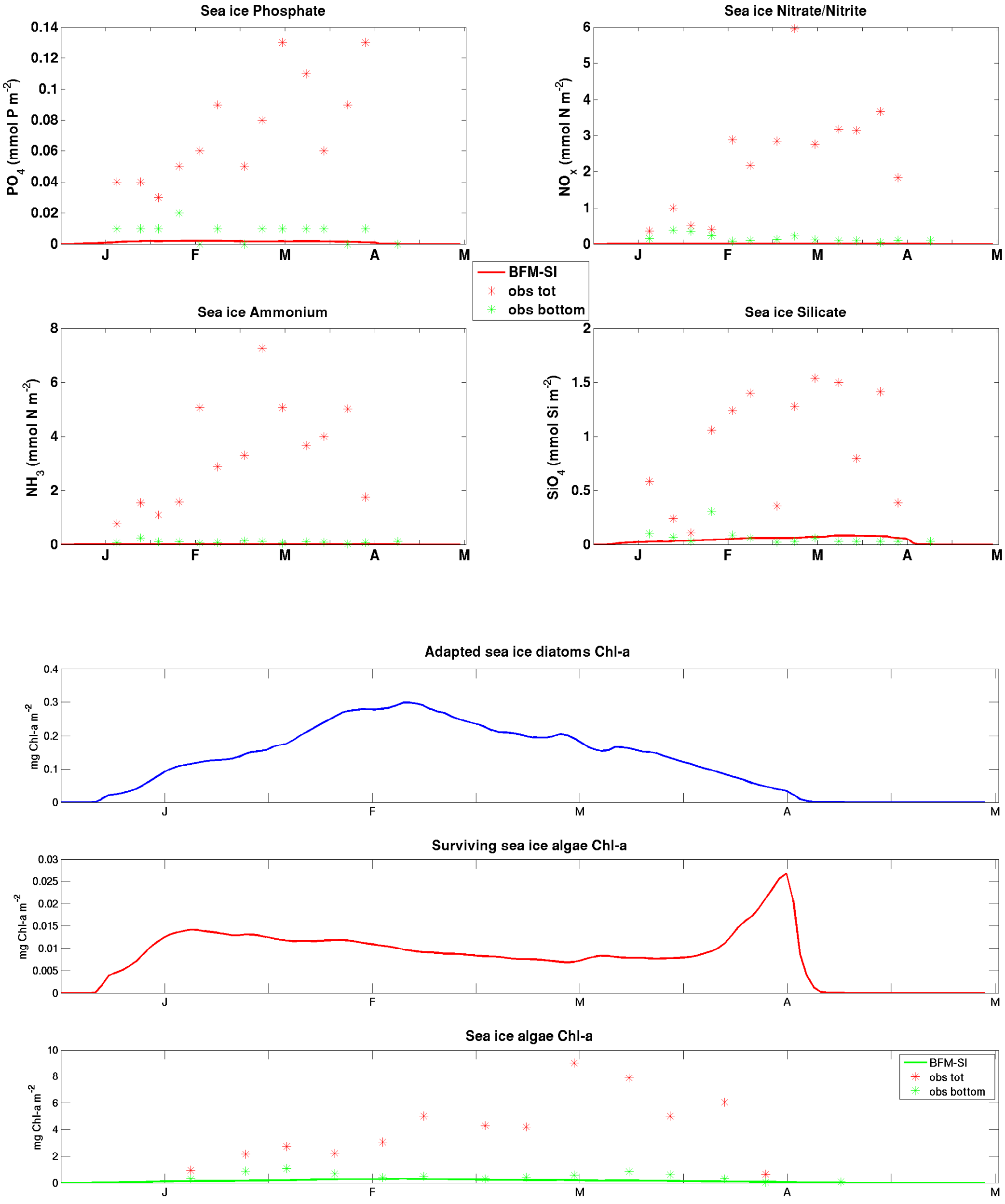

Figure 5.12: BFM-SI nutrients (above) and chlorophyll (below) dynamics compared to observations at Santala Bay considering only the exchange with the ocean.

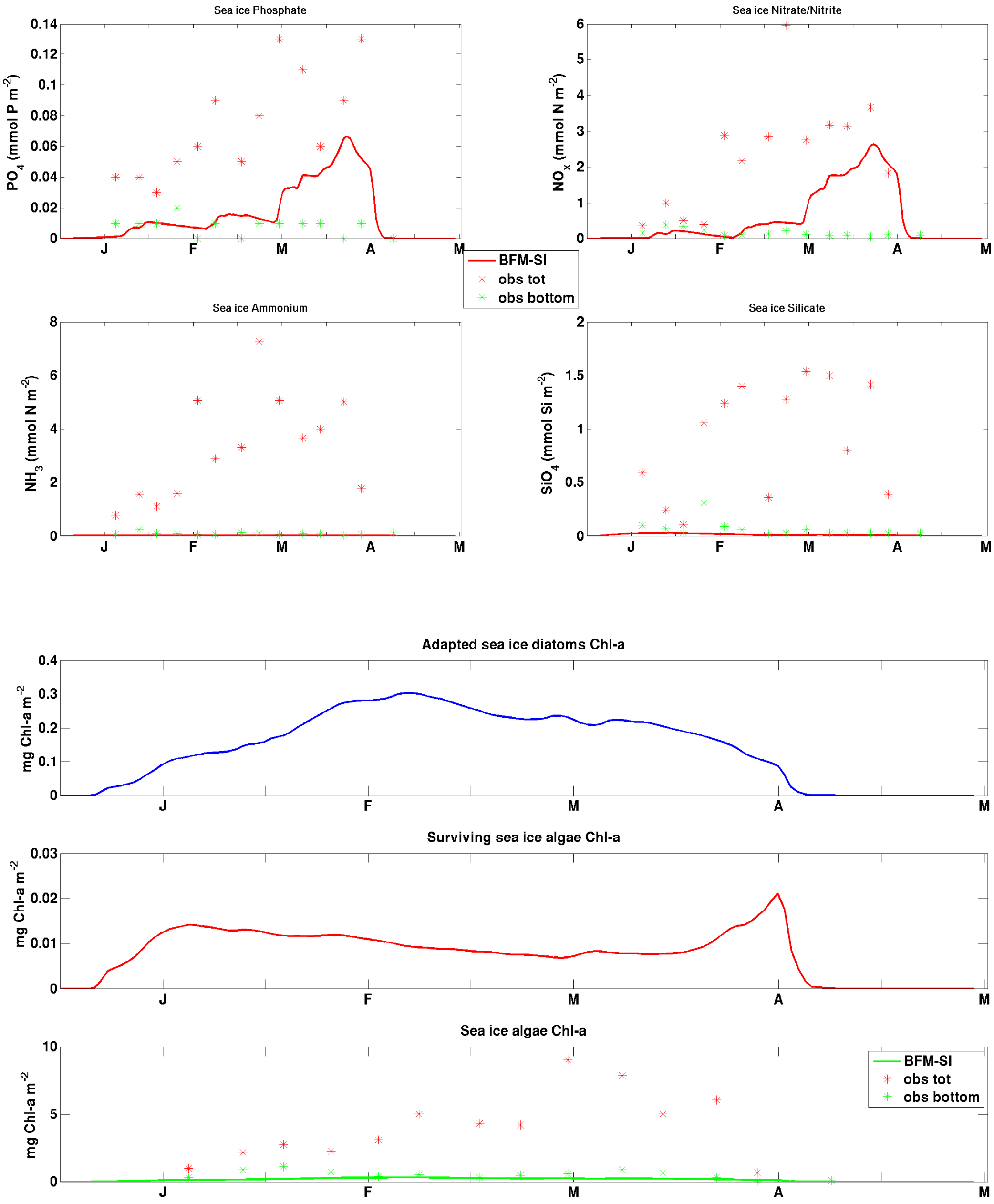

Figure 5.13: BFM-SI nutrients (above) and chlorophyll (below) dynamics compared to observations at Santala Bay considering the exchange with the ocean and the atmospheric deposition of nitrogen and phosphate.

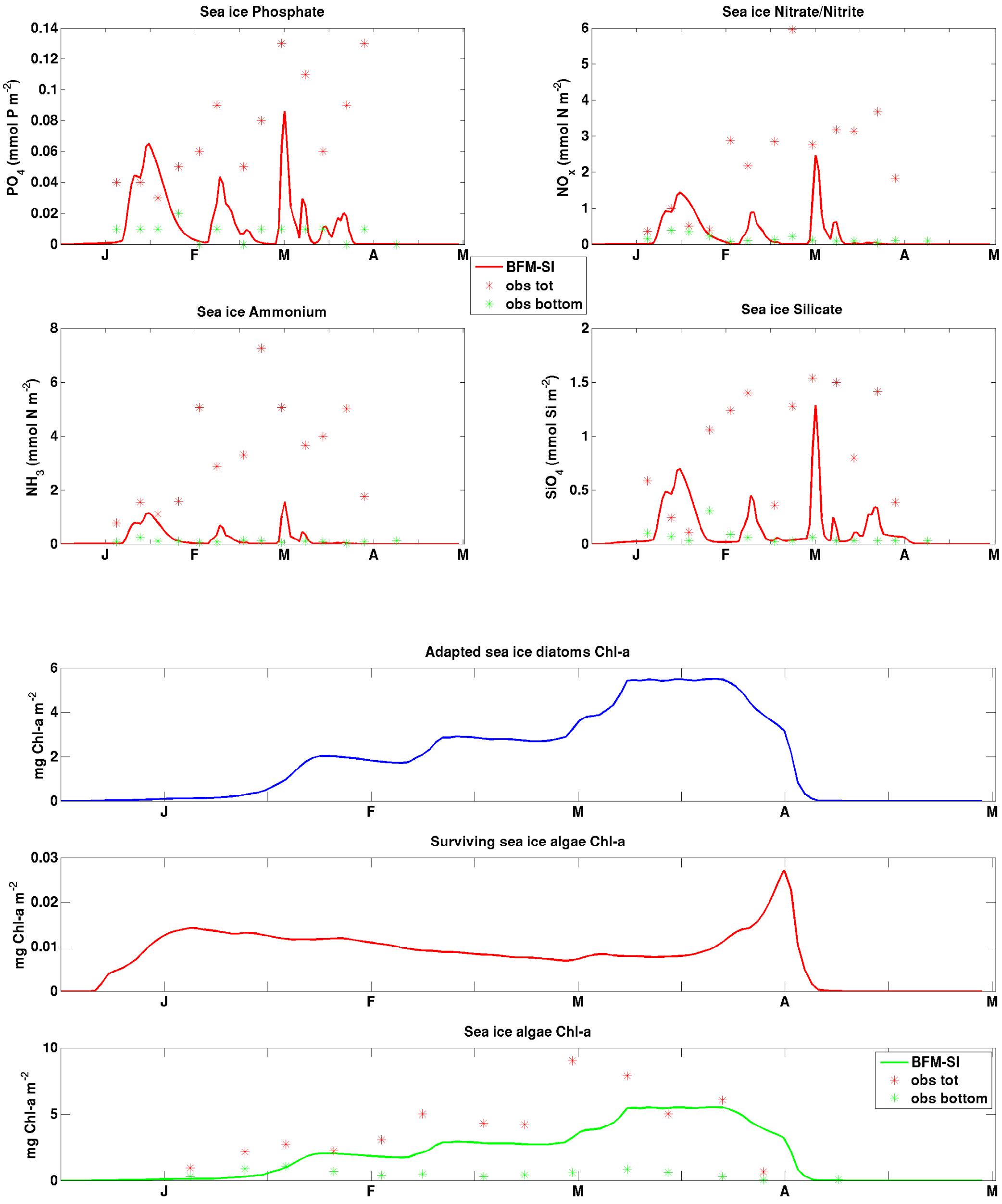

Figure 5.14: BFM-SI nutrients (above) and chlorophyll (below) dynamics compared to observations at Santala Bay considering the exchange with the ocean, the atmospheric deposition of nitrogen and phosphate and the flooding of phosphate, nitrogen and silicate (reference experiment).

only with data from the bottom section of the ice core (0.1 m), thus are only representative of bottom communities. However, the thickness of the BAL at Santala Bay shows to be larger than 0.1 m several times during the ice season (Fig. 5.3). In this case, it is thus necessary to study other mechanism of nutrient replenishment besides the mere entrapment from the ocean. Flushing of snow and snow ice formation reveals, in fact, to be responsible of the biggest fraction of nutrient supply in Santala Bay sea ice (Fig. 5.13 and Fig. 5.14). Only considering these further replenishment of nutrients, chlorophyll results become comparable with observations at Santala Bay.

5.4 Composition of sea ice and pelagic communities

BFM-SI is a useful tool to investigate the living strategies of sea ice algae with respect to pelagic phytoplankton. BFM phytoplankton acclimates to light by regulating the chl:C ratio (Geider et al., 1998). The initial composition of the sea ice community depends on the pelagic populations which are entrapped in sea ice during ice formation. There is currently a debate if phytoplankton simply acts passively during entrapment in sea ice or if it has also the ability to maintain its position at the bottom of the ice, preventing to be entrapped in the ice matrix or be expelled to the water column, as stated for instance by Welch and Bergmann (1989). Also Arrigo et al. (1993) numerically showed that sea ice algae are able to maintain their vertical position at the bottom of the congelation ice during ice growth.

Since more data are to date not yet available, the initial assumption is that there is no active role played by phytoplankton during entrapment in the liquid fraction of sea ice. Different groups of pelagic phytoplankton (diatoms and flagellates in pelagic BFM, Fig. 4.8) are assumed to have the same abundance in seawater and to move to brines, forming the sea ice community (sea ice diatoms and survivors, respectively in BFM-SI, Fig. 4.8). Afterward, the composition of the community changes according to algae adaptation to the new physical environment and/or to the ability of both functional groups to acclimate, that is sea ice algae populations are naturally selected for the new habitat.

This section examines the possible links between the sea ice and pelagic populations and how communities of both systems would be shaped if phytoplankton and ice algae belong to the same or to different communities. The Kobbefjord simulation and data (Fig. 5.5) are used here as reference.

5.4.1 Phytoplankton as sea ice algae

In a region covered by sea ice for most of the year, it would be reasonable to assume that the pelagic community would be more light-adapted to live in sea ice than in seawater. Thus, the community should be characterized in pelagic BFM by the same parameters which describe sea ice algae in BFM-SI (Table 5.1).

The results of this experiment are shown in Fig. 5.15. Being phytoplankton adapted to low-light intensities, it responds actively at the high light intensities in open water and it already blooms prior to ice formation (Fig. 5.15, upper left panel). In particular, flagellates are the major contributors, being characterized by a faster response than diatoms. They deplete the pelagic box model of nitrogen and phosphate (Fig. 5.15, upper right panel).

Because of the high initial bloom, high chlorophyll concentrations are entrapped in sea ice during ice growth (Fig. 5.15, lower left panel). However, the entrapment of nutrients is very small (Fig. 5.15 lower right panel) due to the initial depletion of the water column content. Sea ice algae are thus nutrient-limited at the time when they are supposed to be not light-limited anymore, and when a sea ice algae bloom should be observed (see reference simulation, Fig. 5.5).

Hence, it is rather reasonable to state that pelagic community cannot typically have the same adaptations that sea ice algae show for the sea ice habitat. However, results shown in this experiment would be fairly realistic if it would be assumed that the pelagic community is photoinhibited, in the sense that phytoplankton would be able to lower its productivity by reducing the number of photosynthetic units when exposed to high levels of irradiance (see also Sect. 5.4.3.2).

5.4.2 Sea ice algae as phytoplankton

Opposite to the experiment of the previous section, it may also be reasonable to assume that sea ice algae living in ice-covered regions where the ice season is very short, would have not enough time to acclimate to sea ice conditions and there would be no ecological advantage to be adapted to the sea ice low-light environment. Thus, the sea ice community should be not adapted to the low-light intensities of the sea ice habitat, but it should show instead more adaptation to open waters environmental conditions. This is tested in the following experiments (Fig. 5.16), where sea ice diatoms and survivors have both a low α_{chl}^{0} value of 3.8 e^{-6} mg C (mg chl)$^{-1}$ μE^{-1}m^{2}s, typical of high light-adapted algae.

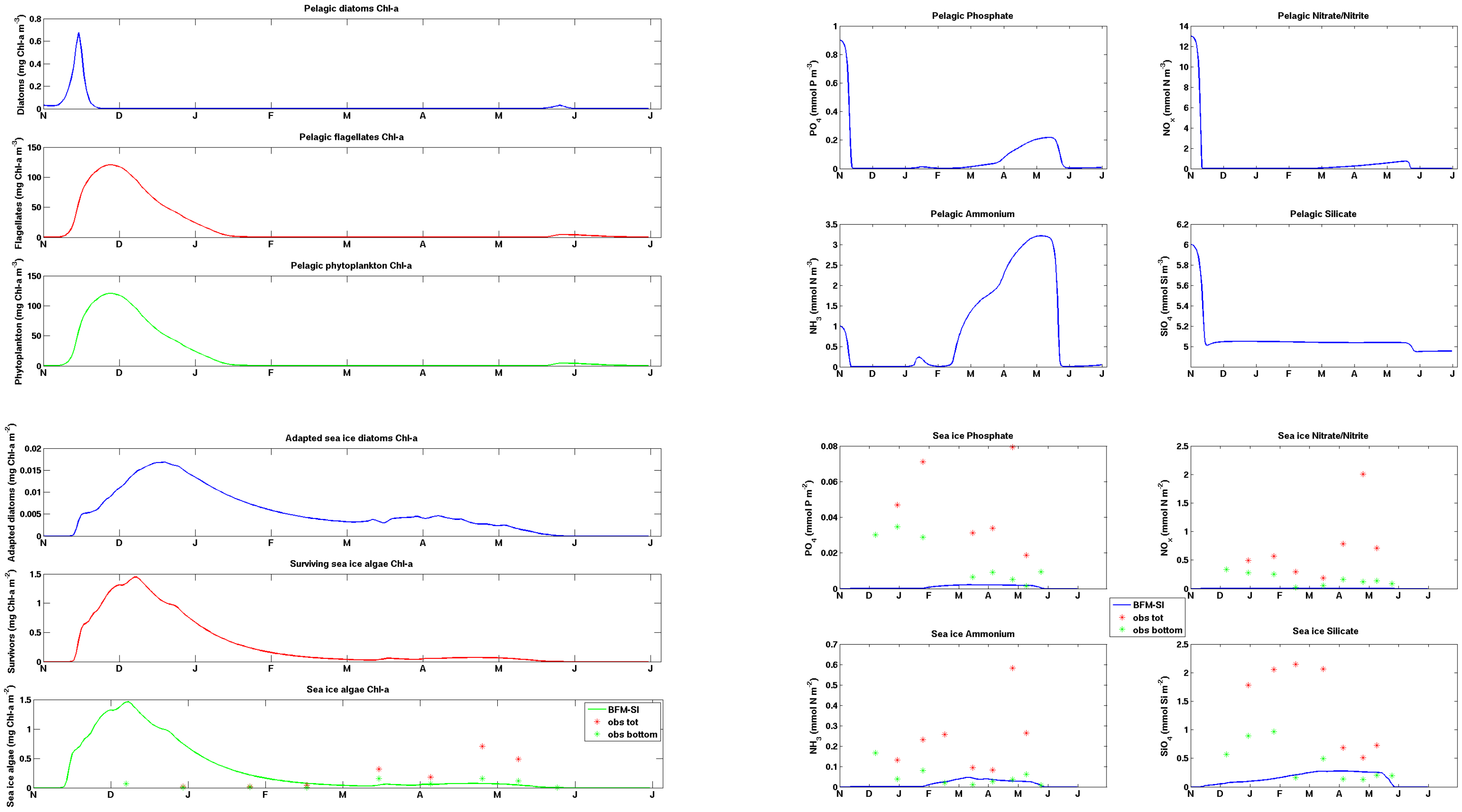

Figure 5.15: Chlorophyll (left) and nutrients (right) dynamics for pelagic (above) and sea ice (below) communities, considering phytoplankton community adapted to the sea ice habitat.

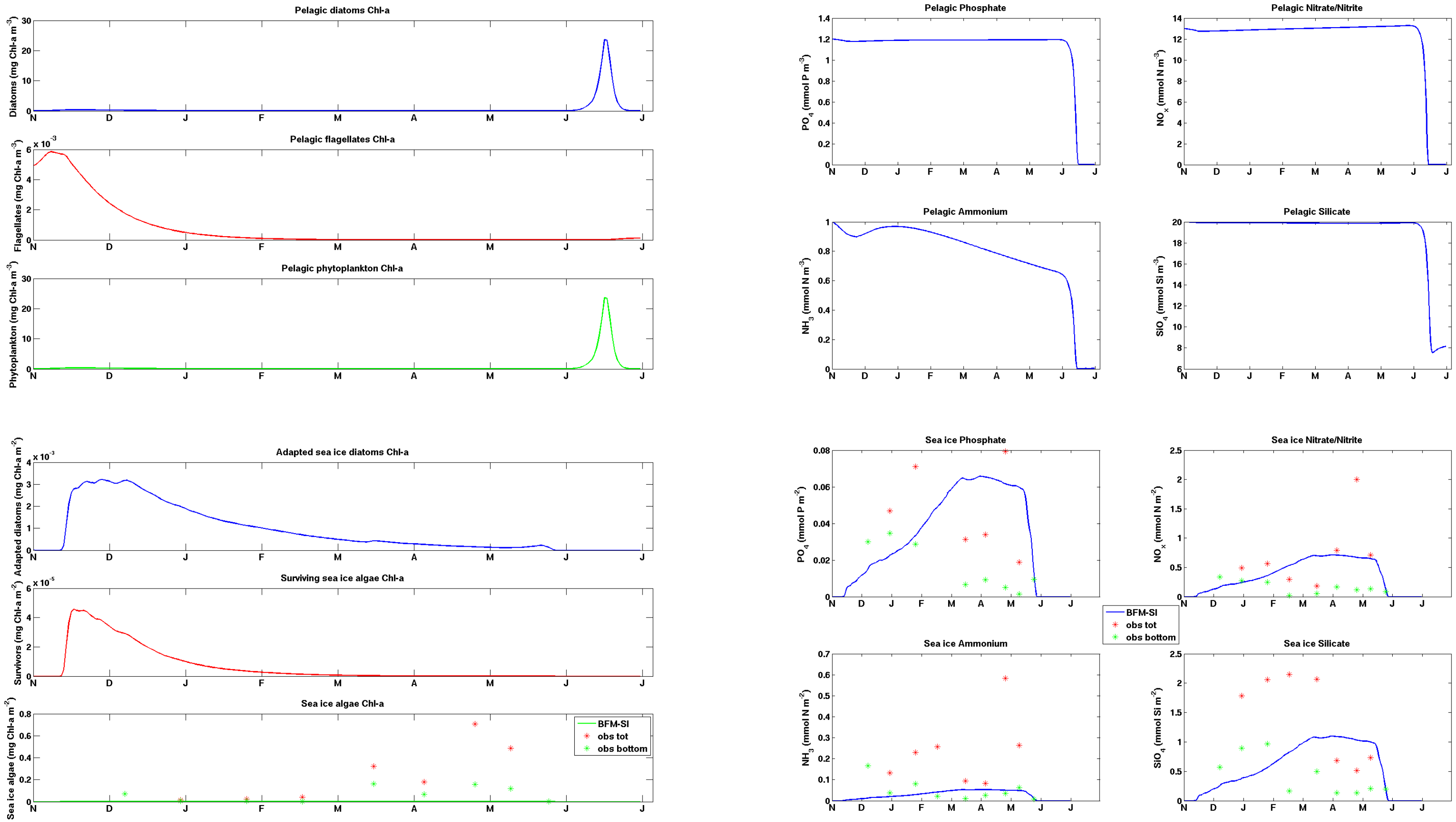

Figure 5.16: Chlorophyll (left) and nutrients (right) dynamics for pelagic (above) and sea ice (below) communities, considering sea ice community adapted to the pelagic habitat.

Total chlorophyll of pelagic community shows low concentrations throughout the ice season. After a few weeks from complete sea ice melting, pelagic diatoms bloom in seawater, showing to dominate with respect to flagellates (Fig. 5.16, upper left panel). The diatom bloom ends for phosphorous and nitrate depletion (Fig. 5.16, upper right panel). The initial entrapment of nutrients would be sufficient for sea ice algae to bloom (Fig. 5.16, lower right panel), but this does not occur (Fig. 5.16, lower left panel) since they are not able to regulate their chl:C ratio in order to take advantage of the nutrient availability. At the irradiance levels found in sea ice, their growth entirely depends on the α^0_{chl} value, which is too low.

Even though this is not the scenario found at Kobbefjord, this experiment clearly shows that sea ice algae living in sea ice depend only on their genetic capability of adaptation or on their phenotypic capacity of acclimation. If a sea ice season is very short, it is quite realistic to assume that the algae community would not be able to acclimate in a short-time period. Hence, their rate of survival and growth in sea ice would likely depend only on their relative presence in the pelagic community. An initial small amount, likely controlled by photo-inhibition, would allow the survival and growth in sea ice (see also Sect. 5.4.3.2).

5.4.3 Sympagic vs. Pelagic community

Several studies in seasonal ice-covered oceans report that the sea ice community and the pelagic community may have either similar or different compositions (e.g., Lancelot et al., 1993; Riebesell et al., 1991; Smith and Nelson, 1985). Similar groups are found in both systems. However, different groups may be responsible for the biggest fraction of the biomass in different habitats. Usually diatoms prevail in the sea ice habitat and flagellates are dominant in seawater after complete ice melting (e.g., Mikkelsen et al., 2008). Thus the communities are referred to as pelagic and sympagic. However, blooms of diatoms in seawater are also reported in regions where the sea ice bloom is also mainly due to diatoms (e.g, Smith and Nelson, 1985).

In the next subsections the composition of the pelagic community, considering mechanisms of (phenotypic) acclimation and (genotypic) adaptation, will be analyzed. The pelagic contribution in terms of chlorophyll and carbon content will be discussed together with the analysis of the nutrients uptake rates of phytoplankton and sea ice algae.

5.4.3.1 Photoacclimatation

Some authors have reported that the composition of the pelagic and sea ice communities sampled at close sites were often characterized by similar composition (e.g., Smith and Nelson, 1985; Garrison et al., 1987; Kang and Fryxell, 1993). Facing different environmental conditions in different habitats, populations of sea ice and pelagic community may be able to completely acclimate in order to live in the different environments.

In the following experiment (Fig. 5.17), it is shown how the pelagic and sea ice communities would be composed if the physiological and ecological parameters representing each group would be the same in different habitats, except for their α^0_{chl} value, which was found in the previous section to be necessarily different ($5.8e^{-4}$ mg C (mg chl)$^{-1}$ μE^{-1}m^{2}s for both sea ice diatoms and survivors, and $3.8e^{-6}$ mg C (mg chl)$^{-1}$ μE^{-1}m^{2}s for both pelagic diatoms and flagellates).

Since the pelagic community is not low-light adapted, both pelagic groups of phytoplankton bloom in seawater after few weeks from complete ice melting (Fig. 5.17, upper left panel). Interestingly, a group succession is found in seawater, with two successive chlorophyll blooms. The first bloom is due to diatoms. Once their bloom starts declining, because of low-nutrients (Fig. 5.17, upper right panel), flagellates start growing with a relevant contribution in terms of total pelagic chlorophyll (Fig. 5.17, upper left panel). Sea ice diatoms start growing later (Fig. 5.17, lower left panel) than in the reference simulation (Fig. 5.5). On the contrary, surviving algae start photosynthesis already in mid March. Even though their contribution is small in terms of total chlorophyll, survivors compete with diatoms for light and nutrients (Fig, 5.17, lower right panel), resulting in a later bloom of sea ice diatoms compared to the reference simulation (Fig. 5.5).

The experiment shown here may thus be the case if pelagic diatoms and flagellates would be able to completely light-acclimate to the new environment found in sea ice.

5.4.3.2 Photoadaptation

Some studies in seasonal ice-covered oceans have also reported that the sea ice community and the pelagic community may often have different compositions (e.g., Riebesell et al., 1991; Mathot et al., 1991; Fripiat et al., 2007).

In the next experiment (Fig. 5.18) it is shown how pelagic diatoms adapted to low-light intensities may show photo-inhibition characteristics and different chlorophyll dynamics than acclimated diatoms (Fig. 5.17). Pelagic diatoms do not change the (high) α^0_{chl} value,

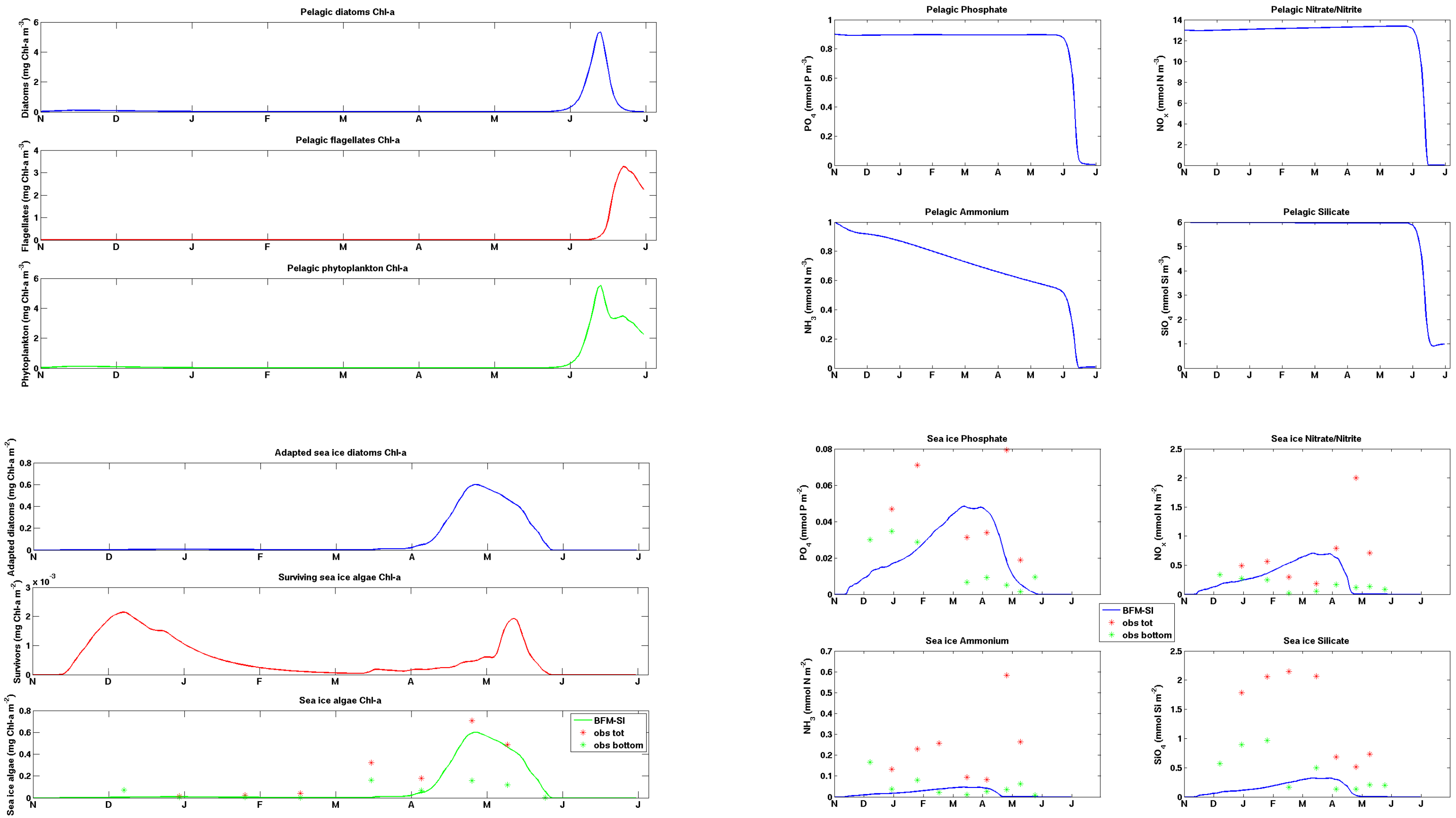

Figure 5.17: Chlorophyll (left) and nutrients (right) dynamics for pelagic (above) and sea ice (below) communities, considering photoacclimatation mechanisms.

but lower the photosynthetic rate when exposed to higher light intensities, while flagellates keeps the same (low) α^0_{chl} value in both environments (sea ice and seawater).

Sea ice algae chlorophyll matches well with observations (Fig. 5.18, lower left panel), as in the reference simulation (Fig. 5.5). At the end of the ice season, the nutrient uptake in sea ice is a bit higher than in the previous experiment since diatoms start growing already in mid May (Fig. 5.18, lower right panel). Flagellates also contributes to the peak of chlorophyll in sea ice, but to a lesser extent, as in the reference simulation (Fig. 5.5).

During the whole ice season, phytoplankton chlorophyll stays low (Fig. 5.18, upper left panel). Once sea ice has completely melted away, diatoms chlorophyll does not significantly increase, showing that the community is photoinhibited at higher irradiance. Flagellates chlorophyll starts increasing since mid July, but later than in the previous experiment (Fig. 5.17), and their peak is also smaller. Opposite to the previous experiment, nutrient concentrations are lowering since the beginning of May, showing that the pelagic phytoplankton starts growing under-ice and earlier than in the previous experiment (Fig. 5.18, upper right panel). However, seawater is not depleted of nutrients at the end of the simulation, as it was in the previous experiment. Even though diatoms chlorophyll stays low in seawater, and despite the fact that nutrients are not limiting, the growth of pelagic flagellates is smaller than in the previous experiment. Hence, some differences may exist in their carbon content.

To understand this, it is further analyzed how adapted and acclimated diatoms, described in the previous experiments (Fig. 5.17 and 5.18) regulate differently their chl:C ratio and what is their contribution in terms of carbon biomass.

Fig. 5.19 compares the chlorophyll (above), carbon (middle) and chl-a:C ratios (below) of acclimated pelagic diatoms (left) analyzed in the first experiment (Fig. 5.17) and of adapted pelagic diatoms (right) described in the second experiment (Fig. 5.18). In both cases the optimal chl:C quotum for pelagic diatoms is 0.03.

In the case of acclimated diatoms (Fig. 5.19, left), the community does not down-regulate its chl:C ratio during the ice season. When light availability is increasing, they slowly lower it and the community blooms in seawater. Once the bloom has expired, their chl:C ratio restarts increasing. The peak of chl-a is about 4.5 mg m^{-3} and corresponds to a peak of carbon biomass of about 250 mg m^{-3}. They start growing at the beginning of July and the peak of chlorophyll and carbon are reached in mid June.

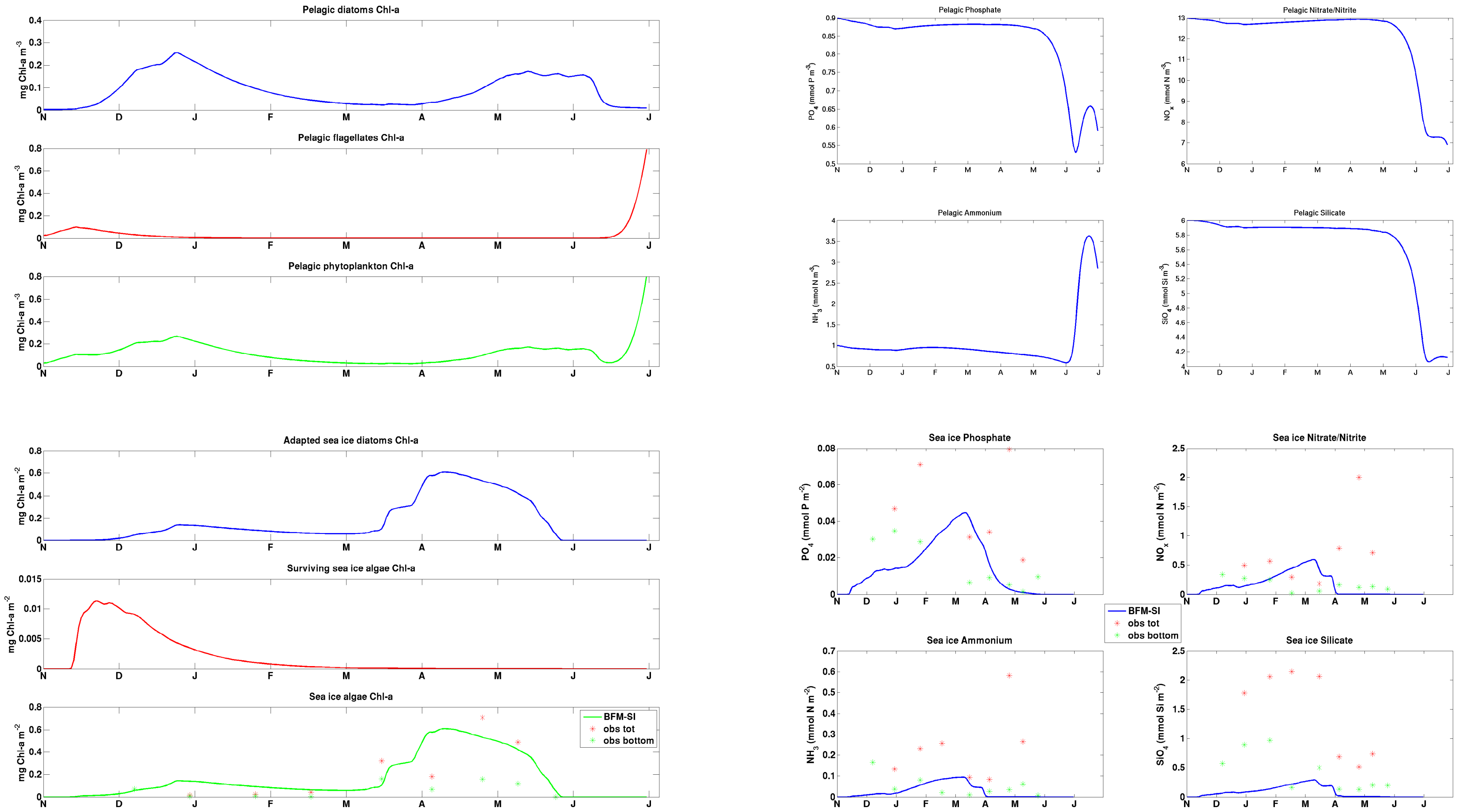

Figure 5.18: Chlorophyll (left) and nutrients (right) dynamics for pelagic (above) and sea ice (below) communities, considering photoadaptation mechanisms.

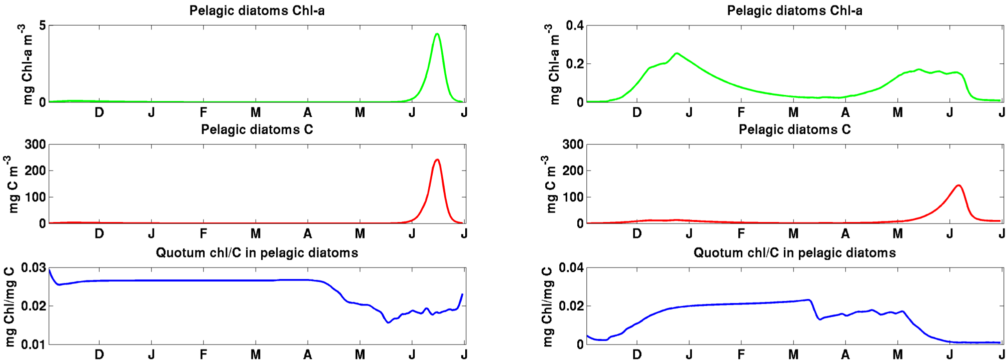

Figure 5.19: Chlorophyll (above), carbon (middle) and chl:C quotum (below) dynamics for an acclimated community (left) and an adapted community (right).

In the case of diatoms adapted to low-light environments (Fig. 5.19, right), the community keeps always a low chl:C ratio when exposed to high-light irradiance, both prior and after the ice season, lowering the number of photosynthetic subunits to avoid photoshock. During the ice season diatoms regulates their adaptation to light by increasing their chl:C ratio. Diatoms chlorophyll stays always low (less than 0.2 mg m^{-3}) during the whole year. However, their capability to lower their chl:C ratio to minimum values, results in a large increase in carbon biomass since May, reaching a peak of about 150 C mg m^{-3} at the beginning of July.

An important outcome of this comparison is thus the necessity of considering different chl:C ratios when dealing with regions where light conditions may change in a very short time-period, as it is in ice-covered regions at the time of the onset of ice or of melting. A model with varying chl:C ratio is therefore needed and chlorophyll should not always be considered as a good proxy for biomass estimations. Several possible scenarios of chl:C ratios should be considered when making estimations of the total carbon biomass of polar and sub-polar regions. Besides, acclimated and adapted diatoms show to start growing at different times. The peak in carbon is reached almost 1 month earlier than in the case of acclimated diatoms. This different behavior may in turn affect the onset of secondary production and the magnitude of it.

5.5 The fate of the sea ice biomass

Sea ice biological loss is an import term of the total biomass budget of ice-covered ocean. Sea ice biomass released to the water column may experience different environmental conditions and its fate can be different also depending on the physiological state of living cells. Pelagic zooplankton can actually play an important role in controlling sea ice algae and phytoplankton blooms.

In the next two subsections the fate of the sea ice biomass is analyzed considering two likely scenarios. In the first case, algae released from sea ice find favorable environmental conditions in sea water: water is stratified, they stay in the upper surface part of the ocean and acclimate, thus becoming an integrated part of total phytoplankton in sea water. In the second case, algae released from sea ice are not viable or die fast, water column is mixed and both sea ice and pelagic diatoms rapidly sink with a nominal sinking velocity of 100 m d^{-1}.

The simulation of Fig. 5.5 is used as reference focusing on the chl:C content and the role of zooplankton in controlling sea ice algae and pelagic phytoplankton.

5.5.1 Seeding effect

Some authors studied the seeding effect in natural water bodies (e.g., Smith and Nelson, 1985) and in mesocosm experiments (e.g., Kuosa et al., 1992). The seeding of a phytoplankton bloom occurs only if sea ice algae released to seawater are viable and find favorable environmental conditions. It also assumes that sea ice algae biomass is of sufficient magnitude to effectively seed a phytoplankton bloom, otherwise they only represent a smaller fraction of total pelagic primary producers. The assumption is thus that the magnitude and extent of the ice-edge bloom is determined by the combined action of meteorological conditions (i.e., winds) and grazing pressure.

The first experiment (Fig. 5.20) shows the results in the pelagic system when considering that the water column is well stratified at the end of the ice season and sea ice algae are viable in seawater. A phytoplankton bloom occurs in July (Fig. 5.20, upper plot). The first chlorophyll peak is reached in the middle of July and is due to diatoms (5 mg chl-*a* m^{-3}), while the second smaller peak found later in July is due to flagellates (3 mg chl-*a* m^{-3}). The biggest fraction of the biomass is due to diatoms (peak of about 270 mg C $m^{-3)}$, while the contribution of flagellates is of about 45 mg C m^{-3} (Fig. 5.20, lower plot). There is a good coupling between the decline of the phytoplankton bloom and bacteria production. A very good coupling is also found between mesozooplankton and phytoplankton growth. However, mesozooplankton biomass is too small compared to that one of phytoplankton (Fig. 5.20, lower plot). Likely, the exhaustion of the phytoplankton bloom is due to nutrients depletion, as shown in Sect. 5.4.3.1. Heterotrophic nanoflagellates and microzooplankton play instead a minor or no role, respectively (Fig. 5.20, lower plot).

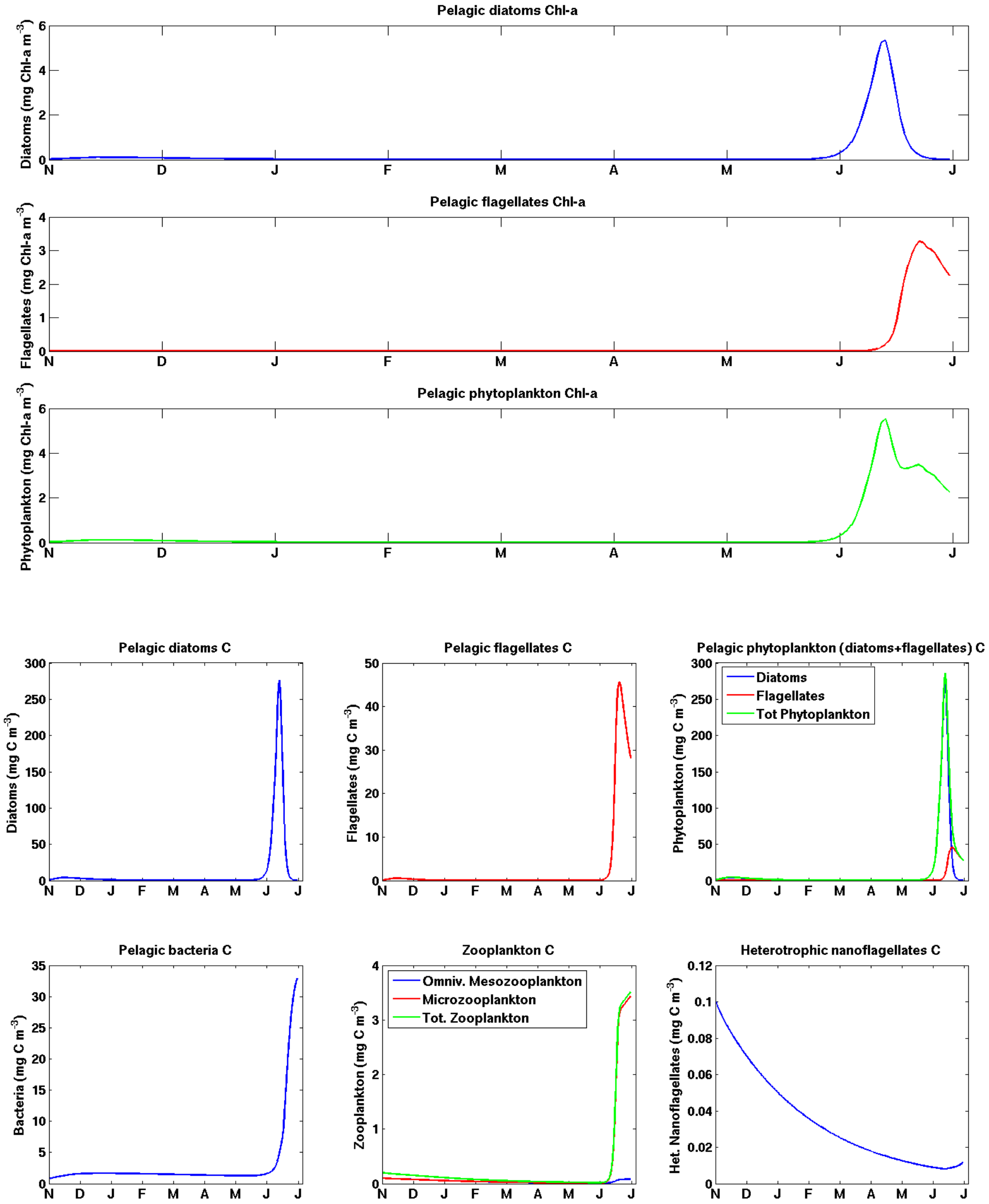

Figure 5.20: Pelagic chlorophyll (above: diatoms, flagellates and total chlorophyll) and carbon (below, clockwise from left: diatoms, flagellates, total carbon, heterotrophic nanoflagellates, zooplankton and bacteria) dynamics in case of seeding.

5.5.2 Sinking

A rapid sink would occur in the case the released sea ice algae population consists of large cells. In this case, both the high size-related sinking velocity and the low grazing pressure may lead to low residence time in the surface layer of the ocean. Similar conditions may occur if the water column is well mixed. Even if sea ice algae can still be viable once released in the water, their removal from the surface illuminated layer would eventually lead to rapid death.

Some studies (e.g., Riebesell et al., 1991; Lancelot et al., 1993) report that ice algae have a strong tendency to form aggregates, with differences for algal assemblages collected from the ice interior and the infiltration layer. Sinking rates of aggregates may be some orders of magnitude higher than those of dispersed ice algae. Thus, ice algae released from the melting sea ice are subject to rapid sedimentation.

In the next experiment (Fig. 5.21 and Fig. 5.22), it is assumed that sea ice algae die once released to the water column. The latter is also well mixed and also pelagic diatoms are affected by a fast sinking velocity (100 m $d^{-1)}$. A smaller phytoplankton bloom (1.5 mg chl-*a* m^{-3}) occurs at the end of July, contemporaneously for both groups: it is due mainly to diatoms and partly to flagellates (Fig. 5.21, upper plot). Carbon biomass of diatoms is also higher than that one of flagellates (Fig. 5.21, lower plot). Again, there is a good coupling between bacteria and phytoplankton growth, event though bacterial production is reduced. A not very good coupling is, instead, depicted for zooplankton, which is not growing prior to the end of the simulated period. Its role may be of lesser importance due to the rapid sinking of diatoms.

In this experiment, when sea ice algae are released to seawater, they are supposed to die and become an integral part of the pelagic dissolved and particulate organic matter (DOC and POC). At Kobbefjord, their partial contribution to total POC and DOC is small compared to that one of the pelagic matter (Fig. 5.22).

The last two experiments show that environmental conditions of the pelagic system (i.e. sinking speed), strongly influence the magnitude of the phytoplankton bloom and the timing of secondary production. Highly mixed waters, which increase the sinking speed of organic matter, results in a small and later phytoplankton bloom. However, since there is less potential material for remineralization, also bacterial activity is lower. Zooplankton is affected by a faster sinking speed as well and its capability of remaining in the upper part of the ocean is reduced, thus also lowering the magnitude of its predation role.

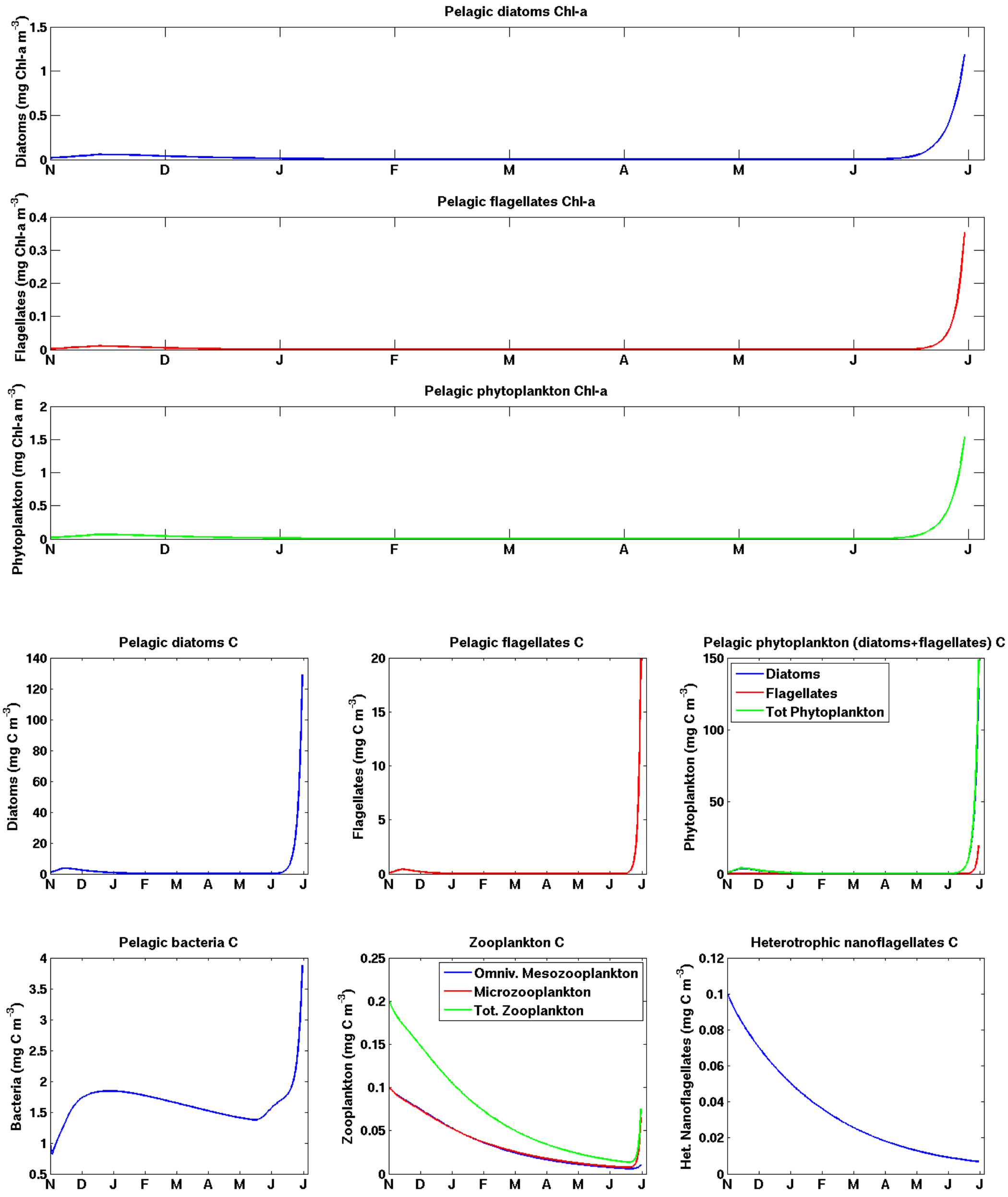

Figure 5.21: Pelagic chlorophyll (above: diatoms, flagellates and total phytoplankton chlorophyll) and carbon (below, clockwise from left: diatoms, flagellates, total phytoplankton carbon, heterotrophic nanoflagellates, zooplankton and bacteria) dynamics in case of sinking.

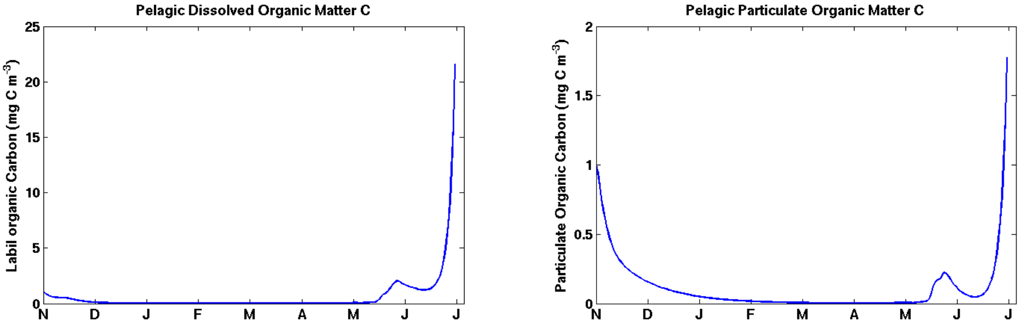

Figure 5.22: Pelagic DOC (left) and POC (right) dynamics in case of sinking.

5.6 Summary

This chapter presented a collection of numerical simulations of sea ice and pelagic biogeochemistry.

The reference BFM-SI simulations have been first visually compared with the observed chlorophyll concentrations at two very different site in terms of productivity: Kobbefjord in the Arctic and Santala Bay in the Baltic.

The physical and biological controlling factors for the evolution of sea ice algae have been analyzed. A sensitivity analysis on a selected set of physical and biological regulating factors indicates that growth in sea ice is primarily controlled by light availability. Nutrients are mostly supplied by the exchange with the ocean waters and may become limiting only if a decline of the algal bloom is observed in sea ice prior to the beginning of the biological loss. However in the studied BFM-SI simulations, this was never the case, even in the more productive site (Santala Bay).

An important contribution to nutrient availability is due to atmospheric depositions in regions where allochtonous dissolved inorganic nutrients accumulate on the surface of sea ice as snow. This is the case for Santala Bay. In area of heavy snow loads, snow ice formation constitutes an additional nutrient supply from the ocean to the sea ice surface.

BFM-SI was also used to study the adaptation and acclimation strategies of different phytoplankton functional groups. Several experiment showed the possible composition of the sea ice and pelagic communities in regions which may be characterized by shorter and longer ice seasons, and by more photo-adapted or more photo-inhibited populations. Different forms of adaptation and acclimation lead to very different contribution of the sea ice and pelagic communities in terms of chlorophyll content and, consequently, in terms of biomass.

Finally, possible scenarios for the fate of the sea ice biomass have been presented. Two different situations for the physical conditions of the pelagic environment and for the viability of the sea ice algae communities showed to produce different results in terms of total chlorophyll and carbon concentrations. Besides, bacteria and zooplankton productions appeared to be better coupled to a viable sea ice algae community in stratified waters than in the opposite situation.

Chapter 6

Conclusions and Outlook

The important thing
is never stop questioning.

(Albert Einstein)

The main conclusions of each chapter of this thesis are summarized and collected here together with the contribution of this work to our knowledge in the field of the polar oceans research and an outlook over the future developments.

6.1 The role of snow and meteoric ice

The initial implementation of ESIM with a thermodynamic component only (ESIM1) showed that, in order to properly simulate an ice season, it was necessary to consider the important physical processes responsible for sea ice/snow accumulation, growth, metamorphism and decay. In the Baltic Sea and in large areas of the Antarctic as the Ross Sea, snow ice plays a very important physical and biological role and gives a relevant contribution to the total ice mass balance of up to 50% (e.g., Kawamura et al., 2004). Additionally, the Baltic Sea is characterized by more complex melt-freeze cycles, mainly due to its mild and wet climate, which requires the inclusion of superimposed ice, a peculiarity of the Baltic Sea (e.g. (e.g., Granskog et al., 2003b)) and the lowest Arctic as the Svalbard area (e.g., Nicolaus et al., 2003). This important component of the sea ice mass balance is usually neglected in models. The modelling structure developed in this work stresses the importance of the snow/ice metamorphism rather than the number of sea ice layers, expanding the simple Semtner-like model and reducing the computational time. These features make the model more suitable for coupled configurations with ocean models.

The sensitivity test to the physical processes showed that ESIM1 does a good job whenever the snow layer is well simulated and it is not necessary to add more sea ice layers to better reproduce the total ice thickness. The model is, instead, very sensitive to the meteoric ice dynamics and snow is the key variable because of its different metamorphoses, high albedo and strong insulating effect. Even though the meteoric ice formation is especially relevant for the Baltic sea ice and for Antarctic first-year ice, in a climate change scenario of thinning of the ice and increasing of precipitation (e.g., Alexander et al., 2004), snow ice and superimposed ice may become more common and important in the Arctic and the rest of the Antarctic as well.

The calibration and the related sensitivity tests to selected model parameters stressed the relevant role of the oceanic heat flux in sea ice modelling. However, the model did not result to be very sensitive to small variations of the surface albedo. Even the highest sensitivity value for winter snow albedo was rather small, showing that ESIM1 is robust to changes in this important parameter for our test-case sites.

Coupled climate models and particularly Earth System Models generally have resolutions comparable or slightly finer than the forcing data used here. A perturbed scenarios analysis demonstrated that the perturbed model simulations do not significantly differ from the control run and it can be concluded that the current coarse resolution of the forcing data can be acceptable for long term simulations of sea ice thermodynamics.

6.2 Salt in sea ice as the link

ESIM2 is a further development of ESIM1 and includes an improved version of the thermodynamic component and a new halodynamic component.

Better results, in terms of thermodynamics, were obtained thanks to a new snow parametrization that collects solid precipitation and allows a more realistic snow compaction. Once again, snow revealed to be a key component of the polar physical system.

The parametrization of gravity drainage in sea ice needed to be adjusted to simulate well the magnitude of the winter desalination of sea ice. The salinity model reproduced well the observed changes in bulk salinity at the Arctic site. However, it did not fully explained the small variability of the brackish Baltic sea ice. The expected increase in precipitation in the Arctic (e.g., Alexander et al., 2004) will have also the effect of lowering sea ice and ocean salinities. Further studies are thus required to better simulate the desalination of low-salinity sea ice.

Salt is not only an important physical property. It showed to be also the most important link between the physics and the biogeochemistry of sea ice. The fractionation of sea ice in the pure solid ice matrix and in liquid salty brines is a necessary information to estimate the available space (brine volume) for microorganisms to grow. Space not only limits the dimensions of the organisms in term of their accessibility to the sea ice environment, but also their vertical distribution, which is possible only in sea ice where brines are interconnected (conventionally larger than 5 % of total ice volume). The brine volume is parametrized as a linear function of sea ice temperature and salinity. A coupled thermodynamic-halodynamic sea ice model such as ESIM2 is thus required to properly estimate the actual space available for the ecosystem to develop.

Depending on the size of the brines, different organisms may compose the sea ice community. Brackish waters lead to the formation of small volumes of brine, where the diversity in species composition may be reduced and the ecosystem highly simplified with few dominant species prevailing. Large brines can instead be inhabited by larger animals, allowing a higher diversity in species composition, but also more trophic levels in the food web.

6.3 Coupling strategy: the Biologically-Active-Layer

The Biologically-Active-Layer (BAL) is the key-concept of this thesis and the strategy for the direct coupling of the physics to the biology of sea ice.

The BAL properties are the mean key-physical properties that ESIM2 computes in the sea ice layer that is continuously physically connected with the underlying ocean. Those are required information for the new biogeochemical flux model in sea ice (BFM-SI), which simulates the physiological and ecological response of the sea ice community to different environmental forcings. This was clearly showed for the BAL simulations at two sites, one in the Baltic and one in the Arctic, characterized by very different physical and biological conditions.

The work done in this thesis represents the first effort to model the physical and biogeochemical properties of a sea ice layer with a time-varying thickness. This ensures a more realistic approach since it is only based on physical formulations.Without any information on the physical properties of sea ice at different latitudes and under different forcing conditions, it may be in fact very hard to realistically prescribe the fraction of sea ice where some biological processes occur.

The BAL concept also allows a proper coupling at the sea ice interface with the ocean. The boundary fluxes reproduce the actual entrapment of organic and inorganic matter at the beginning of ice formation and during the growth period. These are distributed within the BAL depending on its thickness and brine volume: larger brines and a thicker BAL layer allow more nutrients to be entrapped and redistribute within sea ice.

The coupling with the ocean at the onset of the sea ice melting allows to study if the decline of a biological sea ice community is due to physical constraints, such as biological losses during the melting of sea ice, or biological controlling factors, such as nutrients depletion. The fate of the sea ice biomass is in fact an important issue (e.g., Riebesell et al., 1991; Lancelot et al., 1993). There is still an on-going debate on the ability of the algal community to be viable in seawater and seed a phytoplankton bloom. The seeding effect is verified only in localized areas, based on sampling of closed sea ice and open water sites (e.g., Smith and Nelson, 1985). The experiments shown here demonstrates that different environmental conditions, such as water stratification, together with a different physiological state of the cells released to the ocean lead to different contribution in terms of pelagic chlorophyll and carbon biomass, which directly affect the timing of bacteria and secondary production.

6.4 Understanding the sea ice ecosystem

The new biogeochemical flux model implemented in a sea ice system (BFM-SI) is developed starting from the comprehensive Biogeochemical Flux Model.

BFM-SI was calibrated to reproduce the chlorophyll rate of change at two different ice sites in terms of productivity: one in the Arctic and one in the Baltic..

A sensitivity analysis on a selected set of physical and biological regulating factors indicates that growth in sea ice is primarily controlled by light availability. The snow cover showed to be the principal controlling factor for the timing of the bloom initiation.

Nutrients are mostly supplied by the exchange with the ocean waters. An important contribution is shown to be given by atmospheric deposition in regions where allochtonous dissolved inorganic nutrients accumulate on the surface of sea ice as snow. However, model results still underestimate the total content of inorganic nutrient in sea ice. The role of bacteria remineralization and the likely enhancement of nutrient fluxes due to convection in the lower sea ice layer need to be investigated in further experiments.

Several experiments showed that different forms of adaptation and acclimation lead to very different evolutions of the sea ice and pelagic communities in terms of chlorophyll content and carbon biomass. The rapid change in light conditions which characterizes ice-covered oceans has shown to lead to different regulations of the chl:C ratio by differently adapted communities. Biomass estimation of pelagic phytoplankton are often derived form satellite observations of chlorophyll. Several scenarios should be considered for the resulted carbon biomass: prescribing a constant chl:C quotum is thus not a proper method when using chlorophyll as a proxy for biomass estimations. Besides, diversely adapted communities showed to bloom at different times and this in turn affects the onset of secondary production and the magnitude of it.

It has been speculated that a shorter ice season associated with a climate warming scenario would lead to a smaller amount of microorganisms entrapped, a shorter and smaller annual ice algal bloom and lower concentrations of organic and inorganic compounds released into seawater during melting (e.g., Jin et al., 2006). The most obvious consequences may be a reduction in significance of two of the major roles that sea ice ecosystems play: the potential seeding of the following phytoplankton bloom and the potential sink of heavy C-content compounds to the bottom of the oceans.

However, a shorter ice season is also characterized by thinner ice that allows more light to penetrate. This was the case found at one of the studied site during an exceptional mild winter. The model showed that light was never limiting sea ice algae growth. Sea ice total chlorophyll increased since the beginning of the ice formation and throughout the ice season. Compared to a typical ecological succession, sea ice was not characterized by a single bloom at the end of the ice season, but there were several successive blooms. The less adapted algae group (flagellates) also started competing for growth.

Hence, model results suggest that thinner ice may favor higher diversity of biological communities. Higher diversity does not only affect the final biomass of the sea ice community, but it also changes the entity and the magnitude of the matter exported to the pelagic waters during melting. Thinner sea ice sustained higher productivity rates and a larger flux of particulate matter to the surface ocean: if viable, they play a major role in seeding the following (if any) phytoplankton bloom. If non-viable, they become important indirect sink for carbon dioxide. Speculations on thinner sea ice associated to lower sea ice biomass are thus not so straightforward. Many other physical and biological constraints have to be considered and the response of the ecosystem to changing environmental conditions is again complex.

6.5 Towards the implementation of BFM-SI in a General Circulation Model

BFM-SI in coupled configurations with ESIM2 and the pelagic BFM has revealed to be a very useful tool to study several physical and biological processes of the sea ice and pelagic ecosystems. More studies and experiments are still possible, including a more detailed analysis of other CFFs such as sea ice zooplankton and bacteria. BFM-SI may thus still be used for process-studies, as well as for supporting mesocosm experiments. Nonetheless, it also shows higher potentialities for regional and global applications.

One of the future developments include the coupling with a physical model of the ocean to more properly study the influence of the depth of the mixed layer on nutrients transport. For the bottom communities BFM-SI results showed that it may be important to consider mixing/stratification processes. The release of freshwater to the ocean increases the stratification favoring a phytoplankton bloom but also preventing nutrient supply from below.

The study on the contribution and fate of the sea ice biomass is an important and large scale issue. A wider picture on the role, magnitude and contribution of the sea ice export to the pelagic organic matter is not yet achieved. BFM-SI revealed to explain well case-limit scenarios and those considerations may be further tested in a coupled configuration with a physical model of the ocean.

The strategy of coupling ESIM2 to BFM-SI is currently done as an off-line coupling. However, the system is already set up to run with a complete on-line coupling.

In order to move on to 3-D modelling, the necessary requirements are straightforward.

The BAL concept is in fact general. ESIM2 can be coupled to any model of sea ice dynamics, which can provide also the ice concentration as prognostic variable. The theory of the BAL can also be applied to other physical models of sea ice which have salinity and temperature as prognostic variables.

BFM-SI used in this thesis is a box model, which only considers vertical light penetration, while the other model variables are homogeneously distributed in the BAL and are thus mean state variables. Nonetheless, BFM-SI has been built in the same modular way as BFM was originally built. Hence, it can be coupled with multi-dimensional physical models. The physical model would thus define the spatial properties of the system and pass the relevant information to BFM-SI.

Sea ice biota has been studied for over few decades. Few regions have been highly characterized, but sea ice biological variability at different temporal and spatial scales is still lacking. There is an urgent need for more data. Sea ice is one of the largest ecosystem on earth, but is also one of the less sampled: sampling sea ice biota is in fact not an easy task. It is costly and time-consuming and often it is made in severe environmental conditions. Satellite can provide information on surface chlorophyll of the oceans. Unfortunately, this is not the case for ice-covered oceans. However, as ever more information are available, the role of sea ice biota appears to become more important (Arrigo, 2003).

In absence of data and remote sensing facilities, modelling can give a large contribution to the understanding of the sea ice ecosystem, as well as it can provide the wider picture of its qualitative and quantitative importance, which is still missing. Models can be used for process studies, such as the ones described in this thesis. Testing the models in regions where data are available for comparison can provide useful set ups for extending model studies in regions where no data are available. Moreover, regional simulations of Baltic Sea ice biota, supported by more data than other ice-covered oceans, can provide valid reference regional simulations for extending studies of the effect of global warming in polar oceans.

This thesis has presented a novel concept, the one of the Biologically-Active-Layer, which is a new modelling approach at the simulations of sea ice biogeochemistry. It has also shown the complexity of the sea ice system, its sensitivity to several biological and physical factors and the need of building models which can realistically describe these features, such as ESIM and BFM. The sea ice scientific community claims the urgent need to increase our knowledge of the sea ice biota. Interdisciplinary research is needed as well as larger efforts in coupling modelling studies with experimental works. This thesis has shown that the effort is possible. But more work is needed. And this should be a major focus of future work in sea ice ecosystems of ice-covered oceans.

List of Tables

List of Figures

Bibliography

Abels, H. (1892). Observations on the daily course of snow temperatures and the determination of the thermal conductivity of snow as a function of its density (in German). *Repert. Meteorol. (St. Petersburg)*, 16:1–53.

Ackley, S. F. and Sullivan, C. W. (1994). Physical controls on the development and characteristics of Antarctic sea ice biological communities. A review and synthesis. *Deep. Sea Res. Part I*, 41, 10:1583–1604.

Ainley, D. G., Tynan, C. T., and Stirling, I. (2003). Sea ice: A Critical Habitat for Polar Marine Mammals and Birds. In Thomas and Dieckmann, editors, *Sea ice: an introduction to its physics, biology, chemistry and geology*, pages 240–266. Blackwell Science, Oxford.

Alexander, M. A., Bhatt, U. S., Walsh, J., Timlin, M. S., Miller, J. S., and D.Scott, J. (2004). The atmospheric response to realistic Arctic sea ice anomalies in a AGCM during winter. *J. Climate*, 17:890–905.

Allen, J., Blackford, J., Holt, J., Proctor, R., Ashworth, M., and Siddorn, J. (2001). A highly spatially resolved ecosystem model for the North West European Continental Shelf. *Sarsia*, 86:423–440.

Allen, J., Blackford, J., and Radford, P. (1998). A 1-D vertically resolved modelling study of the ecosystem dynamics of the Middle and Southern Adriatic Sea. *J. Mar. Syst.*, 18:265–286.

Arrigo, K. R. (2003). Primary Production in Sea Ice. In Thomas and Dieckmann, editors, *Sea ice: an introduction to its physics, biology, chemistry and geology*, pages 143–183. Blackwell Science, Oxford.

Arrigo, K. R., Dieckmann, G., Gosselin, M., Robinson, D. H., Fritsen, C. H., and SullivanJ, C. W. (1995). High resolution study of the platelet ice ecosystem in McMurdo

Sound, Antarctica: biomass, nutrient, and production profiles within a dense microalgal bloom. *Mar. Ecol. Prog. Ser.*, 127:255–268.

Arrigo, K. R., Kremer, J. N., and Sullivan, C. W. (1993). A simulatec Antarctic fast-ice ecosystem. *J. Geophys. Res.*, 98:6929–6946.

Arrigo, K. R. and Sullivan, C. W. (1992). The influence of salinity and temperature covariation on the photophysiological characteristics of Antarctic sea ice microalgae. *J. of Phycol.*, 28:746–756.

Arrigo, K. R. and Thomas, D. N. (2004). Large scale importance of sea ice biology in the Southern Ocean. *Antarctic Science*, 16,4:471–486, doi: 10.1017/S0954102004002263.

Assur, A. (1958). Composition of sea ice and its tensile strength. In Unknown, editor, *Arctic Sea Ice*, pages 106–138. Publ. Natl. Acad. Sci., U.S.A.

BAAC (2008). *The BACC Author Team Assessment of Climate Change for the Baltic Sea Basin Series: Regional Climate Studies*. Springer Verlag, Heidelberg.

Baretta, J., Ebenhoeh, W., and Ruardij, P. (1995). The European Regional Seas Ecosystem Model, a complex marine ecosystem model. *J. Sea Res.*, 33, 3-4:233–246.

Baretta-Bekker, J., B. J. E. W. (1997). Microbial dynamics in the marine ecosystem model ERSEM II with decoupled carbon assimilation and nutrient uptake. *J. Sea Res.*, 38, 3-4:195–212.

Bennington, K. O. (1963). Some crystal growth feature of sea ice. *J. Glaciol.*, 4, 36:669–688.

Bunt, J. S. and Lee, C. C. (1970). Seasonal primary production in Antarctic sea ice at McMurdo Sound in 1967. *J. of Mar. Res.*, 28:304–320.

Cheng, B. and Launiainen, J. (1998). Modelling of ice thermodynamics in natural water bodies. *Cold Regions Science and Technology*, 27:153–178.

Cheng, B., Vihma, T., Pirazzini, R., and Granskog, M. A. (2006). Modelling of superimposed ice formation during the spring snowmelt period in the Baltic Sea. *Ann. Glaciol.*, 44, 1:139–146(8).

Comiso, J. C. (2003). Large-scale Characteristics and Variability of the Global Sea Ice cover. In Thomas and Dieckmann, editors, *Sea ice: an introduction to its physics, biology, chemistry and geology*, pages 112–142. Blackwell Science, Oxford.

Comiso, J. C., Parkinson, C. L., Gersten, R., and Stock, L. (2008). ccelerated declinein the Arctic sea ice cover. *Geophys. Res. Lett.*, 35:L01703, doi:10.1029/2007GL031972.

Cota, G. F., Legendre, L., Gosselin, M., and Ingram, R. G. (1991). Ecology of bottom ice algae: I Environmental controls and variability. *J. Mar. Syst.*, 2:257–277.

Cox, G. F. N. and Weeks, W. F. (1983). Equations for determining the gas and brine volume in sea-ice sample. *J.of Glaciol*, 29:306–316.

Cox, G. F. N. and Weeks, W. F. (1988). Numerical simulations of the profile properties of undeformed first year sea ice during the growth season. *J. Geophys. Res.*, 93:12444–12460.

Curry, J. A., Schramm, J. L., and Ebert, E. E. (1995). Sea ice-albedo climate feedback mechanism. *J. of Climate*, 8:240–247.

Dieckmann, G. S. and Hellmer, H. H. (2003). The Importance of Sea Ice: An Overview. In Thomas and Dieckmann, editors, *Sea ice: an introduction to its physics, biology, chemistry and geology*, pages 1–21. Blackwell Science, Oxford.

Dieckmann, G. S., Lange, M. A., Ackley, S. F., and Jennings, J. C. (1991). he Nutrient Status in Sea Ice of the Weddell Sea During Winter: Effects of Sea Ice Texture and Algae. *Polar Biology*, 11:449–456.

Eicken, H. (2003). From the Microscopic, to the Macroscopic, to the Regional scale: Growth, Microstructure and Properties of Sea Ice. In Thomas and Dieckmann, editors, *Sea ice: an introduction to its physics, biology, chemistry and geology*, pages 22–81. Blackwell Science, Oxford.

Eicken, H., Grenfell, T. C., Perovich, D. K., Richter-Menge, J. A., and Frey, K. (2004). Hydraulic controls of summer Arctic pack ice albedo. *J. Geophys. Res.*, 109:C08007, doi:10.1029/2003JC001989.

Eicken, H., Krouse, H. R., Kadko, D., and Perovich, D. K. (2002). Tracer studies of pathways and rates of meltwater transport through Arctic summer sea ice. *J. Geophys. Res.*, 107, C10:8046, doi:10.1029/2000JC000583.

Feltham, D. L., Untersteiner, N., Wettlaufer, J. S., and Worster, M. G. (2006). Sea ice is a mushy layer. *Geophys. Res. Lett*, 33:L14501, doi:10.1029/2006GL026290.

Fichefet, T. and Maqueda, M. A. M. (1999). Modelling the influence of snow accumulation and snow-ice formation on the seasonal cycle of the Antarctic sea-ice cover. *Climate Dynamics*, 15:251–268.

Flato, G. M. and Brown, R. D. (1996). Variability and climate sensitivity of landfast Arctic sea ice. *J. Geophys. Res.*, 101, C10:25,767–25,778.

Fripiat, F., Cardinal, D., Tison, J. L., Worby, A., and Andre, L. (2007). Diatom-induced silicon isotopic fractionation in Antarctic sea ice. *J. Geophys. Res.*, 112:G02001, doi:10.1029/2006JG000244.

Garrison, D. L., Buck, K. R., and Fryxel, G. A. (1987). Algal assemblages in Antarctic pack ice and in ice-edge plankton. *J. Phycol.*, 23:564–572.

Geider, R., MacIntyre, H., and Kana, T. (1998). A dynamic regulatory model of phytoplanktonic acclimation to light, nutrients, and temperature. *Limnol. Oceanogr.*, 43, 3:679–694.

Gibson, J. K., Kallberg, P., Uppala, S., Noumura, A., Hernandez, A., and Serrano, E. (1997). *ERA Description.* Blackwell Science, Reading, UK, ecmwf re-analysis project report series, 1 edition.

Gill, A. E. (1973). Circulation and bottom water production in the Weddell Sea. *Deep Sea Research*, 20:111–140.

Golden, K. M., Ackley, S. F., and Lytle, V. I. (1998). The percolation phase transition in sea ice. *Science*, 282:2238–2241.

Gosselin, M., Legendre, L., Demers, S., and Ingram, R. G. (1985). Responses of Sea-Ice Microalgae to Climatic and Fortnightly Tidal Energy Inputs (Manitounuk Sound, Hudson Bay). *Canadian Journal of Fisheries and Aquatic Sciences*, 42, 5:999–1006, doi:10.1139/CJFAS–42–5–999.

Gosselin, M., nad Wheeler P. A., L. M., A., H. R., and C., B. B. (1997). New measurements of phytoplankton and ice algal production in the Arctic Ocean. *Deep Sea Research Part II: Topical Studies in Oceanography*, 44-8:1623–1644.

Granskog, M. A. and Kaartokallio, H. (2004). An estimation of the potential fluxes of nitrogen, phosphorous and cadmium and lead from sea ice and snow in the northern Baltic Sea. *Water Air and Soil Pollution*, 154:331–347.

Granskog, M. A., Kaartokallio, H., Kuosa, H., Thomas, D. N., and Vainio, J. (2006a). Sea ice in the Baltic Sea: A review. *Estuarine, Coastal and Shelf Science*, 70:145–160.

Granskog, M. A., Kaartokallio, H., and Shirasawa, K. (2003a). Nutrient status of Baltic sea: Evidence for control by snow-ice formation, ice permeability, and ice algae. *J. Geophys. Res.*, 108, C8:3253, doi: 10.1029/2002JC001386.

Granskog, M. A., Leppäranta, M., Kawamura, T., Ehn, J., and Shirasawa, K. (2004). Seasonal development of the properties and composition of landfast sea ice in the Gulf of Finland, the Baltic Sea. *J. Geophys. Res.*, 109:C02020, doi: 10.1029/2003JC001874.

Granskog, M. A., Martma, T. A., and Vaikmäe, R. A. (2003b). Development, structure and composition of land-fast sea ice in the northern Baltic Sea.

Granskog, M. A., Uusikivi, J., Sequeiros, A. B., and Sonninen, E. (2006b). Relation of ice growth rate to salt segregation during freezing of low-salinity sea water (Bothnian Bay, Baltic Sea). *Annales of Glaciology*, 44:134–138.

Grossi, S. M., Kottmeier, S. T., Moe, R. L., Taylor., G. T., and Sullivan, C. W. (1987). Sea ice microbial communities. VI. Growth and primary production in bottom ice under graded snow cover. *Mar. Ecol. Prog. Ser.*, 35:153–164.

Haapala, J., Meier, M., and Rinne, J. (2001). Numerical investigations of future ice conditions in the Baltic Sea. *Ambio*, 30, 4-5:237–244.

Hägstrom, A., Azam, F., Kuparinen, J., and L.Zweifel, U. (2001). Pelagic plankton growth and resource limitations in the Baltic Sea. In Wulff, F. V., R. L. A. L. F., editor, *A System Analysis of the Baltic Sea*, pages 177–210. Springer-Verlag.

Hibler, W. D. (1979). A dynamic thermodynamic sea ice model. *J. Phys. Oceanogr.*, 9:817–846.

Holland, M. M. and Bitz, C. M. (2003). Polar amplification of climate change in coupled models. *Climate Dynamics*, 21:221–232.

Ikävalko, J. (1998). Further observations on flagellates within sea ice in northern Bothnina Bay, the Baltic Sea. *Polar Biology*, 19:323–329.

Jin, M., Deal, C. J., Wang, J., Shin, K. H., Tanaka, N., Whitledge, T. E., Lee, S. H., and Gradinger, R. R. (2006). Controls of the landfast ice-ocean ecosystem offshore Barrow, Alaska. *Ann. Glaciol.*, 44:63–72.

Johnsen, J. and Hegseth, E. N. (1991). Photoadaptation of sea ice microalgae in the Barents Sea. *Polar Biology*, 11:179–184.

Kaartokallio, H. (2004). Food web components, and physical and chemical properties of Baltic Sea ice. *Marine ecology Progress series*, 273:49–63.

Kaartokallio, H., Kuosa, H., Thomas, D. N., Granskog, M. A., and Kivi, K. (2006). Biomass, composition and activity of organism assemblages along a salinity gradient in sea ice subjected to river discharge in the Baltic Sea. *POlar Biology*, 30, 2:183–197.

Kalnay, E., Kanamitsu, M., Kistler, R., Collins, W., Deaven, D., Gandin, L., Iredell, M., Saha, S., White, G., Woollen, J., Zhu, Y., Leetmaa, A., Reynolds, B., Chelliah, M., Ebisuzaki, W., Higgins, W., Janowiak, J., Mo, K., Ropelewski, C., J., J. W., Jenne, R., and Joseph, D. (1994). The NCEP/NCAR 40-Year Reanalysis Project. *Bull. Amer. Meteor. Soc.*, 77:437–471.

Kang, S. H. and Fryxell, G. A. (1993). Phytoplankton in the Weddell Sea, Antarctica: Composition, abundance and distribution in water-column assemblages of the marginal ice-edge zone during austral autumn. *Mar. Biol*, 116:335–348.

Kantha, L. H. and Klaison, C. A. (1994). An improved mixed layer model for geophysical applications. *J. Geophy. Res.*, 99:25235–25266.

Kawamura, T., Jeffries, M. O., Tison, J. L., and Krouse, H. R. (2004). Superimposed ice formation in summer on Ross Sea pack ice floes. *Ann. Glaciol.*, 39, 1:563–568.

Kirst, G. O. and Wiencke, C. (1995). Ecophysiology of polar algae. *J. Phycol.*, 31:181–199.

Kottmeier, C., Olf, J., Frieden, W., and Roth, R. (1992). Wind Forcing and Ice Motion in the Weddell Sea Region. *J. Geophys. Res.*, 97(D18):20373–20383.

Kuosa, H. and Kaartokallio, H. (2006). Experimental evidence on nutrient and substrate limitation of Baltic sea ice algae and bacteria. *Hydrobiologia*, 554:1–10.

Kuosa, H., Norrman, B., Kivi, K., and Brandini, F. (1992). Effects of Antarctic sea ice biota on seeding as studied in aquarium experiments. *Polar biology*, 12, 3-4:333–339.

Lancelot, C., Mathot, S., Veth, C., and de Baar, H. (1993). Factors controlling phytoplankton ice-edge blooms in the marginal ice-zone of the northwestern Weddell Sea during sea ice retreat 1988: Field observations and mathematical modelling. *Polar Biology*, 13, 6:377–387.

Larsen, J., Kuosa, H., Ikävalko, J., Kivi, K., and Hällfors, S. (1995). A redescription of Scrippsiella hangoei (Schiller) comb. nov. a red tide dinoflagellate from the northern Baltic. *Phycologia*, 34:135–144.

Lavoie, D., Denman, K., and Michel, C. (2005). Modeling ice algae growth and decline in a seasonally ice- covered region of the Arctic (Resolute Passage, Canadian Archipelago). *J. Geophys. Res.*, 110:C11009, doi: 10.1029/2005JC002922.

Legendre, L., Ackley, S. F., Dieckmann, G. S., Gulliksen, B., Horner, R., Hoshiai, T., Melnikov, I. A., Reeburgh, W. S., Spindler, M., and Sullivan, C. W. (1992). Ecology of sea ice biota: 2. global significance. *Polar Biology*, 12:429–444.

Leppäranta, M. (1981). On the structure and mechanism of pack ice in the Bothnian Bay. *Finnidh Marine Research*, 248:3–86.

Leppäranta, M. (1983). A growth model for black ice, snow-ice and snow thickness in subarctic basins. *Nordic Hydrol.*, 14:59–70.

Leppäranta, M. and Manninen, T. (1983). The brine and gas content of sea ice with attention to low salinity and high tempertaure. Technical report, Finnish Institute of Marine Research Internal Report, Helsinki.

Leppäranta, M. and Myrberg, K. (2009). *Physical Oceanography of the Baltic Sea*. Springer Verlag, Helsinki.

Leventer, A. (2003). Particle Flux from Sea Ice in Polar Waters. In Thomas and Dieckmann, editors, *Sea ice: an introduction to its physics, biology, chemistry and geology*, pages 303–332. Blackwell Science, Oxford.

Lizotte, M. P. (2003). The Microbiology of Sea Ice. In Thomas and Dieckmann, editors, *Sea ice: an introduction to its physics, biology, chemistry and geology*, pages 184–210. Blackwell Science, Oxford.

Lizotte, M. P. and Sullivan, C. W. (1991). Photosynthesis-irradiance relationships in microalgae associated with Antarctic pack ice: evidence for in situ activity. *Mar. Ecol. Prog. Ser.*, 71:175–184.

Lytle, V. I., Massom, R., Bindoff, N., Worby, A., and Allison, I. (2000). Wintertime heat flux to the underside of east Antarctic pack ice. *J. Geophys. Res.*, 105(C12):28759–28769.

Maslanik, J. A., Fowler, C., Stroeve, J., Drubota, S., Zwally, J., Yi, D., and Emery, W. (2008). A younger, thinner Arctic ice cover: Increased potential for a rapid extensive sea-ice loss. *Geophys. Res. Lett.*, 34:L24501, doi:10.1029/2007GL032043.

Mathot, S., Bequevort, S., and Lancelot, C. (1991). Microbial communities from the sea ice and adjacent water column at the time of ice melting in the northwestern part of the Weddell Sea. *Polar Research*, 10, 1:267–276.

Maykut, G. A. (1985). An introduction to ice in the polar oceans. Technical report apl-uw 8510, Department of Atmospheric Sciences, University of Washington.

Maykut, G. A. and McPhee, M. G. (1995). Solar heating of the Arctic mixed layer. *J. Geophys. Res.*, 100, C12):24691–25703.

Maykut, G. A. and Untersteiner, N. (1971). Some results from a time dependent thermodynamic model of sea-ice. *J. Geophys. Res.*, 76, 6:1550–1575.

McDougall, T., Feistel, R., Millero, F. J., Jackett, D. R., Wright, D. G., King, B. A., Marion, G. M., Chen, C.-T. A., and Spitzer, P. (2009). *Calculation of the Thermodynamic Properties of Seawater.*

Meiners, K., Fehling, J., Granskog, M. A., and Spindler, M. (2002). Abundance, biomass and composition of biota in Baltic sea ice and underlying water (March 2000). *Polar Biology*, 25:761–770.

Melnikov, I. A. and Bounderchuk, L. L. (1987). To the ecology of the mass aggregations of colonial diatom algae under the Arctic drifting sea ice. *Okeanology*, 27:317–321.

Mikkelsen, D. M., Rysgaard, S., and Glud, R. N. (2008). Microalgal composition and primary production in Arctic sea ice - a seasonal study from Kobberfjord/Kangerluarsunnguaq, West Greenland. *Mar. Ecol. Prog. Ser.*, 368:65–74.

Nicolaus, M., Haas, C., and Bareiss, J. (2003). Observations of superimposed ice formation at melt-onset on fast ice on Kongsfjorden, Svalbard. *Phys. Chem. Earth*, 28, 28-32:1241–1248.

Nishi, Y. and Tabeta, S. (2005). Analysis of the contribution of ice algae to the ice-covered ecosystem in Lake Saroma by means of a coupled ice-ocean ecosystem model. *Journal of Marine Systems*, 55:249–270.

Notz, D. and Worster, M. G. (2006). A 1-D enthalpy model of sea ice. *Ann. Glaciol.*, 44:123–128.

Obernosterer, I., Ruardij, P., and Herndl, G. (2001). Spatial and diurnal dynamics of dissolved organic matter (DOM) fluorescence and H2O2 and the photochemical oxygen demand of surface water DOM across the subtropical Atlantic Ocean. *Lymnol. Oceanogr.*, 46, 3:632–643.

Omstedt, A. and Hansson, D. (2006). The Baltic Sea ocean climate system memory and response to changes in the water and heat balance components. *Continental Shelf Research.*, 26:236–251.

Perovich, D. K. (1993). A theoretical model of ultraviolet light transmission through Antarctic sea ice. *J. Geophys. Res.*, 98, C12:22579–22588.

Perovich, D. K. (1996). *The optical properties of sea ice*, volume 96-1. CREEL monograph.

Petihakis, G., Triantafyllou, G., Allen, I. J., Hoteit, I., and Dounas, C. (2002). Modelling the spatial and temporal variability of the Cretan Sea ecosystem. *J. Mar. Syst.*, 36:173–196.

Pirazzini, R., Vihma, T., Gransgok, M. A., and B. Cheng, B. (2006). Surface albedo measuraments over sea ice in the Baltic Sea during the spring snowmelt period. *Ann. Glaciol.*, 44:7–14.

Raick, C., Delhez, E. J. M., Soetaert, K., and Gregoire, M. (2005). Study of the seasonal cycle of the biogeochemical processes in the Ligurian Sea using a ID interdisciplinary model. *J. Mar. Syst.*, 55:177–203.

Räisänen, J. (2002). CO2-induced changes in inter-annual temperature and precipitation variability in 19 CMIP2 experiments. *Journal of Climate*, 15:2395–2411.

Raymond, J. A., Sullivan, C. W., and DeVries, A. L. (1994). Release of an ice-active substance by Antarctic sea ice diatoms. *Polar Biology*, 14-1:71–75.

Reinart, A., Arsta, H., Blanco-Sequeiros, A., and Herlevi, A. (1998). Relation between underwater irradiance and quantum irradiance in dependence on water transparency at different depths in the water bodies. *J. Geophys. Res.*, 103(C4):7749–7752.

Riaux Goben, C., Treguer, P., Paulin, M., and Vetion, G. (2000). Nutrinets, algal biomass and communities in land-fast ice and seawater off Adelie Land (Antarctica). *Antarctic Science*, 12:160–171.

Riebesell, U., Schloss, I., and Smetacek, V. (1991). Aggregation of algae released from melting sea ice: implications for seeding and sedimentation. *POlar biology*, 11, 4:239–248.

Ruardij, P., Haren, H. V., and Ridderinkhof, H. (1997). The impact of thermal stratification on phytoplankton and nutrient dynamics in shelf seas: a model study. *J. Sea Res.*, 38,3:311–331.

Saloranta (2000). Modeling the evolution of snow, snow ice and ice in the Baltic Sea. *Tellus*, 52, 1:93–108.

Semtner, A. J. (1976). A model for the thermodynamic growth of sea ice in numerical investigation of climate. *J. Phys. Oceanogr.*, 6:379–389.

Shine, K. P. and Pederson-Heller, A. (1985). The sensitivity of a thermodynamic sea ice model to changes in surface albeo parametrizations. *J. Phys. Oceanogr.*, 90:2243–2250.

Smith, W. S. and Nelson, D. M. (1985). Phytoplankton Bloom Produced by a Receding Ice Edge in the Ross Sea: Spatial Coherence with the Density Field. *Science*, 227, 4683:163–166, doi: 10.1126/science.227.4683.163.

Stefan, J. (1891). Über die Theorie der Eisbildung, insbesondere über Eisbildung im Polarmeere. *Ann. Phys.*, 42, 2:269–286.

Stigebrandt, A. (2001). Physical oceanography of the Baltic Sea. In Wulff, F. V., R. L. A. L. F., editor, *A System Analysis of the Baltic Sea*, pages 18–74. Springer-Verlag.

Taylor, A. H., Allen, J. I., and Clark, P. A. (2002). Extraction of a weak climatic signal by an ecosystem. *Nature*, 416:629–632.

Tedesco, L. and Vichi, M. (2009). BFM-SI: a novel tool for numerical simulations of sea ice biogeochemistry. *In preparation*, xx:xx–xx.

Tedesco, L., Vichi, M., Haapala, J., and Stipa, T. (2009a). An enhanced sea ice thermodynamic model applied to the baltic sea. *Boreal Enviromental Research*, 14:68–80.

Tedesco, L., Vichi, M., Haapala, J., and Stipa, T. (2009b). The Biologically-Active-Layer: a modeling approach to sea ice biogeochemistry. *J. Geophys. Res.*, Submitted.

Thomas, D. N. and Dieckmann, G. S. (2002). Antartic sea ice - a habitat for extremophiles. *Science*, 295, 5555:641–644.

Thomas, D. N. and Papadimitriou, S. (2003). Biogeochemistry of Sea Ice. In Thomas and Dieckmann, editors, *Sea ice: an introduction to its physics, biology, chemistry and geology*, pages 267–302. Blackwell Science, Oxford.

Thorndike, A. S. D. A. R., Maykut, G. A., , and Colony, R. (1975). The thickness distribution of sea ice. *J. Geophys. Res.*, 80, 33:4501–4513.

Untersteiner, N. (1964). Calculations of temperature regime and heat budget of sea-ice in the central Arctic. *J. Geophys. Res.*, 69, 22:4755–4766.

Untersteiner, N. (1968). Natural desalination and equilibrium salinity profile of perennial sea ice. *J. Geophys. Res.*, 73:1251–1257.

Vancoppenolle, M., Bitz, C. M., and Fichefet, T. (2007). Summer landfast sea ice desalination at Point Barrow, Alaska: Modeling and observations. *J. Geophys. Res.*, 112:C04022, doi:10.1029/2006JC003493.

Vichi, M., Masina, S., and Navarra, A. (2007a). A generalized model of pelagic biogeochemistry for the global ocean ecosystem. Part II: Numerical simulations. *J. Mar. Sys.*, 64, 1-4:110–130.

Vichi, M., May, W., and Navarra, A. (2003a). Response of a complex ecosystem model of the northern Adriatic Sea to a regional climate change scenario. *Clim. Res.*, 24:141–159.

Vichi, M., Oddo, P., Zavatarelli, M., Coluccelli, A., Coppini, G., M, C., Umani, S. F., and Pinardi, N. (2003b). Calibration and validation of a one-dimensional complex marine biogeochemical fluxes model in different areas of the northern Adriatic shelf. *Ann. Geophys*, 21:413–436.

Vichi, M., Pinardi, N., and Masina, S. (2007b). A generalized model of pelagic biogeochemistry for the global ocean ecosystem. Part I: Theory. *J. Mar. Sys.*, 64, 1-4:89–109.

Vichi, M., Ruardij, P., and Baretta, J. W. (2003c). Link or sink: a modelling interpretatio of the open Baltic biogeochemistry. *Biogeosciences*, 1:79–100.

Vichi, M., Zavatarelli, M., and Pinardi, N. (1998). Seasonal modulation of microbial-mediated carbon fluxes in the Northern Adriatic Sea. *Fisheries Oceanogr.*, 7, 3:182–190.

Vihma, T. and Haapala, J. (2009). Geophysics of sea ice in the Baltic Sea: a review. *Progress in Oceanography*, in press.

Wadhams, P. (2000). *Ice in the Oceans*. Gordon and Breach Scinece Publisher, Amsterdam.

Wadhams, P., Lange, M., and Ackley, S. F. (1987). The ice thickness distribution across the Atlantic sector of the Antarctic Ocean in midwinter. *J. Geophys. Res.*, 92:14535–14552.

Weeks, W. F. and Ackley, S. F. (1986). The growth, structure and properties of sea ice. In N., U., editor, *The Geophysics of Sea Ice*, page 156. Plenum Press, New York.

Welch, H. E. and Bergmann, M. A. (1989). Seasonal development of ice algae and its prediction from environmental factors near Resolute, NWT, Canada. *Canadian Journal of Fisheries and Aquatic Sciences*, 46:1793–1804.

Whitman, W. G. (1926). Elimination of salt from seawater ice. *Am. J. Sci. Ser.*, 211:126–132.

Zavatarelli, M. J. B., Baretta-Bekker, J., and Pinardi, N. (2000). The dynamics of the Adriatic Sea ecosystem; an idealized model study. *Deep-Sea Res. Part 1, Oceanogr. Res.*, 47:937–970.

Thanks

A hundred times every day
I remind myself that my inner and outer life
depend on the labors of other men,
living and dead,
and that I must exert myself
in order to give in the same measure
as I have received and am still receiving.

(Albert Einstein)

My foremost thanks are due to my supervisor, Marcello Vichi. Above everything else, it was his humanity, his insight, his ability to transfer his knowledge and his helpfulness that made the work described in this thesis as challenging and enjoyable as it was. He believed in me and built a modeler from beginning, while allowing me the room to work in my own way. I share with him all satisfactions I had during the years we have been working together.

I thank my tutor, Nadia Pinardi, for giving me the chance to start my PhD at the University of Bologna and to work in a so much exciting environment as CMCC is.

My special thanks also to my co-supervisor, Jari Haapala, for teaching me everything about the physical nature of sea ice. I began writing my first line of Matlab code with him and I ended up to develop my own physical model.

My thanks also to my other co-supervisor, Tapani Stipa, for the possibility he gave me to join the (ex-)Finnish Institute of Marine Research, for valuable discussions, and for providing me with hospitality every time it was needed.

I am grateful to many of the students, postdocs and scientists working with me at CMCC in Bologna for all the scientific, technical and human support I received. In particular, I am very grateful to Enrico and Fabrizio, for their extreme patient and helpfulness all the times my Linux machine was simply just a stranger to me.

In my daily work I have been blessed with a friendly and cheerful group of PhD students: Daniele and our long-lasting non-sense chats, Ida and the many laughs, Lavinia and the good moods, Michela, my virtual flatmate, Tete and his huge repertoire of anecdotes and Toto, always taking care that none of us went thirsty. We never ended up in a comune, but we were definitely already a comune. My years spent in Bologna would have never been so great without you around.

I'm very grateful to many scientists at FMI/FEI in Helsinki. I thank all the members of the sea ice group at FMI, in particular Bin, Roberta and Timo for all the valuable discussions during our meetings. Thanks also to many of the biologists at FEI, especially to Harri and Hermanni for all the scientific discussions we had about that wonderful world that is the sea ice biology. My special thanks to my Finnish biologist friends, Eeva and Jonna, for all the science and non-science we shared while drinking liters of coffee (and beer) together.

I'm very grateful to Harri Kuosa and Mats Gransgok for accepting to referee my PhD thesis and for their useful feedbacks.

My thanks also to David Thomas for being such an inspiration to me and to my work and for joining me the day of the defense of my thesis.

I thank all of the people who provided me with data for models comparison: Ari Seina for sea ice and snow thickness data in the Finnish Baltic, Mats Granskog and Jari Uusikivi for physical data at Hailuoto and Santala Bay, Ditte Mikkelsen for physical and biological data from Kobbefjord, Hermanni Kaartokallio for physical and biological data from Santala Bay and David Thomas and Milla Johansson for physical and biogeochemical data of the ISPOL cruise. Modelers definitely need data and all the experimentalists deserve my deepest admiration for such a hard work they do.

This thesis was supported by the Italian project VECTOR of the Italian Ministry of the University and Scientific Research, which I very much acknowledge. Special thanks also to IPY, NMA, Nord Forsk and NetICE project for supporting many of my sometimes costly trips.

Without the support of my family, none of this would have been possible. I thank my parents and my sister for their love and for everything they have done for me throughout the years.

So many people I met during the last few years. With many I discussed of science, from many I received many hints and with many I exchanged dozens of emails. And many now also stay good friends. Too many people would deserve to be mentioned. Which is why I simply stop here.

Allez, allez il n’y a pas de barrière

nous sommes tous enfants de la même mer

il n’y a pas de pirate il n’y a pas d’émigrant

nous sommes tous des navigants.

(Eugenio Bennato)